

# Undular hydraulic jumps

---

B.A. Wols

M.Sc. Thesis

Graduation committee  
Prof. Dr. Ir. G.S. Stelling  
Dr. Ir. W.S.J. Uijttewaai  
Ir. R.J. Labeur  
Ir. P.J. van Overloop

June 23, 2005  
Delft University of Technology  
Faculty of Civil Engineering and Geosciences  
Section of Environmental Fluid Mechanics



# Preface

In this master thesis an experimental and numerical study is described on the undular hydraulic jump. The work has been carried out within the framework of the Faculty of Civil Engineering at Delft University of Technology.

I would like to thank my graduation committee, prof. dr. ir. G.S. Stelling, dr. ir. W.S.J. Uijtewaal, ir. R.J. Labeur and ir. P.J. van Overloop for their assistance and comments. I would also like to thank the staff members of the laboratory for their help in constructing the weir and for the assistance during the experiment.

B.A. Wols

Delft  
June 23, 2005



# Abstract

The undular jump occurs at Froude numbers a little larger than 1 and is characterized by free-surface waves (undulations). A special case of the undular hydraulic jump is the formation of undulations behind a weir, which have more or less the same properties as the undular jump. The present research will concentrate on the undulations downstream of a weir. Knowledge of the characteristics and the formation of undular hydraulic jumps is important for the design of canals and the maintenance of natural channels. Undular jumps are also popular for recreational activities. More insight in the formation of undular jumps might also be useful for the planning of water sports, such as canoeing, rafting and surfing.

The undular jump is considered as a free-surface flow with a non-hydrostatic pressure distribution, which makes it a good example to evaluate different modelling approaches. It is interesting to find out whether the model can predict the occurrence of undulations and the correct wave characteristics. A second objective is to gain a better insight in the physical processes governing the undulations downstream of a weir. An experimental program is executed to achieve these objectives.

A weir is designed that consist of three parts, each of which can be removed. In that way, different shapes of the weir could be investigated. An experimental program is defined based upon the limitations of the numerical models and the physical processes, that need to be examined. This program results in measurements for five different weir shapes. The flow conditions for the transition zones (from undulations to no undulations) are measured together with the characteristics of the undulations. Local velocities are measured with a laser Doppler anemometer (LDA) and the water depths are measured with a photo camera.

Undulations occur for a certain range of the degree of submergence. This also depends on the shape of the weir. Two cases can be distinguished: a weir with an abrupt change in bottom profile on the downstream side and a weir with a smooth downstream part. For an abrupt change in bottom profile, undulations occur for lower degrees of submergence and the wave characteristics are different: undulations are more pronounced, wave lengths are two times larger and wave heights are up to four times larger. Wave lengths for the abrupt change in bottom profile are comparable to wave lengths of the undular hydraulic jump on a horizontal bottom from the literature.

A criterion for standing waves should be that the flow velocity equals the wave celerity. This depends on the choice of the flow velocity: the mean flow velocity is too low, because of the non-uniform velocity distribution, but the velocity at the free surface is too high. Furthermore, there seems to be a dependency of the factor  $\frac{U}{c}$  (flow velocity divided by wave celerity) with the Froude number.

The velocity profile has a large influence on the undulations. For the abrupt change in bottom profile, a recirculation zone is visible and it seems to have a wavy shape similar to the

undulations.

One of the used models is based upon the linearized Boussinesq equations. An analytical expression for the wave length can be derived depending on the Froude number only. This expression is in good agreement with the measured wave lengths when the shape of the horizontal velocity profile is taken into account. In case of an abrupt change in bottom profile, a triangular shaped velocity profile is applied, while for the weir with the smooth downstream part an uniform velocity profile is applied. These velocity profiles are in good agreement with the measured velocity profiles. An analytical expression for the wave height can be derived when a cosine shaped weir is assumed. The wave heights are in good agreement with the measurements, even for the weir with an abrupt change in bottom profile. This is remarkable, but can be explained by looking at the streamlines, which follow more or less a cosine shape.

Another model on free-surface flows is based upon the Euler equations. Multiple layers can be applied over the height. The one-layer case is considered resulting in too short waves for the abrupt change in bottom profile.

It can be concluded that 1D modelling is not valid for the undulations behind an abrupt change in bottom profile, which is also clearly visible in the velocity profiles. The FINEL 3D model, a finite element model that allows variations over the height, provides the correct wave lengths and predicts the upper and lower limit for the occurrence of undulations in a good manner.

# Summary (in Dutch)

Een ondulaire watersprong is een speciaal geval van de watersprong en wordt gekenmerkt door vrije oppervlakte golven (ondulaties). De watersprong treedt op voor Froude-getallen tussen de 1 en 1.7. Ondulaties, die ontstaan benedenstrooms van een overlaat, hebben min of meer dezelfde eigenschappen als de ondulaire watersprong op een vlakke bodem. Dit onderzoek beperkt zich tot de ondulaties benedenstrooms van een overlaat. Kennis over de eigenschappen van de ondulaties en de stromingscondities, waaronder ze gevormd worden, is belangrijk voor het ontwerp en/of onderhoud van kanalen en rivieren. Bovendien zijn ondulaire watersprongen populair voor recreatieve activiteiten, zoals kanoën, raften en surfen.

De ondulaire watersprong wordt beschouwd als een vrije oppervlakte stroming met een niet-hydrostatische drukverdeling. Het is daarom een geschikt voorbeeld voor het evalueren van verschillende modelleringen. Bovendien vindt er een golf-stroom interactie plaats. Het is interessant of de modellen het optreden van en de karakteristieken van de ondulaties kan voorspellen. Een tweede doelstelling van het onderzoek is om een beter inzicht te krijgen in de fysische processen, die plaatsvinden in de ondulaties benedenstrooms van een overlaat. Hiervoor is een experimenteel onderzoek uitgevoerd.

Een overlaat, bestaande uit drie delen, is ontworpen, zodat verschillende vormen onderzocht konden worden. De definitieve vormen zijn gebaseerd op de eisen gesteld door de numerieke modellen en de fysische processen, die onderzocht moeten worden. Gemeten is onder welke stromingscondities ondulaties wel of niet optreden en wat de karakteristieken zijn van de ondulaties. Lokale snelheden zijn gemeten met een LDA (Laser Doppler Anemometer) en de waterstanden met een foto camera.

Het optreden van ondulaties hangt af van de maat van verdrunkenheid (verhouding waterstand benedenstrooms van de overlaat tot de waterstand bovenstrooms ervan). Dit verschilt per vorm van de overlaat. Twee gevallen kunnen onderscheiden worden: een overlaat met een abrupte overgang aan de benedenstroomse kant en een overlaat met een gladde benedenstroomse kant. Voor het eerste geval treden ondulaties op voor een lagere maat van verdrunkenheid en de golven zijn hoger en langer. Deze ondulaties zijn qua golflengtes te vergelijken met uitdrukkingen uit de literatuur voor de ondulaire watersprong op een vlakke bodem.

Het snelheidsprofiel heeft een grote invloed op de ondulaties. In het geval van de overlaat met een abrupte overgang, ontstaat een recirculatie zone benedenstrooms van de overlaat. De snelheidsverdeling is dan niet meer uniform over de hoogte. De recirculatie zone heeft net als de ondulaties een golvende vorm.

Eén van de gebruikte modellen is gebaseerd op de Boussinesq vergelijkingen. Deze vergelijkingen bevatten de ondiep-water vergelijkingen, waaraan een term voor de niet-hydrostatische drukverdeling is toegevoegd. De Boussinesq vergelijkingen zijn gelineariseerd met als gevolg dat een an-

alytische uitdrukking voor de golflengte bepaald kan worden, die alleen van het Froude getal benedenstrooms van de overlaat afhangt. Voor de overlaat met een gladde benedenstroomse kant blijkt deze uitdrukking goed te kloppen. Echter, voor de overlaat met een abrupte overgang dient de niet uniforme snelheidsverdeling in rekening gebracht te worden. Als een driehoekigvormige snelheidsverdeling wordt aangenomen komen de golflengtes van het model aardig overeen met de gemeten golflengtes. Als voor de overlaat een cosinus vorm wordt aangenomen, kunnen de gelineariseerde Boussinesq vergelijkingen analytisch opgelost worden, wat resulteert in een analytische uitdrukking voor de golfhoogte. Opmerkelijk genoeg, blijkt deze uitdrukking voor alle vormen van de overlaat te kloppen met de metingen. Voor de overlaat met een abrupte overgang kan dit verklaart worden door te kijken naar de stroomlijnen, welke min of meer een cosinus vorm volgen.

Een ander niet-hydrostatisch model is gebaseerd op de Euler vergelijkingen. Meerdere lagen over de hoogte kunnen toegepast worden. In dit geval is echter het éénlagenmodel beschouwd, welke resulteert in te korte golven voor de overlaat met een abrupte overgang. Zoals al eerder uit de snelheidsprofielen opgemaakt is, blijkt één dimensionaal modelleren van ondulaties na een overlaat met abrupte overgang een te grove benadering te zijn. Het FINEL 3D model, een eindig elementen model, welke de variaties over de hoogte in rekening brengt, geeft wel de correcte golflengtes weer. Bovendien is het het enig gebruikte model dat de onder- en bovengrens voor de maat van verdronkenheid, waartussen de ondulaties optreden, juist voorspelt.



# Contents

<b>1</b>	<b>Introduction</b>	<b>1</b>
1.1	General . . . . .	1
1.2	Study objectives . . . . .	2
1.3	Methodology . . . . .	3
1.4	Outline of the thesis . . . . .	3
<b>2</b>	<b>Background information</b>	<b>5</b>
2.1	Introduction . . . . .	5
2.2	Undular hydraulic jump on a horizontal bottom . . . . .	5
2.2.1	General information . . . . .	5
2.2.2	Origin of the waves . . . . .	5
2.2.3	Historical background . . . . .	7
2.2.4	Classification of the undular jump . . . . .	8
2.2.5	Important parameters . . . . .	8
2.3	Undulations behind a weir . . . . .	9
2.3.1	Occurrence of undulations . . . . .	9
2.3.2	Discharge coefficient . . . . .	12
2.3.3	Characteristics of the undulations . . . . .	13
2.4	Conclusion . . . . .	14
<b>3</b>	<b>Experimental setup</b>	<b>15</b>
3.1	Introduction . . . . .	15
3.2	Preliminary experiment . . . . .	15
3.3	Experimental design . . . . .	17
3.3.1	Requirements of the weir . . . . .	17
3.3.2	Experimental program . . . . .	20
3.3.3	Measurements . . . . .	20
3.3.4	Instrumentation . . . . .	22
3.3.5	Flow conditions . . . . .	24
3.3.6	Accuracy of the measurements . . . . .	24
3.4	Conclusion . . . . .	26
<b>4</b>	<b>Interpretation experimental data</b>	<b>27</b>
4.1	Introduction . . . . .	27
4.2	Observations . . . . .	27

4.3	Occurrence of undulations . . . . .	30
4.3.1	Discharge coefficient . . . . .	32
4.4	Wave characteristics . . . . .	32
4.4.1	Wave lengths . . . . .	33
4.4.2	Wave celerities . . . . .	35
4.4.3	Wave heights . . . . .	39
4.4.4	Error analysis . . . . .	41
4.5	Interpretation velocity profile . . . . .	41
4.5.1	Recirculation zones . . . . .	42
4.5.2	3D effects . . . . .	43
4.6	Hypothesis . . . . .	45
4.7	Conclusion . . . . .	46
<b>5</b>	<b>Modelling</b>	<b>47</b>
5.1	Introduction . . . . .	47
5.2	Boussinesq model . . . . .	47
5.2.1	Overview . . . . .	47
5.2.2	Linearized equations . . . . .	49
5.2.3	Non-linear Boussinesq equations . . . . .	53
5.2.4	Numerical implementation . . . . .	54
5.3	Non-hydrostatic model . . . . .	54
5.4	FINEL 3D . . . . .	54
5.5	Conclusion . . . . .	54
<b>6</b>	<b>Numerical experiments</b>	<b>55</b>
6.1	Introduction . . . . .	55
6.2	Boussinesq model . . . . .	55
6.2.1	Linear Boussinesq model . . . . .	55
6.2.2	Non-linear Boussinesq model . . . . .	58
6.3	Non-hydrostatic 1D . . . . .	59
6.4	FINEL 3D . . . . .	64
6.5	Conclusions . . . . .	66
<b>7</b>	<b>Conclusions and Recommendations</b>	<b>67</b>
7.1	Conclusions . . . . .	67
7.2	Recommendations . . . . .	68
	<b>Notations</b>	<b>73</b>
	<b>References</b>	<b>73</b>
<b>A</b>	<b>Dataprocessing</b>	<b>75</b>
A.1	Velocities . . . . .	75
A.2	Water depths . . . . .	76
A.3	Pressure . . . . .	76
A.4	Discharge . . . . .	76

<b>B</b>	<b>Water Profiles</b>	<b>77</b>
<b>C</b>	<b>Verification LDA-measurement</b>	<b>91</b>
<b>D</b>	<b>Velocities and Reynoldsstresses</b>	<b>93</b>
<b>E</b>	<b>Water Profiles Wave celerity</b>	<b>99</b>
<b>F</b>	<b>Numerical implementation Boussinesq equations</b>	<b>107</b>
F.1	Linearized equations . . . . .	107
F.2	Non-linearized equations . . . . .	108



# List of Figures

1.1	Types of undular jump . . . . .	2
2.1	Undular jump on a horizontal bottom . . . . .	6
2.2	Physics initiation of undulations. . . . .	7
2.3	Classification of undular jumps, taken from Ohtsu et al (2003) . . . . .	9
2.4	Flow regimes over a weir . . . . .	10
2.5	Theoretical relation submergence and Froude for different Reynolds numbers. . .	11
2.6	Discharge reduction coefficient . . . . .	12
2.7	Definition of the variables concerning the undulations behind a weir . . . . .	13
3.1	Different shapes of the weir used in the preliminary experiment . . . . .	16
3.2	Preliminary experiment . . . . .	16
3.3	The weir consists of three parts . . . . .	17
3.4	Shape of the weir . . . . .	20
3.5	Experimental flume . . . . .	20
3.6	Requirements measured variables . . . . .	22
3.7	Sideview flume . . . . .	22
3.8	Camera view from above . . . . .	23
3.9	Velocity points over the depth . . . . .	23
4.1	Photo water profile series 4 $Q=45$ l/s . . . . .	28
4.2	Photo from above series 2 $Q=60$ l/s . . . . .	29
4.3	Photos water profile series 2 $Q=45$ l/s . . . . .	29
4.4	Water profile derived from the photos . . . . .	30
4.5	Occurrence of undulations . . . . .	31
4.6	Discharge reduction coefficient . . . . .	32
4.7	Water depth profile . . . . .	33
4.8	Definition of wavelengths . . . . .	34
4.9	Dimensionless wave number against Froude number . . . . .	34
4.10	Froude number against wave celerity . . . . .	35
4.11	Vector plot series 1 . . . . .	37
4.12	Vector plot series 2 . . . . .	38
4.13	Definition of the wave heights for weirs with and without a downstream part . .	40
4.14	Waveheights . . . . .	40
4.15	Recirculation zone for series 1 . . . . .	42
4.16	Sketch top view . . . . .	45

5.1	Definition of the variables in the Boussinesq equations . . . . .	49
5.2	Schematisation of the horizontal velocity profile . . . . .	50
5.3	Wavenumber against Froude for different horizontal velocity distributions . . . .	52
5.4	Waveheight determined by the analytical solution of the linear Boussinesq equation	53
6.1	Example of a simulation of the linear Boussinesq model . . . . .	55
6.2	Comparison wave numbers measurements to linear Boussinesq model . . . . .	56
6.3	Comparison wave heights measurements to linear Boussinesq model, calculated wave heights are inaccurate for the weir with the abrupt change in bottom profile. The solid line represents an analytical solution in case of a cosine shaped weir. .	57
6.4	Comparison wave celerities measurements to linear Boussinesq model . . . . .	58
6.5	Comparison wave numbers measurements to non linear Boussinesq model . . . .	59
6.6	Comparison wave heights measurements to non linear Boussinesq model . . . .	60
6.7	Example non-hydrostatic 1D model . . . . .	60
6.8	Comparison wave numbers measurements to non-hydrostatic 1D model . . . . .	62
6.9	Comparison wave heights measurements to non-hydrostatic 1D model . . . . .	63
6.10	Example of a simulation of the FINEL3D model for series 1. . . . .	64
6.11	Occurrence of undulations for the FINEL 3D model . . . . .	65
6.12	Measured wave lengths compared to the FINEL 3D model. . . . .	65
6.13	Measured wave heights compared to the FINEL 3D model . . . . .	66
C.1	Calibration sharp weir . . . . .	92
C.2	Calibration horizontal bottom . . . . .	92

# List of Tables

2.1	Types of hydraulic jumps (rough classification)(Chow 1973) . . . . .	6
3.1	Overview geometry flumes . . . . .	15
3.2	Overview requirements from numerical model . . . . .	18
3.3	Overview hypothesis . . . . .	19
3.4	Experimental program . . . . .	21
3.5	Flow conditions experiment . . . . .	25
3.6	Absolute error in measured parameters . . . . .	25
4.1	Overview experiments . . . . .	28
4.2	Values of ( $\frac{u}{c}$ ) for the horizontal velocity at the free surface . . . . .	39
4.3	Relative errors . . . . .	41
4.4	Comparison discharges . . . . .	43
4.5	Relative error discharges . . . . .	44
6.1	Upper boundary occurrence of undulations . . . . .	61
6.2	Overview numerical models . . . . .	66
C.1	Sharp weir . . . . .	91
C.2	Flow over a horizontal bottom . . . . .	91





# Chapter 1

## Introduction

### 1.1 General

Most models on free-surface flows, based upon the shallow water equations, make use of the assumption of a hydrostatic pressure distribution (neglecting the vertical accelerations). Modelling free-surface flows that can handle rapidly-varied flows requires more sophisticated models. These models have to account for the effect of the non-hydrostatic pressure. A phenomenon possessing these properties is the undular hydraulic jump. This undular jump seems to be a good example to evaluate different model approaches for free-surface flows. Moreover, the undular jump combines flow and wave phenomena, which are often treated separately.

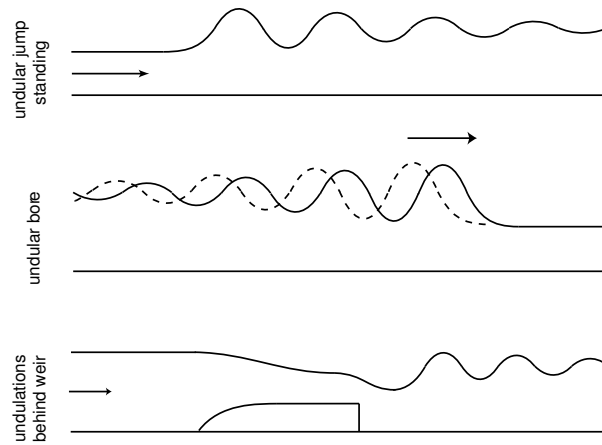
The undular hydraulic jump is a special case of the hydraulic jump. The hydraulic jump occurs at the transition from a rapid to tranquil flow in an open channel. This is a spectacular phenomenon with a lot of turbulence, air entrainment and energy losses. The undular hydraulic jump is characterized as a hydraulic jump of low height with free-surface waves. These standing waves are called undulations, which can stretch out over a great length, because of the low dissipation of the waves. Whether the jump is undular or not, depends on the flow situation (see Chapter 2).

The formation of undular jumps can be observed in different circumstances. Three types are distinguished with more or less the same behaviour (see Figure 1.1). The first type is a standing undular jump on a flat bottom. This type may occur in irrigation and water supply channels, in estuaries (during some periods of the tides), in narrow or shallow straights subjected to strong currents and in case of a coming flood flow in a river during some stages of the flood. For a flow below a sluice gate, supercritical flow develops downstream of this structure, which may as well result in an undular jump. Also, in the transition region from steep to mildly sloping channels this type of undular jump is observed. The second type is a moving undular hydraulic jump, which is called an undular surge. It is observed in tidal rivers, where the geometry of the river causes a sharp tidal front, on which undulations can occur. Undulations may as well originate downstream of a weir (third type). The weir can be an arbitrary obstacle on the bottom (like groynes in the river, summer dikes etc.).

The undulations may cause bank and bottom erosion and lead to additional loads to hydraulic structures downstream of the jump. The waves can also hinder navigation. Therefore knowledge of the characteristics and the formation of undular hydraulic jumps is important for the design of canals and the maintenance of natural channels. Undular jumps are also popular for

recreational activities. So, more insight in the formation of undular jumps might be useful for the planning of water sports, such as canoeing, rafting and surfing.

Most research on undular jumps has been conducted for a standing hydraulic jump in flat channels (type 1). Still, the characteristics and the formation of an undular hydraulic jump are not fully understood. The hydraulic parameters governing the undular jumps have not been fully clarified. The present research will concentrate on the formation of undulations behind an obstacle. This coincides with the renewed interest for research on weirs nowadays at the Delft University of Technology: The Dutch Department of Public Works (Rijkswaterstaat) is interested in the resistance of obstacles (weirs), that are situated in the riverbanks. This influences the height of the flood wave during an extreme high discharge through the river, which determines the design height of the dikes.



**Figure 1.1:** Types of undular jump

## 1.2 Study objectives

Two objectives of the study are formulated:

1. Obtain a proper dataset of the flow situation and characteristics of the undulations behind a weir to evaluate different modelling approaches.
2. To gain a better insight in the physical processes, that determine the undulations behind an obstacle.

Ad 1.

It is important that the model can describe under what hydraulic conditions the undulations occur. Two transitions need to be determined: when the undular jump moves over into a classical hydraulic jump (with a surface roller) and when the undulations disappear. The characteristics of the undulations need to be clarified for a proper verification of the model. Also, the application of the models for different shapes of the obstacle needs to be investigated.

Ad 2.

The objective is to determine what physical processes influence the occurrence and the characteristics of the undulations and to translate this into a few parameters. The importance of a certain physical process can be determined by investigating different shapes of the obstacle, which corresponds to the dominant physical process.

### 1.3 Methodology

A literature study is conducted for the undular jump on a horizontal bottom. The important parameters, that determine the undular jump are described. For the undulations behind an obstacle, the main characteristics are determined, that are necessary for a good interpretation and for the comparison of the experiment with the model.

An experiment is needed to determine the flow conditions and wave characteristics. A preliminary experiment is conducted to get some general idea on the undular hydraulic jump behind an obstacle, under which conditions it occurs and for what obstacle shape the most pronounced undulations occur. The next step is the design of a weir shape, that meets the requirements of the numerical models and is capable of investigating the physical processes. In that way, hypotheses, that correspond to a physical process, are formulated. Experiments are conducted for five different weir shapes under different flow conditions.

The results of the measurements are investigated: the relation between the flow conditions and the occurrence of the undulations, between the flow conditions and the wave characteristics, influence of the obstacle shape on the undulations.

The final step is the evaluation of the different model approaches. The experimental data is compared to the numerical models. The flow conditions, under which the undulations occur and the wave characteristics are compared to each other. This results in an overview of the applicability of the numerical models for different obstacles.

### 1.4 Outline of the thesis

In Chapter 2, background information on the undular hydraulic jump is given. It contains an overview of the past research on undular jumps and the basic concepts of undulations behind a weir. The experimental setup is presented in chapter 3. The results and interpretation of the experiment are described in chapter 4. The numerical models used to describe the undulations, are presented in chapter 5. The comparison between the measurements and the numerical simulations is given in chapter 6. Finally the conclusions and recommendations are described in chapter 7.



# Chapter 2

## Background information

### 2.1 Introduction

This chapter provides an overview of the past research on the undular jump. Most research is conducted for an undular jump on a horizontal channel. The undulations behind the weir are a special case of the undular jump, which means that the same concepts can be applied. Furthermore, the important parameters that describe the characteristics of the undulations are defined. These parameters are used for the interpretation of the experiment and evaluation of the models.

### 2.2 Undular hydraulic jump on a horizontal bottom

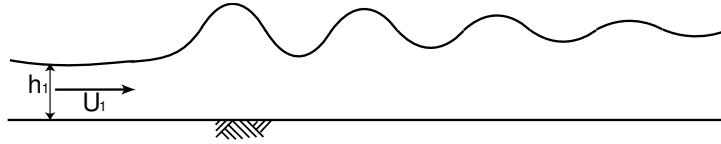
#### 2.2.1 General information

A hydraulic jump occurs at the transition from supercritical flow to subcritical flow. The Froude number determines whether the flow is subcritical or supercritical. It is given by ( $U$ =mean flow velocity,  $h$ =water depth):

$$F = \frac{U}{\sqrt{gh}}$$

Supercritical flow occurs for Froude numbers larger than 1 and is characterized by high velocities and low water depths. Subcritical flow occurs for Froude numbers smaller than 1 and is characterized by low velocities and high water depths. The transition occurs at  $F = 1$ . A hydraulic jump only forms when the inflow is supercritical.

There are different types of hydraulic jumps, which depend on the inflow Froude number. A rough classification for hydraulic jumps in rectangular channels is given by Chow (1973) (see Table 2.1). An undular hydraulic jump occurs for relatively small inflow Froude numbers (between 1 and 1.7). Figure 2.1 contains a sketch of the undular jump on a horizontal bottom.



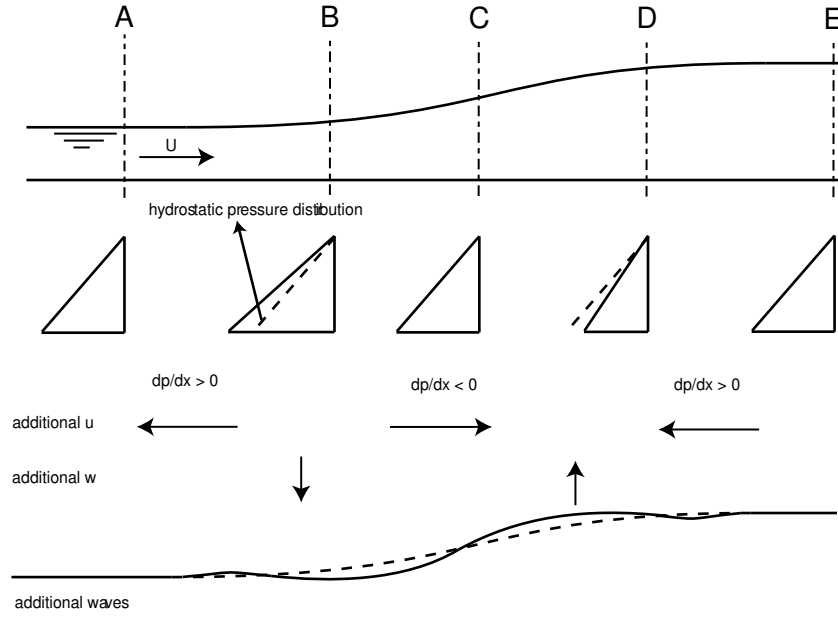
**Figure 2.1:** Undular jump on a horizontal bottom, undulations develop for inflow Froude numbers between 1 and 1.7

Type jump	Froude nr.	Description
Strong jump	$F > 9$	Rough jump, lot of energy dissipation.
Steady jump	$4.5 < F < 9$	Considerably energy losses.
Oscillating jump	$2.5 < F < 4.5$	Unstable oscillating jump. Production of large waves of irregular period.
Weak jump	$1.7 < F < 2.5$	Little energy loss.
Undular jump	$1.0 < F < 1.7$	Free-surface undulations downstream of the jump. Negligible energy losses.

**Table 2.1:** Types of hydraulic jumps (rough classification)(Chow 1973)

### 2.2.2 Origin of the waves

The origin of the waves can be explained by the sketch, given in Figure 2.2 (Frazao and Zech 2002). The transition from supercritical to subcritical flow leads to a curved water surface. Due to this curvature of the water surface, the pressure distribution is not hydrostatic. The dotted lines in the pressure distributions (at cross-sections B and D in Figure 2.2) refer to the hydrostatic pressure. At position A, C and E, the pressure is hydrostatic, while at position B, the pressure is higher than the hydrostatic pressure, while at position D, the pressure is lower. This means that horizontal pressure gradients develop, leading to additional horizontal and vertical velocities: An additional flow develops in the direction of position D away from position C and E. The opposite occurs at position B, where an additional flow develops away from position B towards position A and C. This leads to a decline in the water level at position B and an incline at position D: additional waves develop at the free surface. This process will continue until it reaches an equilibrium or the waves break.



**Figure 2.2:** Physics initiation of undulations, the horizontal pressure gradients cause additional waves

### 2.2.3 Historical background

Darcy and Bazin (1865) observed undular jumps in the Canal de Bourgogne with undulations stretching out over lengths up to 150m. Most research is conducted to the flow conditions, for which the undular jump occurs. An upper limit of the Froude number, for which undulations still develop, is often proposed. Bradley and Peterka (1957) found experimentally an upper limit of the Froude number  $F_{limit} = 1.7$ . Ippen and Harleman (1954) assumed an analogy between an undular surge and an undular jump. The upper limit of the Froude number ( $F_{limit} = \sqrt{3}$ ) is obtained when the velocity at the first wave crest becomes zero. Iwasa (1955) and Hager and Hutter (1984) proposed an upper limit of the Froude number ( $F_{limit} = 1.4 - 1.7$ ) based on the cnoidal wave height and the solitary wave height. In some textbooks the upper limit of the Froude number is 1.7 (Chow 1973), (Henderson 1966). Montes (1978) and Ryabenko (1990) performed independent investigations and rejected an analogy between an undular surge and an undular jump. They observed an upper limit for the Froude number between 1 and 3.7. Chanson and Montes (1995a) supposed that the transition depends on the Froude number and aspect ratio of the flow cross-section ( $h/B$ ,  $B$ =width of the channel). They found an upper limit for the Froude number ( $F_{limit} = 1.5 - 2.9$ ), depending on the aspect ratio: for a relatively wide channel, the upper limit of the Froude number increases. Ohtsu et al. (2001) also investigated the influence of the development of the turbulent boundary layer on the formation of undular hydraulic jumps. They found an upper limit of the Froude number for a developing flow of  $F_{limit} = 1.3 - 2.3$ . For a fully developed flow, they found an upper limit of  $F_{limit} = 1.7$ . Ohtsu et al. (2003) investigated the influence of the Reynolds number on the formation of the hydraulic jump. General agreement for the formation of an undular hydraulic jump has not been obtained.

### 2.2.4 Classification of the undular jump

The undular jump seem to have different appearances: the waves may break and shock waves from the sides can develop interfering with the undulations. A classification is used for a better understanding. Ohtsu et al. (2003) proposes the following classification for undular jumps (see Figure 2.3):

- Non-breaking undular jump ( $1.0 < F < F_{limit}$ )
  - The undular surface is two dimensional, shock waves are not visible. The amplitude of the undulations is small. ( $1.0 < F < 1.2$ )
  - Lateral shock waves develop ( $1.2 < F < F_{limit}$ ). Two cases are distinguished, that depend on the width of the channel (aspect ratio). For case I, relatively wide, the shock waves don't reach the middle of the channel, the amplitude of the undulations is smaller near the sidewalls than in the middle of the channel. For case II, relatively small, the lateral shock waves intersect at the top of the first wave.
- Breaking undular jump. ( $F_{limit} < F < F_u$ )
 

The first wave breaks at the central zone of the channel and stable undulations develop downstream of the first wave. For case I, the undulations near the sidewalls are negligible, while for case II the undulations near the sidewalls are clearly visible. For Froude number higher than  $F_u$ , a classical jump is formed and no undulations are observed.

Chanson and Montes (1995a) provides a slightly different classification, which for that reason will not be discussed here.

### 2.2.5 Important parameters

Important parameters, that influence the transition from undular to classical jump on a horizontal bottom, are:

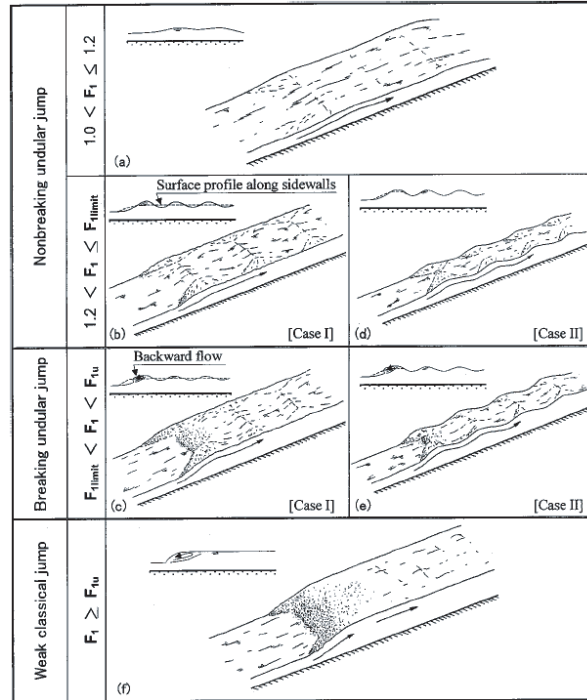
- Inflow Froude number
- Aspect ratio:
  - $\frac{y_c}{B}$  (Chanson and Montes 1995a),  $y_c$  is the critical flow depth (where  $F = 1$ ).
  - $\frac{B}{h_1}$  (Ohtsu et al. 2003),  $h_1$  is the flow depth at the toe of the jump.
 These parameters are related to each other ( $B$  = width of the channel):

$$\frac{B}{h_1} = \frac{F_1^{2/3}}{\frac{y_c}{B}}$$

The aspect ratio influences the upper limit of the inflow Froude number. A relatively wide channel leads to an increase in the upper limit of the Froude number.

- Development of boundary layer
  - $\frac{\delta}{h_1}$  (Ohtsu et al. 2001)
  - $\delta$  is the thickness of the boundary layer at the bottom or the wall, which also depends on the roughness of the bottom and wall. For a fully developed boundary layer, the upper





**Figure 2.3:** Classification of undular jumps, taken from Ohtsu et al (2003)

limit of the Froude number is 1.7. No undulations occur when the boundary layer is not developed at all.

- Reynoldsnumber  $Re = \frac{uD}{\nu}$   
 $Re > 6.5 \cdot 10^4$ : no influence on formation of the undular hydraulic jump.  
 $Re < 6.5 \cdot 10^4$ : if  $Re$  decreases, undular jumps are possible for higher Froude numbers, probably due to viscous effects. Furthermore, if  $Re$  decreases, the amplitude and wavelength of the undulations increase (Ohtsu et al. 2003).

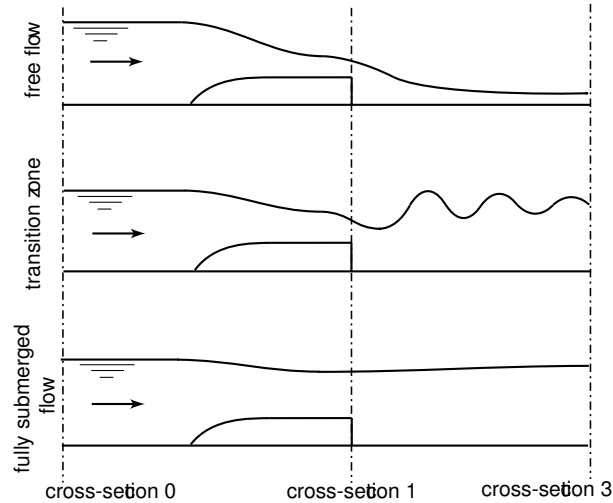
## 2.3 Undulations behind a weir

The most important issues, concerning the undulations behind a weir, are: under which flow conditions they occur, and what the characteristics of these undulations are. Three cross-sections are defined (see Figure 2.4): section 0 is upstream of the weir, where the water surface is horizontal. Section 1 is at the end of the horizontal part of the weir. Section 3 is at a distance downstream of the weir. The index of a variable refers to these cross-sections.

### 2.3.1 Occurrence of undulations

Three flow regimes are distinguished by Kolkman (1989) for the flow over a weir (see Figure 2.4):

- Free flow (perfect weir). The flow above the weir becomes supercritical and is independent of the downstream water depth. Downstream of the weir a hydraulic jump can occur at some distance.
- Transition zone. This is the transition from free flow to submerged flow, where surface waves develop downstream of the weir.
- Fully submerged flow. The water surface is almost horizontal, the flow above the weir is subcritical and depends on the upstream and downstream water depth.



**Figure 2.4:** Flow regimes over a weir, type of flow regime depends on the degree of submergence.

Starting from the free flow, the transition zone is reached by increasing the downstream water depth. Fully submerged flow is reached by further increasing the downstream water depth. The degree of submergence ( $S$ ), given as the downstream water depth ( $h_3$ ) divided by the upstream water depth ( $h_0$ ), gives some information about the expected flow regime.

The point of interest is the transition zone, where the undulations occur. This can be seen as a special case of the undular jump on a flat bottom. In that case, the Froude number at the toe of the undular jump is the most important parameter that determines whether the jump is classical or undular. For a certain range of the Froude number ( $F = 1 - 1.7$ ) undulations occur, for higher Froude numbers the undular jump transforms into a classical jump. The same process takes place for the undulations behind the weir. But it is difficult to determine the correct Froude number, because the highest Froude number is somewhere between the end of the weir and the first wave trough. At this position, the flow is not uniform over the depth: a recirculation zone develops behind the weir. So, the mean velocity is much lower than the velocity in the upper layer. The Froude number at the end of the weir can be derived more easily, because the flow is more or less uniform over the depth at this position. A relation between this Froude number and the degree of submergence can be derived analytically by the principle of energy conservation and momentum balance (for a weir with an abrupt change in

bottom profile).

Applying Bernoulli between cross-section 0 and cross-section 1 along the water surface, no energy is lost between these sections:

$$h_0 + \frac{U_0^2}{2g} = h_1 + a_{weir} + \frac{U_1^2}{2g} \quad (2.1)$$

This expression is valid as long as the curvature of the streamlines is small. When the curvature is large, the velocity at the free surface drops, so that the assumption of the mean velocity in equation 2.1 is not allowed.

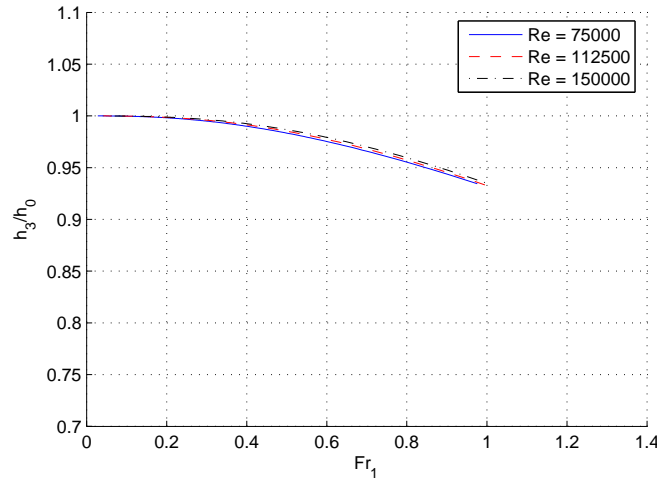
Applying the momentum balance between section 1 and section 3 yields:

$$\frac{1}{2}\rho g(h_1 + a_{weir})^2 + \rho U_1^2 h_1 = \frac{1}{2}\rho g h_3^2 + \rho U_3^2 h_3 \quad (2.2)$$

This equation is only valid when the pressure distribution is hydrostatic. For a strongly curved water surface, a non-hydrostatic pressure distribution arises leading to a different momentum balance. When Froude numbers are higher than 1, the curvature in the water surface increases in order that the energy balance and momentum balance as defined in equation 2.1 and 2.2 become inaccurate. Rearranging leads to an expression for  $S$  (valid for  $Fr_1 < 1$ ):

$$\frac{h_3}{h_0} = S = f(Fr_1, q)$$

When a constant kinematic viscosity is assumed,  $S$  is also a function of  $Fr_1$  and  $Re$ . In Figure 2.5, this relation is given. The influence of the Reynolds number is small. In the expression



**Figure 2.5:** Theoretical relation degree between the degree of submergence and the Froude number for different Reynolds numbers.

for the degree of submergence, the upstream and downstream water level are referred to the bottom and not to the weir height. For the former, the relation of the Froude number with the

submergence is more or less independent of the discharge.

Similar to the undular jump on a horizontal bottom, where the occurrence of undulations is defined as a function of the inflow Froude number, the existence of undulations behind a weir can be characterized by the Froude number at the end of the weir or equivalent to this, the degree of submergence.

### 2.3.2 Discharge coefficient

The discharge coefficient  $C_{dv}$  in case of a perfect weir is given by:

$$C_{dv} = \frac{Q}{\frac{2}{3}BH_1\sqrt{\frac{2gH_1}{3}}} \quad (2.3)$$

$H_1$ =energy level [m]

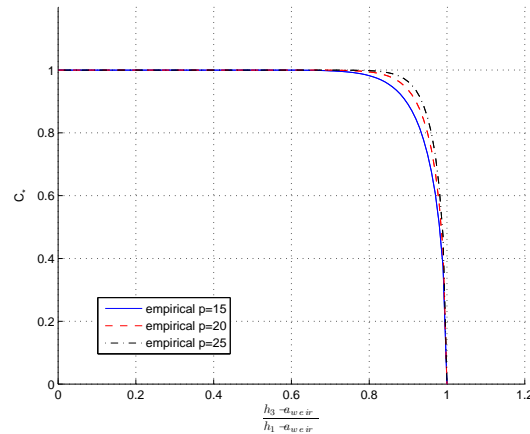
$B$  = width of the flume [m]

$Q$  = discharge [ $m^3/s$ ]

The value of  $C_{dv}$  depends on the upstream flow conditions only. For the transition zone from perfect weir to imperfect weir, there is no simple discharge relation. A relative simple approach is to use a discharge reduction coefficient  $C_*$ , which is a function of the submergence. This discharge reduction coefficient is a reduction factor to the discharge coefficient for the perfect weir (free flow):

$$C_* = \frac{Q}{C_{dv}\frac{2}{3}BH_1\sqrt{\frac{2}{3}gH_1}} \quad (2.4)$$

There are empirical formulas for the relation between  $C_*$  and the submergence. Villemonte



**Figure 2.6:** Discharge reduction coefficient, the fitting parameter  $p$  accounts for the influence of the geometry of the weir.

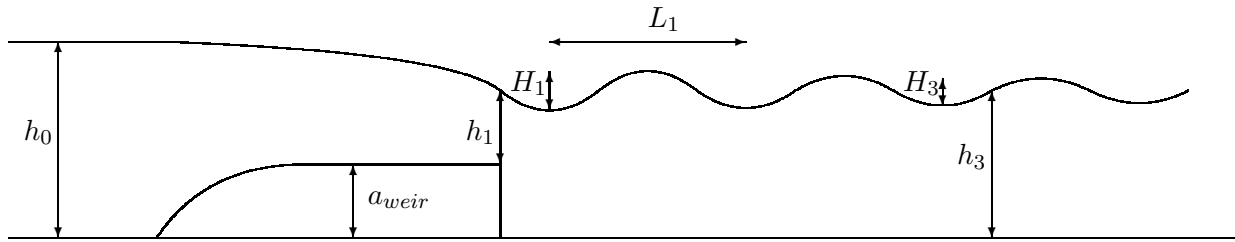
(1947) uses:

$$C_* = \sqrt{1 - \left( \frac{h_3 - a_{weir}}{h_0 - a_{weir}} \right)^p}$$

The parameter  $p$  is a fitting parameter, that accounts for the influence of the geometry of the weir. The value of  $p$  increases with weir length. An example of the discharge reduction coefficient as a function of the submergence is presented in Figure 2.6. The empirical relation is given for  $p = 15$ ,  $p = 20$  and  $p = 25$ . The line moves closer to the upper right corner with increasing  $p$ .

### 2.3.3 Characteristics of the undulations

For a better understanding of the measurements and a proper evaluation of the models, the wave characteristics are investigated. First of all, a definition sketch is given in Figure 2.7 for the undulations behind a weir in a channel with a horizontal bottom. The indices for the wavelengths and wave heights (see chapter 4) correspond to different cross-sections than the cross-sections for the water depths defined by Figure 2.4. The characteristics are governed by



**Figure 2.7:** Definition of the variables concerning the undulations behind a weir

the following parameters:

- Dimensionless wave number ( $kh_i$ ):

$$kh_i = \frac{2\pi h_i}{L_i} \quad (2.5)$$

$h_i$  = water depth at cross-section i

$L_i$  = wave length at cross-section i

- Dimensionless wave height ( $\frac{H_i}{a_{weir}}$ ). Wave height is expected to be proportional to the weir height.
- Velocity divided by wave celerity ( $\frac{U_i}{c_i}$ ). This parameter defines the relation between the mean flow velocity ( $U$ ) under the waves and the wave celerity ( $c$ ). It is expected that  $U/c = 1$  is a criterion for standing waves (the wave celerity equals the flow velocity). A complication is that the flow velocity is not uniform over the height, so the mean velocity can differ from the velocity at the surface.

The wave celerity is given by the linear dispersion relation:

$$c_i = \sqrt{\frac{g}{k_i} \tanh kh_i} \quad (2.6)$$

In this way, the parameter  $\frac{U}{c}$  can be determined:

$$\frac{U_i}{c_i} = \sqrt{F_i^2 \frac{kh_i}{\tanh kh_i}} \quad (2.7)$$

This seems to be a function of the Froude number and the dimensionless wave length.

- Froude number. The specific property of the wave often depends on the Froude number.

These parameters are used for the interpretation of the measurements in chapter 4 and for comparison with the model in chapter 6.

## 2.4 Conclusion

Different types of hydraulic jumps are described with characteristics that depend on the inflow Froude number. For Froude numbers little higher than 1, the jump is undular. The undular jump has different appearances, depending on the width of the channel and inflow Froude number. The undulations behind a weir have the same properties as the undular jump. The occurrence of undulations depend on the degree of submergence or equivalent to this, the Froude number at the end of the weir. The parameters that describe the wave characteristics are the dimensionless wave number, dimensionless wave height, velocity divided by the wave celerity and the Froude number.

# Chapter 3

## Experimental setup

### 3.1 Introduction

A short description is given of the major observations of some preliminary experiments. A weir shape is designed, that meets the requirements from the numerical model and which is applicable to investigate the most important physical processes. From this, the experimental program can be derived. In this program, the measured variables are determined, which result in the instrumentation. Also, the different flow conditions for which the measurements will be conducted are defined.

### 3.2 Preliminary experiment

Some preliminary experiments were conducted in different flumes to get insight in the occurrence of an undular hydraulic jump. Table 3.1 gives an overview of the flumes.

Flume	Length	Width	Height
Short flume	4.40	0.20	0.40
Demonstration flume	9.0	0.20	0.40
Long tilting flume	14.30	0.40	0.40

**Table 3.1:** Overview geometry flumes

#### Short flume and demonstration flume

In the middle of both the flumes, a long-crested weir is situated (height of the weir is 15cm). Various discharges can be realised. A sharp-edged weir controls the downstream water depth (tailwater depth). For a certain range of tailwater depths, undulations occur behind the weir. Lower tailwater depths lead to a classical hydraulic jump behind the weir, higher tailwater depths lead to the disappearance of the hydraulic jump. The undulations are not very stable, the amplitude increases and the wave becomes steeper until it breaks. This process repeats itself. In case of a classical hydraulic jump, a recirculation zone occurs at the water surface, while in

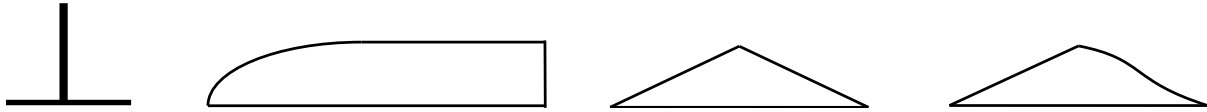
case of an undular jump, a recirculation zone occurs at the bottom. The three-dimensional nature of the flow in the hydraulic jump is remarkable.

### Long tilting flume

Different sort of shapes are placed in the long tilting flume to investigate the influence of the shape of the weir on the undulations (see Figure 3.1). The bottom is set horizontal.

The following shapes were used:

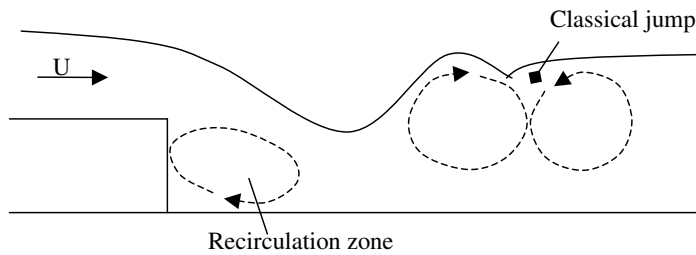
- Sharp-crested weir
- Long weir
- Triangular weir
- Triangular weir with smooth downstream part (cosine squared)



**Figure 3.1:** Different shapes of the weir used in the preliminary experiment

The discharge and the tailwater depth are controlled. The degree of submergence  $S$  (downstream water depth divided by the upstream water depth) indicates when the undulations occur.

The best undulations were observed behind the long weir. Stable undulations occur when the downstream water depth ( $S \approx 0.85$ ) is proper adjusted. For lower tailwater depths ( $S \approx 0.8$ ), a classical jump (with air entrainment) still develops after the first undulation. A special case is observed for a lower degree of submergence ( $0.80 \leq S \leq 0.85$ ), where one wave originates until a classical jump occurs. The flow pattern is visible from entrained air bubbles. This is interesting, because it shows that the recirculation zones under the first wave top and in the classical jump have an opposite sense of rotation (see Figure 3.2).



**Figure 3.2:** Preliminary experiment, the recirculation zone under the first wave top and the classical jump have an opposite sense of rotation



### Conclusion preliminary experiment

From the preliminary experiments it can be concluded that for the most kind of shapes (triangular, long and sharp-crested), undulations occur when the tailwater depth is between 0.8 and 0.95 of the upstream water depth. The largest undulations occurred behind a long-crested weir. The question is whether this is due to the horizontal streamlines above the weir or to the sharp drop in height downstream of the weir.

## 3.3 Experimental design

### 3.3.1 Requirements of the weir

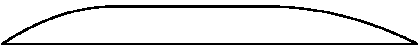
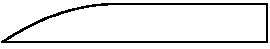

The next step is to design a weir shape, which is applicable for a good comparison with the model and provides more insight in the physical processes. For the last, different hypotheses are defined, which can be verified by a shape that represents an extreme case of the hypothesis. The weir will consist of three parts (see Figure 3.3) to obtain some flexibility in varying the shape. The weir exists of an upstream part, a middle part and a downstream part. The height of the weir is set to 15cm, a commonly used height: a greater height will cause the flume to overflow at high discharges, a lower height makes the measurements of the undulations more difficult (the height of the undulations is proportional to the weir height). The middle part has a constant height, with a length long enough to get horizontal streamlines. In the 1D numerical model, a length of 1m is sufficient to get uniform flow even at the highest discharges. A larger crest length will only increase bottom friction losses, so a length of 1m (maximal energy head loss approximate:  $c_f Fr^2 L \approx 0.5cm$ ) is good. The shape of the upstream and downstream part of the weir depends on different requirements, prescribed by the numerical model and the physical process that is to be investigated.



**Figure 3.3:** The weir consists of three parts

### Limitations from the numerical model

A numerical model based on the non-hydrostatic free-surface flow (Stelling and Zijlema 2003) is used to calculate the undulations. One version of this model has difficulties with sudden changes in bottom geometry, which may cause additional waves and inaccuracies, which are not physical. So the shape of the weir must be streamlined and smooth. For some tests in the numerical model, the upstream part of the weir needs a smooth shape with a length of at least 0.75m to reduce the effect of additional waves. A cosine-squared shape is a good solution and gives no additional waves. A cosine shape gives some additional waves, but this effect is neglected, because the streamlines are horizontal above the middle part of the weir. A cosine shape with a length of 0.75m is chosen for the upstream part based upon the requirement from the non-hydrostatic model.

	Requirement from model		L/h	Configuration of the weir
1	Compare measurements to non-hydrostatic free surface flow	Type model that can't handle sudden changes in bottom topography	7	
		Type model that can handle sudden changes in bottom topography	0	
2	Compare measurements to analytical solution of Boussinesq model	Cosine shaped weir	5	




**Table 3.2:** Overview requirements from numerical model

The upstream and middle part of the weir are determined. The downstream part of the weir has some contradicting requirements. An analysis on which hypothesis has to be investigated will define the definite shape of the downstream part together with the requirements from the numerical model. The last one is summarized in Table 3.2 with the following explanation.

1. The downstream part needs an average slope of 1/7 to prevent flow separation. This requires a length of at least 1m for the downstream part of the weir. Another version of this model can handle sudden changes in bottom geometry better, so a comparison can be made with and without this downstream part of the weir.
2. An analytical solution of the Boussinesq model can be derived for a pure cosine shape (see chapter 5). The downstream part must have the same length as the upstream part resulting in an average slope of 1/5.

### Physical processes

Different hypotheses are formed, that describe the most important physical processes. A hierarchical overview of hypotheses and/or investigations is given in Tabel 3.3.

	Hypothesis / Investigation		L/h	Configuration of the weir
1	Influence separation zone on the undulations	No separation zone	7	
		Separation zone	0	
2	Abrupt change in bottom profile causes undulations	No abrupt change in bottom profile	7	

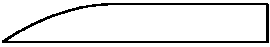
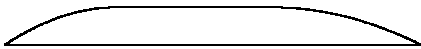
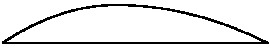
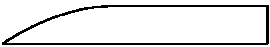
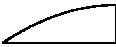
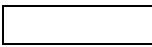
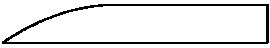
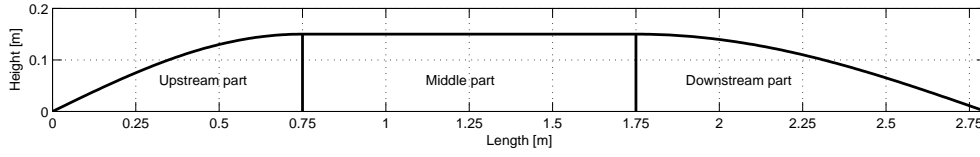
		Abrupt change in bottom profile	0	
3a	Undulations depend on the curvature of the streamlines above the weir	Horizontal streamlines	7	
		Strongly curved streamlines	7	
3b	Undulations depend on the curvature of the streamlines above the weir	Horizontal streamlines	0	
		Strongly curved streamlines	0	
4	Influence upstream shape of weir on undulations	Large influence Vertical upstream part	0	
		Little influence	0	

Table 3.3: Overview hypothesis

### Explanation

1. The length of a separation zone is estimated at 7 times the weir height. So, for a downstream cosine shape with an average slope of  $1/7$ , a separation zone will probably not occur. By comparing the case without a separation zone to the case with a separation zone, the influence of the separation zone on the undulations can be determined.
2. In the boussinesq model, which is applied to internal waves, the waves depend on the shape of the streamlines. When there is an abrupt change, the streamlines will have a sort of cosine shape (similar to the case without an abrupt change). According to this, the abrupt change will have little effect on the waves.
3. In the preliminary experiment, the amplitude of the undulations for the triangular weir was much less than for the long weir. A reason might be the curvature of the streamlines: for horizontal streamlines above the weir, the undulations are larger than for strongly curved streamlines. By removing the middle part, the streamlines above the weir are not horizontal. This can be investigated with the presence (4a) or the absence (4b) of the upstream downstream part.
4. The shape of the upstream part of the weir influences the streamlines at the upstream part. It is interesting whether this effect has an influence on the undulations.

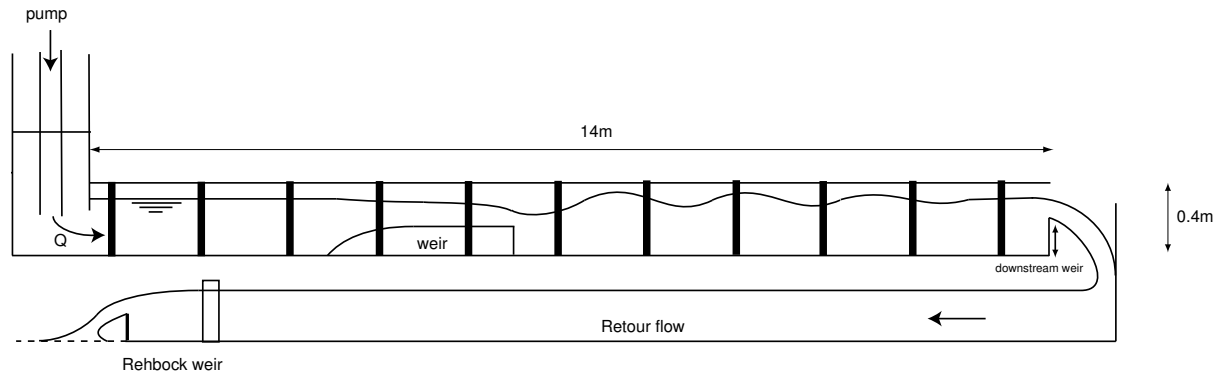
Taking account of the hierarchy of the hypothesis and the requirements from the models (Table 3.2), the shape of the downstream part of the weir is set to a cosine shape with a length of 1.05m. This results in the definite shape of the weir (see Figure 3.4).



**Figure 3.4:** Shape of the weir

### 3.3.2 Experimental program

The experiments are conducted in the long tilting flume (see Figure 3.5). All the hypotheses (given in Table 3.3) can be tested by using five different configurations of the weir. This leads to a program of experiments (see Table 3.4). The five configurations are called series, where the series number refers corresponds to the weir shape given in Table 3.4.




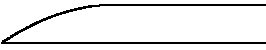

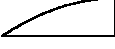

**Figure 3.5:** Experimental flume, the incoming discharge from the left can be controlled as well as the downstream water depth.

For the first and second experiment extensive measurements are needed in order to achieve a good comparison with the numerical model. For the last three experiments less variables (water depths and discharges) are needed to check the hypothesis.

### 3.3.3 Measurements

Important parameters in this experiment are:

- Upstream water depth to determine the upstream flow conditions.
- Downstream water depth to determine the degree of submergence and the boundary condition in the model.

Series	Shape weir
1	
2	
3	
4	
5	

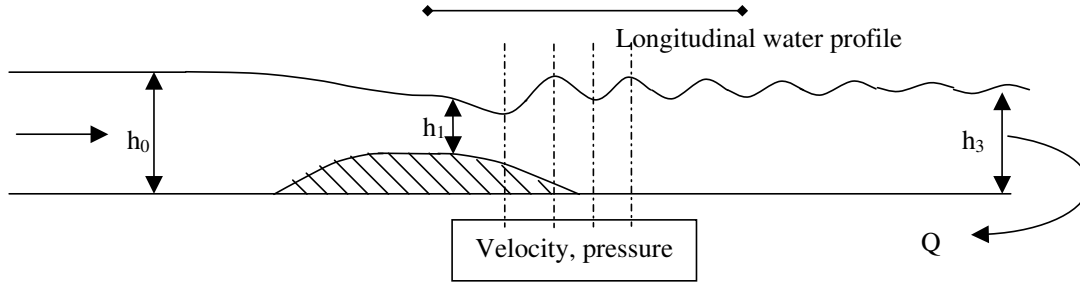
**Table 3.4:** Each series corresponds to a different shape of the weir.

- Water profile above the weir to check if the flow is uniform and to determine the Froude number above the weir.
- Wave heights, for comparison of the numerical model with the measurements and comparison of the different weir shapes.
- Wave lengths, for comparison of the numerical model with the measurements and comparison of the different weir shapes.
- Damping of the wave height, for comparison of the numerical model with the measurements.
- Length of the separation zone (dye injection for an estimation) to compare the influence of the different shapes on the separation zone and to investigate the influence of the separation zone on the undulations.
- Horizontal mean velocity profile (under wave trough and wave crest), for comparison with the numerical model, to investigate the existence of a separation zone and to investigate the influence of the velocity profile (velocity gradient, shear stresses) on the undulations.
- Vertical mean velocity profile (under wave trough and wave crest) for comparison with the numerical model.
- Pressure at the bottom (under first wave trough and first wave crest), in order to determine the deviation from the hydrostatic pressure distribution under the first wave trough and wave crest.
- Discharge to determine the Froude number and velocities. The discharge is also an upstream boundary condition.

This leads to the following requirements for the measurements (see Figure 3.6):

- Longitudinal profile of the water depths, in the middle of the flume (width) , (time averaged), starting at the horizontal part of the weir to approximately four waves.

- Velocity profile (horizontal and vertical) in the middle of the flume (width) at the following positions:
  - Under the first and second wave through
  - Under the first and second wave crest
- Discharge
- Pressure (time averaged) at positions:
  - Under the first and second wave through
  - Under the first and second wave crest

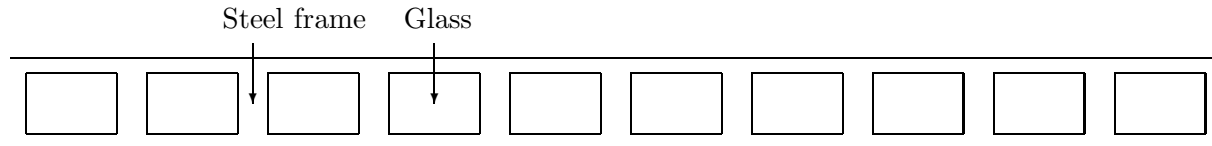


**Figure 3.6:** Requirements measured variables

### 3.3.4 Instrumentation

#### *Water depth*

Taking photos through the glass will record the longitudinal profile of the water depth. A transparent squared paper is attached to the glass window to check the deformation of the image. At some points (with a distance of 1.10m) there are steel tubes (width of 10cm), which obstruct the view of the water surface (see Figure 3.7). In order to reduce these effects, the position of the weir in the flume has to be chosen carefully. In the preliminary experiment, the undulations tend to move a little upstream and downstream. This effect also has to be determined in an observational experiment. A few water depths will be measured with a pointer gauge to verify the measurements with the camera ( $h_0$ ,  $h_1$ ,  $h_3$  in Figure 3.6). In the photos, the best visible water depth is at the glass wall nearest to the camera, so the water depth is measured at one of the sides. (see Figure 3.8).

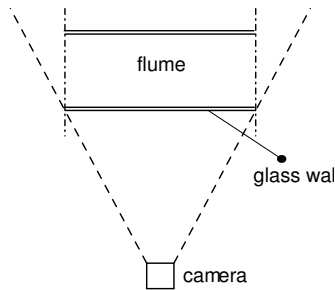


**Figure 3.7:** Sideview flume, steel tubes obstruct the view of the water depth at some points.

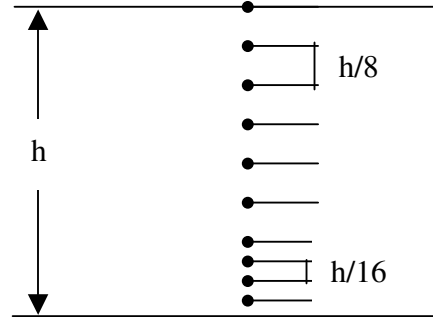
### Velocity

Velocities will be measured with a LDA (Laser Doppler Anemometry). Most fluids contain little particles of around 1 micrometer. A laser beam is directed in the fluid, where the particles reflect the laser beam in every direction. The biggest part is reflected in forward direction, which is intercepted by a receiver. When the particles move, the frequency of the reflected laser beam changes from the frequency of the incoming laser beam, which is called the Doppler shift. This frequency shift is proportional to the velocity of the fluid. A reference laser beam is also directed into the fluid to determine the frequency shift. The laser beams intersect in the fluid, which determines the measuring volume. The size of the measuring volume is around  $H*B*L = 0.5*0.5*15mm$ , over which the measured velocity is averaged. By using two incoming laser beams and one reference beam, the velocity can be measured in two directions. The horizontal and vertical velocity will be measured for different points over the water depth (50 samples per second). The mean velocity is calculated by time averaging over a certain period. This period should be long compared to the characteristic time scale of the turbulent motions, but short with respect to the time scale, in which the mean motion varies. In the flume, the flow situation is steady, but a complication is the movement of the undulations (in upstream and downstream direction), which might have the same time scale as the turbulent motions. The duration of the movement of the undulations is around 10 seconds, which is in good agreement with the natural frequency of the flume ( $L$ =length from weir to end flume  $\approx 8m$ ,  $h = 0.3m$ ):

$$f = \frac{\sqrt{gh}}{2L} \approx 0.1Hz$$



**Figure 3.8:** Camera view from above



**Figure 3.9:** Velocity points over the depth

For a good statistical average, a measurement for a single point has to take at least 10 minutes (in order to include the effect of the movement of the undulations). Also, the cross-sections, where the velocity is measured, have to be visible (not at the steel tubes). Around 10 points over the height are measured to get a sufficient reliable velocity profile. The points near the bottom are interesting for the determination of a possible recirculation zone, so the first velocity points taken from the bottom are at a distance of  $1/16$  of the water depth from each other (see Figure 3.9). Closer to the water surface, the distance between the velocity points is increased to  $1/8$  of the water depth.

### Pressure

The time-averaged pressure at the bottom is measured at first wave crest and first wave through to determine the deviation from the hydrostatic pressure distribution. Chanson and Montes (1995b) measured a deviation of 25% from the hydrostatic pressure distribution under the first wave through and of 10% under the first wave crest. A pressure device mounted in the bottom will be problematic, because it has a fixed position, while the position of the first wave crest and wave through changes with discharge (wave length is larger at higher discharges). Chanson and Montes (1995a) use a pitot tube to measure the pressure. This causes an obstacle in the flow. Also, pressure fluctuations can not be measured. But it gives an idea of the deviation from the hydrostatic pressure distribution. The pitot tube is more flexible than a fixed pressure device, which is necessary due to the different weir shapes and different positions of the wave top and wave trough. So, the pitot tube is used to determine the pressure at the bottom.

#### *Other instrumentation*

- Rail-mounted pointer gauge positioned over the channel's centerline.
- Pointer gauge in the Rehbock weir
- Meter line

Requirements for the position of the weir in the flume:

- Downstream length of about 10 wave lengths to measure damping of the undulations (approximate 6 m), in addition to this 1m to guarantee no effects of the downstream weir at the end of the flume.
- Upstream velocity distribution. For the upstream part there is 5,2m left ( $14m - 7m - 1,8m$ ), too little for a fully developed boundary layer.
- Visibility of the undulations for measuring with the camera and the LDA (no obstruction of the steel tubes).

### 3.3.5 Flow conditions

In all the experiments, the variables will be measured for different discharges (see Table 3.5). As a reference, measurements are conducted when no undulations occur: in case of the transition from classical to undular and from undular to no jump. These measurements will also be compared to the model. Starting from a classical jump, the tailwater depth will be raised until undulations occur. In the transition zone from a classical jump to an undular jump, the largest undulations occur, but these undulations are not very stable (breaking waves etc), so the tailwater depth will be raised until stable undulations occur. For this situation, the water depth, velocities and pressure are measured.

### 3.3.6 Accuracy of the measurements

The reliability of the comparison of the measurements with the models depends on the accuracy of the measurements. The absolute and relative errors of the measurements need to be determined. An estimation of the absolute error in the measured variables is given in Table 3.6. The absolute error depends on the accuracy of the measuring device, but also on the flow



Experimental runs	Q [l/s]	$h_3/h_0$	
1	30	$0 \rightarrow 1$	Reference
	30	$0.80 \rightarrow 0.95$	Undulations
2	45	$0 \rightarrow 1$	Reference
	45	$0.80 \rightarrow 0.95$	Undulations
3	60	$0 \rightarrow 1$	Reference
	60	$0.80 \rightarrow 0.95$	Undulations

**Table 3.5:** Flow conditions experiment

Variable		Absolute error	Average low value	Relative error
Photos				
Wave height	$H_i$	3mm	5cm	6%
Wave length	$L_i$	10mm	20cm	5%
Water depth 3	$h_3$	3mm	25cm	1.2%
Pointer gauge				
Water depth	$h_0$	0.5mm	30cm	0.17%
Water depth	$h_1$	0.5mm	10cm	0.5%
Water depth	$h_3$	3mm	25cm	1.2%
Rehbock weir	$h_R$	1mm	10cm	1%
Meter line				
Width flume	$B$	0.5mm	40cm	0.125%
Width Rehbock weir	$B_{weir}$	0.5mm	43.2cm	0.116%
LDA				
Signal 1	$X_1$	0.01 m/s	1 m/s	1%
Signal 2	$X_2$	0.01 m/s	1 m/s	1%

**Table 3.6:** Absolute error in measured parameters

conditions. For example, the value of the water depth at cross-section 3 varies a little due to the undulations, so the error is larger. The wave heights and wave lengths taken from the photos are not very accurate, because of the movements of the undulations, the transformation of the photos and the limited number of photos (3 or 4). The maximal relative error occurs at the lowest values of the measured parameters. For the LDA, the relative error of the measuring device is approximately 1%, which corresponds to an absolute error of  $1\text{cm/s}$  for a flow velocity of  $1\text{m/s}$ . A complication is the movement of the undulations in longitudinal direction and the turbulent motions (see section 4.5).

### 3.4 Conclusion

A weir is designed that consist of three parts, each of which can be removed. In that way, different shapes of the weir are investigated. An experimental program is defined based upon the requirements from the numerical models and the physical processes, that needs to be examined. This program results in measurements for five different shapes of the weir. The flow conditions for the transition zones (from undulations to no undulations) are measured and the characteristics of the undulations. Local velocities are measured with a laser doppler anemometry (LDA) and the water depths are measured with a photo camera.

# Chapter 4

## Interpretation experimental data

### 4.1 Introduction

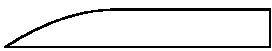
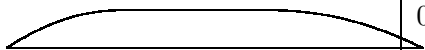

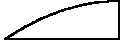
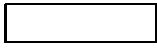
In this chapter, the measured data are presented and interpreted. In Appendix A, the method of dataprocessing is described. First of all, important observations from the measurements are presented. The occurrence of the undulations and the wave characteristics for the different shapes of the weir are considered. Furthermore, emphasis is put on the the velocity profile. Finally, the hypotheses, defined in the experimental design, are verified.

### 4.2 Observations

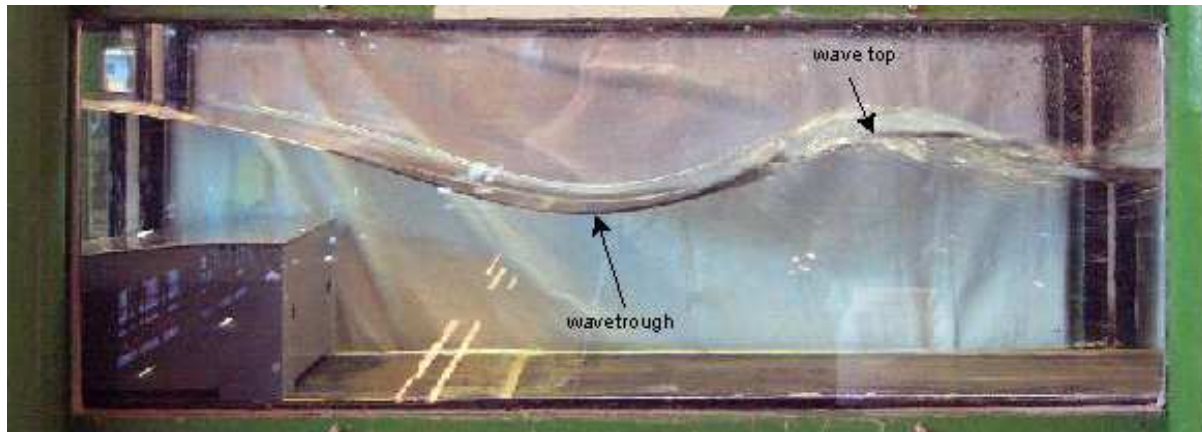
The experiment is divided into five series, which all correspond to a different shape of the weir. Table 4.1 gives an overview for these series with the corresponding shapes of the weir and the upper and lower limit of the degree of submergence, under which undulations occur. Three different discharges ( $Q=30$  l/s,  $Q=45$  l/s and  $Q=60$ l/s) are investigated for every series, except for series 5, because the weir would be carried away at the highest discharge.

Main observations in a qualitative manner, which form a start for a more quantative analysis of the experiment, are:

- The undulations occur for a certain range of the degree of submergence  $S$  (waterdepth downstream of the weir  $h_3$  divided by the water depth upstream of the weir  $h_0$ ). For lower values of  $S$ , a classical hydraulic jump occurs behind the weir. For higher values of  $S$ , no hydraulic jump or undulations occur. This corresponds to the flow regimes described in chapter 2.
- For series 1 and 4 (abrupt change in bottom profile), large and smooth undulations develop directly behind the weir (see Figure 4.1 and 4.4). There is no variation over the width. At the end of the weir, a steep downward facing slope of the water level is visible. This results in the first wavetrough, after which the water level increases again, resulting in the first wavetop. A few wave lengths downstream of the weir, the undulations are less pronounced and look disorderly. Also, the undulations tend to move a little up- and downstream with the same frequency as the resonance frequency of the flume ( $f \approx 0.1Hz$ ). Sometimes, the undulations become steeper and steeper until they break. This happens mainly for lower values of  $S$ . The undulations for series 1 and series 4 show a lot of resemblance.

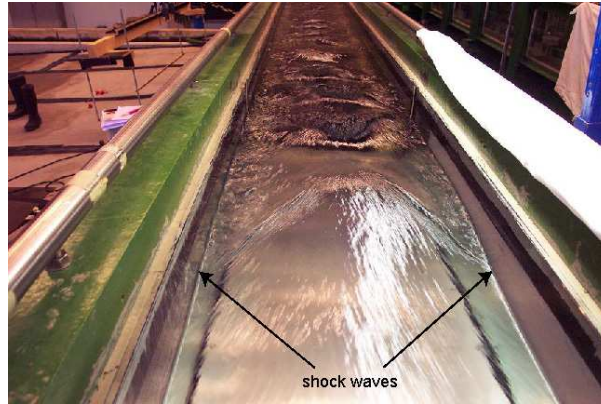
Series	Shape weir	Undulations	Wavel.(cm)	Description
1		$0.75 \leq S \leq 0.90$	54	Large waves
2		$0.90 \leq S \leq 0.97$	26	Small waves, shock waves from the wall develop
3		$0.94 \leq S \leq 0.98$	24	Small waves, shock waves from the wall develop
4		$0.78 \leq S \leq 0.95$	50	Large waves
5		$0.71 \leq S \leq 0.88$	54	Large waves behind weir
		$0.90 \leq S \leq 0.97$	30-60	Waves above weir

**Table 4.1:** Overview experiments, wavelength at  $Q=45$  l/s. The degree of submergence  $S$  prescribes when undulations occur.

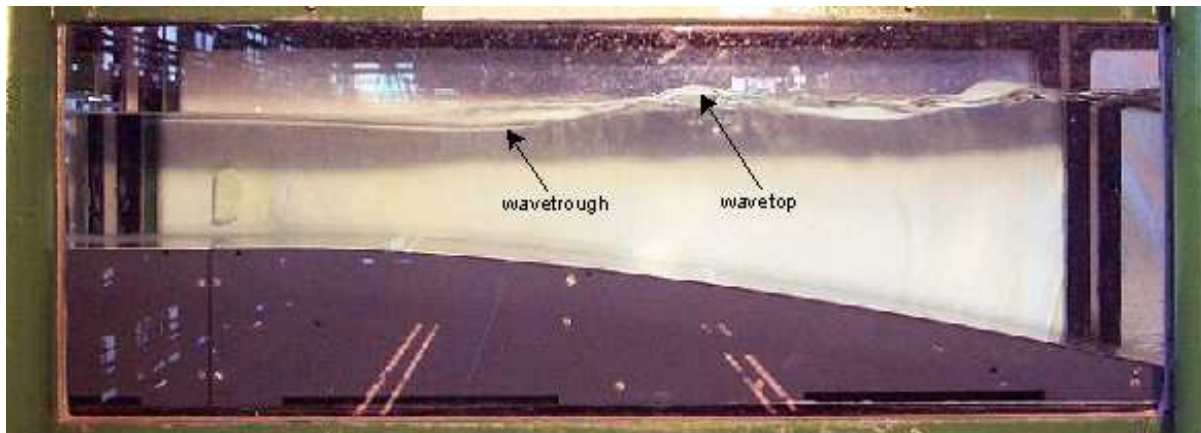


**Figure 4.1:** Photo water profile for series 4 ( $Q=45$  l/s), large undulations develop downstream of the weir.

- For series 2 and 3, small undulations develop above the downstream part of the weir (see Figure 4.3 and 4.4). There seems to be a variation over the width, shock waves develop from the sides and intersect in the middle of the flume at the wave top (Figure 4.2). The wave heights are much smaller than in case of an abrupt change in bottom profile. The wave lengths are also two times smaller. The absence of the middle part of the weir (series 3) does not seem to make a difference for the characteristics of the undulations.



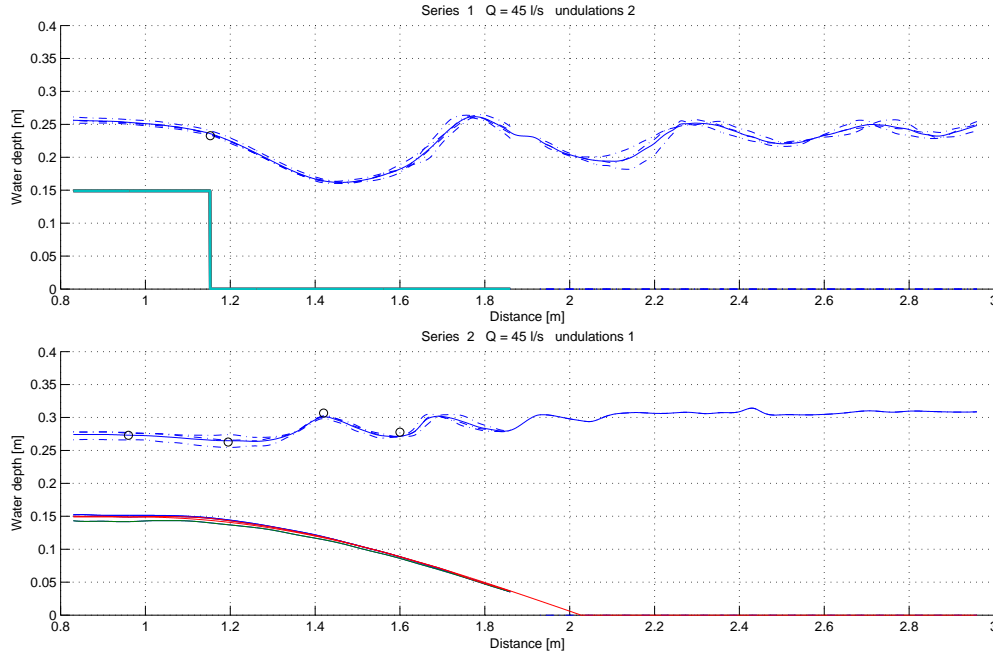
**Figure 4.2:** Photo from above for series 2 ( $Q=60$  l/s), shock waves develop from the sides of the flume.



**Figure 4.3:** Photo water profile for series 2 ( $Q=45$  l/s), small undulations develop at the downstream side of the weir.

- For series 5 (block shaped weir), a distinction is made between two different types of undulations. In case of the first type, undulations develop behind the weir. This happens for the lower degrees of submergence. They resemble the undulations of series 1 and 4. Increasing the downstream water depth (degree of submergence  $S \approx 0.89$ ) leads to the disappearance of the undulations. Further increasing the downstream water depth leads

to the second type of undulations. These undulations develop above the weir. The wave length depends on the degree of submergence: a higher submergence leads to a higher water depth above the weir resulting in lower velocities and accordingly a shorter wave length.



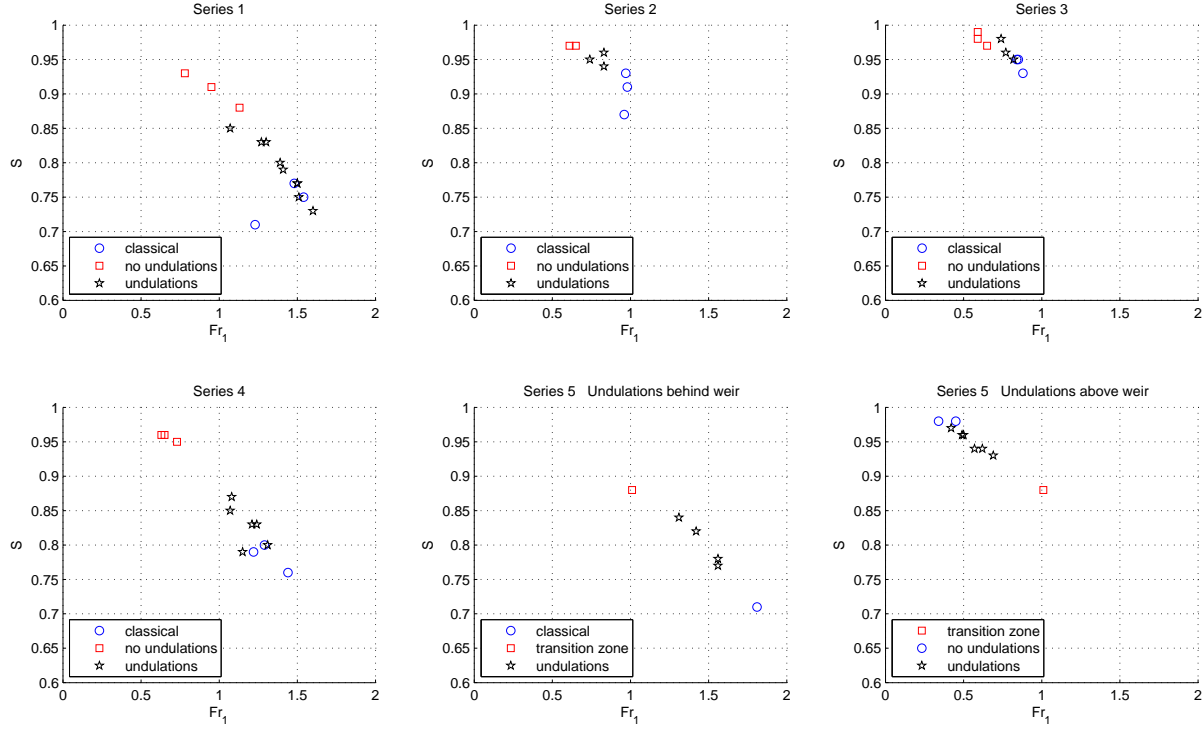
**Figure 4.4:** Water profile derived from the photos, the circles correspond to the pointer gauge measurements, the solid line is the average of a few water profiles dotted lines).

### 4.3 Occurrence of undulations

All the flow situations are summarized in Figure 4.5. The degree of submergence ( $\frac{h_3}{h_0}$ ) is plotted against the Froude number in case of a classical jump, in case of undulations and in case of no undulations. In the last case, the flow is submerged and no undulations occur. The transition zone in series 5 refers to a transition (where no undulations occur) from undulations behind the weir to undulations above the weir. The Froude number at section 1 is positioned at the end of the horizontal part of the weir (series 1, 2 and 5) or, in absence of a horizontal part, at the end of the upstream part (series 3 and 4). As mentioned in chapter 2, there is an obvious relation between these parameters determined by the principle of energy conservation and the momentum balance. The upstream and downstream water depths are related to the bottom instead of the weir height, because the submergence is in that case more or less independent of the discharge.

For series 1, 4 and 5 (abrupt change in bottom profile), undulations occur for lower degrees of submergence or higher Froude numbers (between 1 and 1.5). This is comparable to the undular jump on a horizontal bottom, where in general undulations occur for Froude numbers between 1

and 1.7. The upper limit is somewhat higher, but this can be explained by considering that the Froude number still increases downstream of the weir due to the strongly curved water surface. For series 2 and 3 (smooth downstream part of the weir), the undulations occur for higher degrees of submergence and lower Froude numbers. The Froude number above the end of the horizontal part of the weir is even lower than 1. This indicates the big difference between the weir with and without the smooth downstream part.



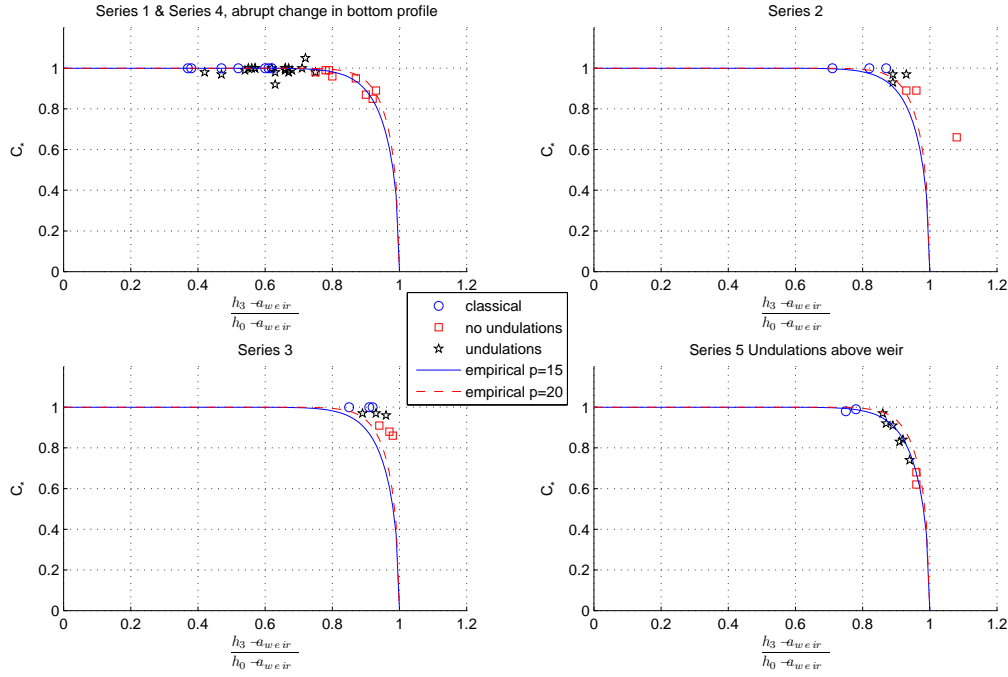
**Figure 4.5:** Occurrence of undulations, for all the flow situations the degree of submergence is plotted against the Froude number determined above the end of the horizontal part of the weir, classical refers to a classical jump without undulations, no undulations refers to the submerged case.

### 4.3.1 Discharge coefficient

The discharge reduction coefficient is plotted against the submergence (the upstream and downstream water depth are calculated from the top of the weir), see Figure 4.6. In case of an abrupt change in bottom profile, the measurements coincide with the empirical relation of Villemonte (When the fitting parameter  $p$  is set to 15):

$$C_* = \sqrt{1 - \left( \frac{h_3 - a_{weir}}{h_0 - a_{weir}} \right)^p}$$

The undulations seem to have little effect on the discharge coefficient. For series 2 and 3 (smooth downstream part), the measurements deviate from the empirical relation (even for  $p = 20$ ). This is expected for series 2, which has the longest weir resulting in higher values of  $p$ . But it is not clear for series 3, since the weir has the same length as the weir in series 1. Anyway, it can be seen that the undulations do not have a notable influence on the discharge relation.



**Figure 4.6:** Discharge reduction coefficient. Undulations seem to have little effect on the discharge coefficient. Classical refers to a classical jump, no undulations to the submerged case.

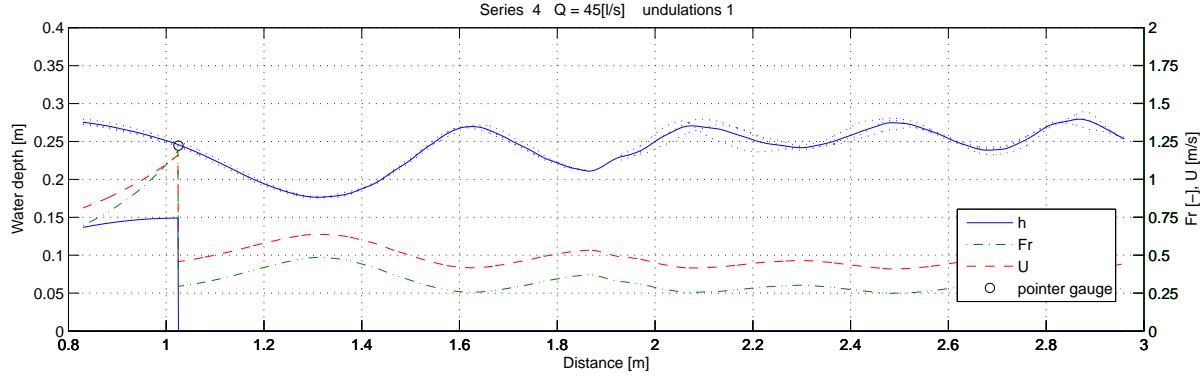
## 4.4 Wave characteristics

After identifying under which conditions undulations occur, the next step in the analysis of the experiment is to determine the characteristics of the undulations. Wave lengths, wave celerities and wave heights are considered.



#### 4.4.1 Wave lengths

The wave lengths are derived from the photos of the water depth (see Appendix B). An example of the water depth profile is given in Figure 4.7. The wave characteristics are derived from these profiles.



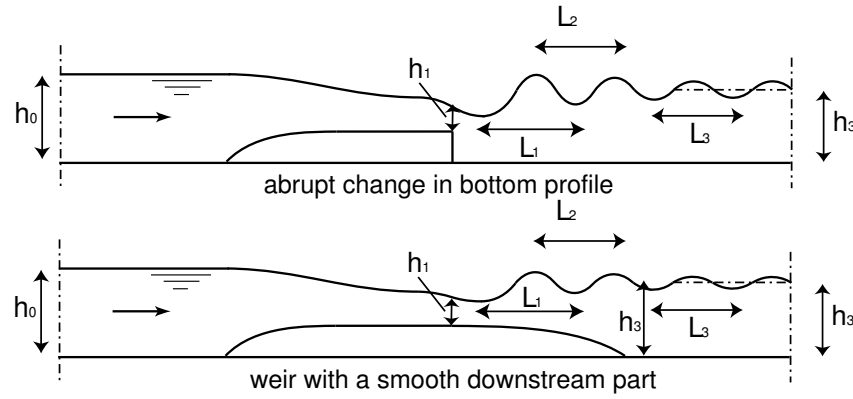
**Figure 4.7:** Water depth profile, wave lengths and wave heights are derived from this profile

For each case, three different wave lengths are determined (see Figure 4.8):

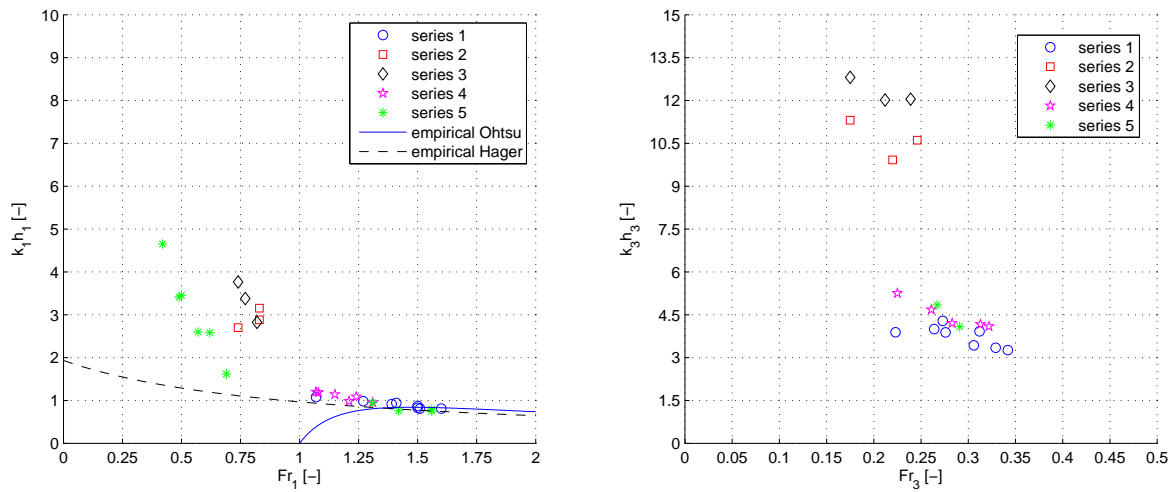
- Wave length given by the distance between the first and second wavetrough ( $L_1$ ).
- Wave length given by the distance between the first and second wavetop ( $L_2$ ).
- Wave length 1m behind the horizontal part of the weir ( $L_3$ ). This means at the end of the weir for the weir with the smooth downstream part (series 2 and 3). At this position, the weir with a smooth downstream part has ended and the recirculation zone for the weir with the abrupt change in bottom profile has almost ended. So, the whole water depth can be used.

Generally, the first wave length is longer than the second wave length. This is caused by a decreasing velocity in upstream direction, which leads to shorter waves according to the linear dispersion relation. The dimensionless wavenumber ( $kh$ ), given by equation 2.5, is plotted against the Froude number in Figure 4.9 for the waves directly behind the weir (cross-section 1) and 1m downstream of the weir (cross-section 3). The wave numbers directly behind the weir are smaller (larger wavelengths). The Froude numbers at section 1 are based upon the water depth above the end of the weir ( $h_1$ ).

- For series 1, 4 and 5 (undulations behind weir), the series with the abrupt change in bottom profile, the wave numbers decrease a little (wave lengths increase) with increasing Froude number. The wave numbers directly behind the weir are comparable to empirical relations between wave numbers and Froude numbers found in the literature for the undular jump on a horizontal bottom (Ohtsu et al. (2003), Reinauer and Hager (1995)). This confirms the analogy between the undulations behind an abrupt change in bottom profile and the undular jump on a horizontal bottom.



**Figure 4.8:** Definition of wavelengths for the weirs with and without a downstream part.



**Figure 4.9:** Dimensionless wave number against Froude number, both directly behind the weir (figure on the left) and 1m downstream of the horizontal part of the weir (figure on the right). The empirical relations correspond to the undular jump on a horizontal bottom

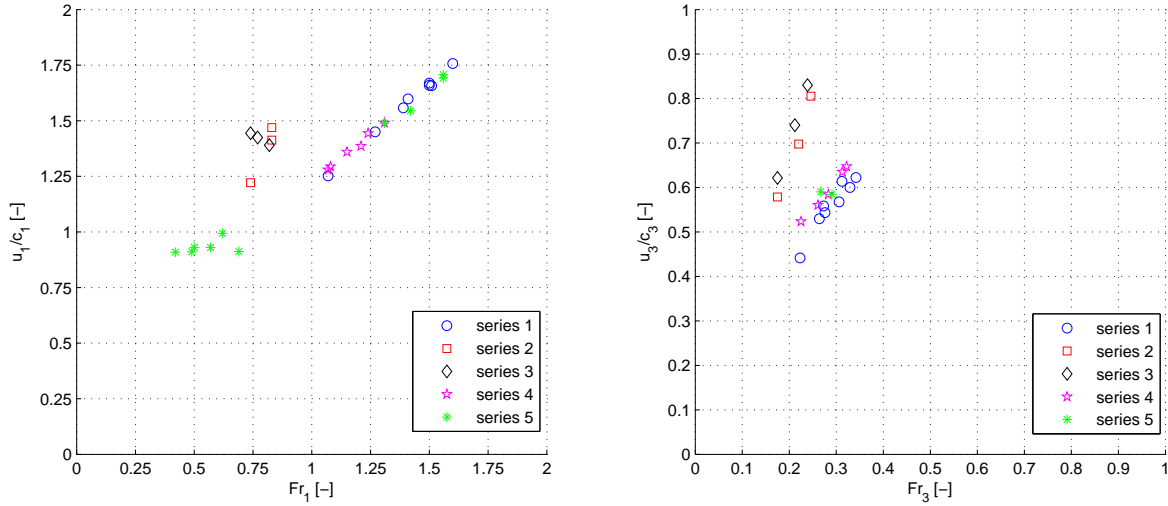
- For series 2 and 3, the dimensionless wavenumbers are much higher and show a weak relation with the Froude number at cross-section 1 as well as cross-section 3.
- For series 5 (undulations above weir), the values of the dimensionless wave numbers depend on the Froude number above the weir: A larger Froude number implies larger waves.

In chapter 5 and chapter 6, where the linear Boussinesq model will be discussed, an expression for the wave length depending on the Froude number (at cross-section 3) will be derived, that coincides with the measured wave lengths.

#### 4.4.2 Wave celerities

The wave celerity is calculated according to linear wave theory (equation 2.6). The wave moves in upstream direction and is stationary when the flow velocity is equal to the wave celerity. So, the wave celerity divided by the flow velocity ( $\frac{u}{c}$ ) should be around 1. When the velocity above the weir is higher than the wave celerity, the waves will be blocked behind the weir. In Figure 4.10, the Froude numbers are plotted against the values of  $\frac{u}{c}$ .

For series 5, in case of undulations above the weir (Figure 4.10 on the left), the values of ( $\frac{u_1}{c_1}$ )

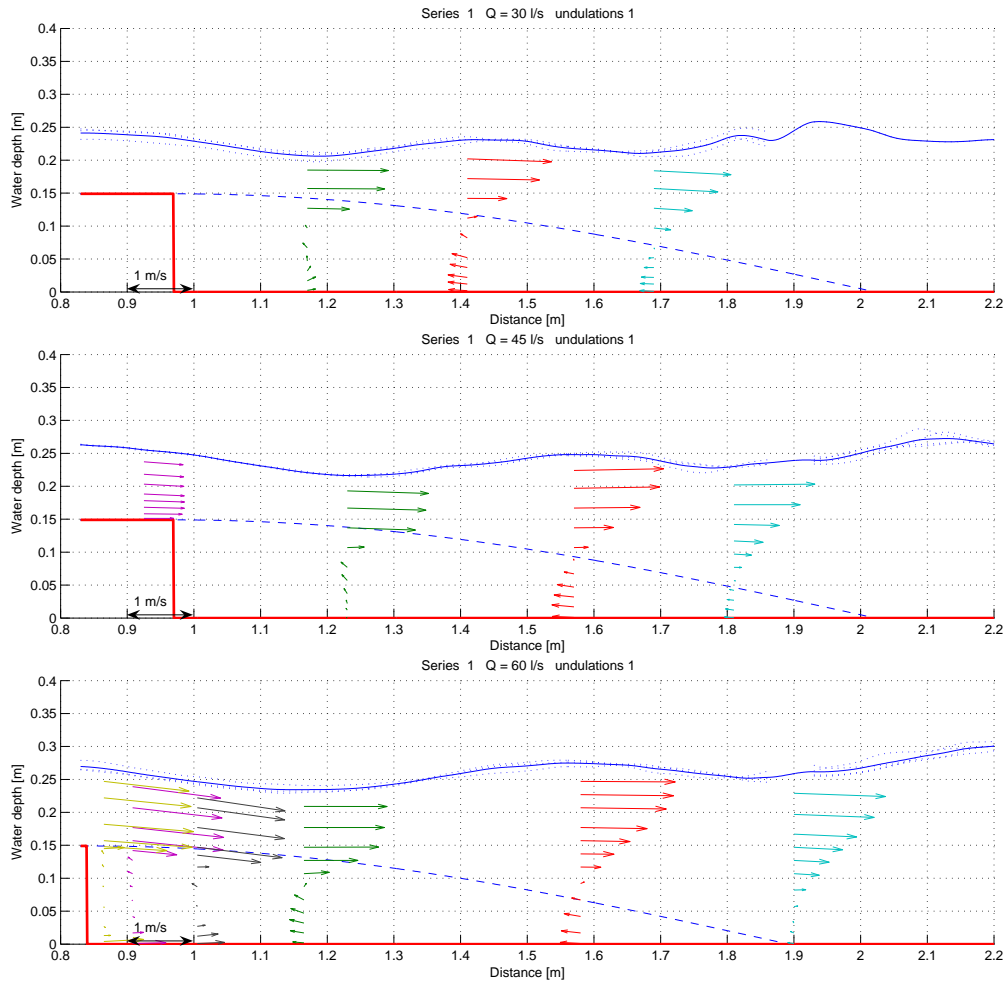


**Figure 4.10:** Froude number against wave celerity,  $c_1$  is the wave celerity calculated from the wave length of the first wave,  $u_1$  is the mean velocity above the end of the weir,  $c_3$  is the wave celerity 1m downstream from the horizontal part of the weir,  $u_3$  the mean velocity at this point

are around 1. The velocity above the weir is equal to the wave celerity. A higher degree of submergence leads to lower Froude numbers and lower velocities above the weir, resulting in smaller waves. In all the other cases, ( $\frac{u_1}{c_1}$ ) is higher than 1. The explanation for this is that the velocity above the end of the weir ( $u_1$ ) is higher than the velocity at the position of the first wave. But 1m downstream of the horizontal part of the weir (section 3), in Figure 4.10 on the right, the values of ( $\frac{u_3}{c_3}$ ) are much lower than 1. So, somewhere between cross-section 1 and 3, the value of ( $\frac{u}{c}$ ) is around 1. In Appendix E, the values of ( $\frac{u}{c}$ ) are plotted in longitudinal direction. The mean velocity is calculated by the discharge, width of the flume and the water

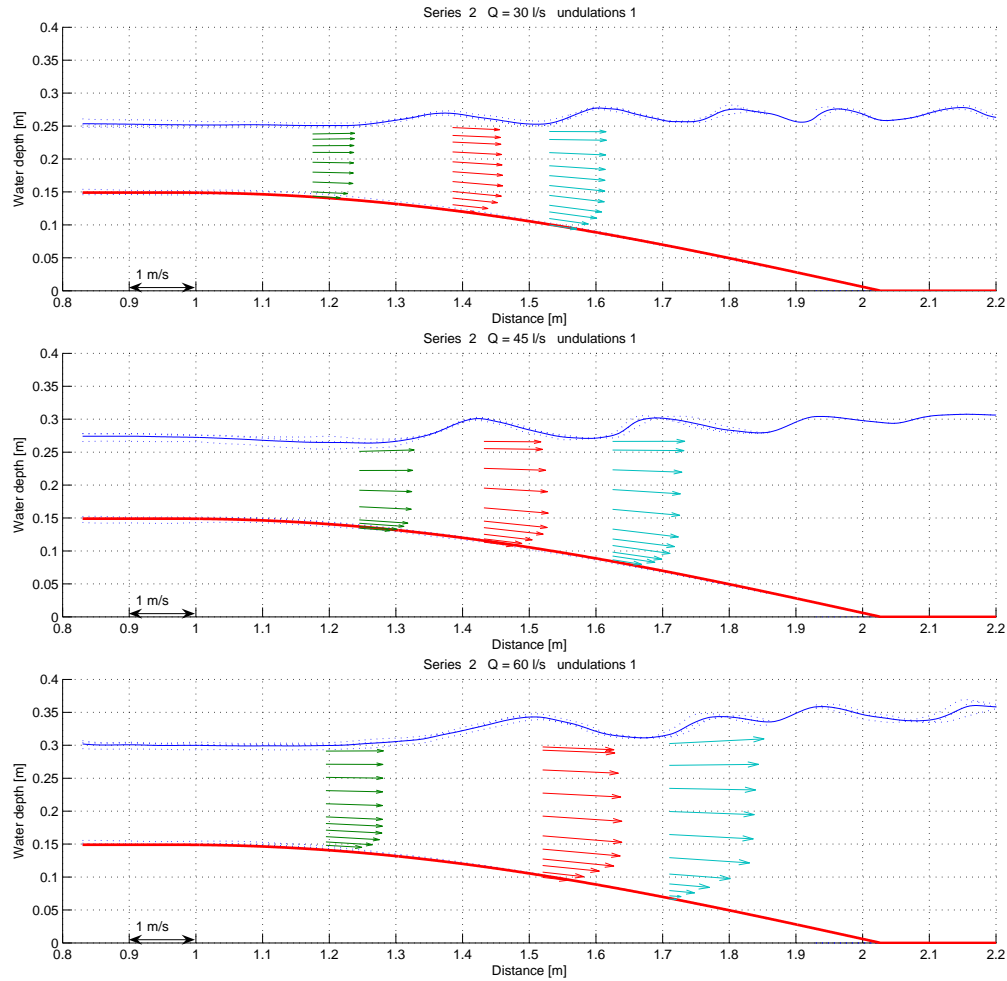
depth. For the abrupt change in bottom profile, a recirculation zone is assumed with a cosine shape with a mean slope of  $1/7$ . In this way, the water depth is defined in order to calculate the mean velocity. At the first wave trough the mean velocity is very high, the assumption for the shape of the recirculation zone is not valid here. It seems that the shape of the recirculation zone is influenced by the shape of the water surface, which will be discussed in section 4.5.1. The ratio ( $\frac{u}{c}$ ) is around 1 between the first wave trough and first wavetop. Further downstream the value of ( $\frac{u}{c}$ ) is much lower than 1. Apparently, the 1D linear theory, which uses the mean velocity, is not valid any more. A closer look to the velocity profile gives a better insight.

**Velocity profiles** The velocity profiles for series 1 (discharges  $Q=30$  l/s,  $Q=45$  l/s and  $Q=60$  l/s) measured by the LDA-device are plotted in Figure 4.11. Also, the water level derived from the photos is given. The existence of the recirculation zone is clearly visible. Two circulation zones, which are rotating in an opposite direction, develop behind the weir: A small recirculation zone directly behind the weir and a bigger recirculation zone further downstream. The direction of the velocities at the water surface seem to agree with the slope of the water level. The highest velocities are observed near the free surface. The velocity profile for the part above the recirculation zone becomes less uniform in downstream direction: the velocity gradient spreads over the height. The velocity profile 1m downstream of the weir (cross-section 3) has a sort of triangular shape.



**Figure 4.11:** Vector plot series 1, derived from LDA measurements for different velocity points over the height at different cross-sections. The non-uniform velocity profile is clearly visible.

The velocity profiles for series 2 are plotted in Figure 4.12. The smooth downstream side of the weir prevents flow separation, so no recirculation zone develops. The velocity profile is more uniform than for series 1. Also, the velocity profile under the wavetop and wavetrough look the same.



**Figure 4.12:** Vector plot series 2, from LDA measurements for different velocity points over the height at different cross-sections. The velocity profile is almost uniform.

From the velocity profiles, it is clearly visible that for series 1 the one-dimensional approach is not valid any more. The profile has a sort of triangular shape, the velocity at the water surface is much higher than the mean velocity. For series 2, the velocity profile is more uniformly distributed at the measured positions (first wavetrough and wavetop, second wavetrough). In that case,  $(\frac{u}{c})$  is closer to 1.

A better approach is to compare the wave celerity to the velocity at the free surface. For series 1 and series 2, the velocity at the free surface is derived from the velocity profile and compared to the wave celerity (see Table 4.2). The wave celerity is calculated from the wave length of the first wave and the water depth at transition first wave trough to first wavetop.

The values of  $(\frac{u}{c})$  are too high. But taking the highest velocity (at the free surface) might be a little exaggerated. The waves are influenced by a larger flow depth than just at the surface. This indicates the importance of the velocity profiles on the undulations. The velocity profile determines which flow velocity is needed for the parameter  $\frac{U}{c}$ . But the velocity profile changes in longitudinal direction as well as the wave celerity due to changes in the water depth and wave length.

Series 1	First wavetrough	First wavetop	Second wavetrough
Q=30 [l/s]	1.63	1.38	1.50
Q=45 [l/s]	1.57	1.35	1.46
Q=60 [l/s]	1.57	1.26	1.26
Series 2			
Q=30 [l/s]	1.48	1.15	1.23
Q=45 [l/s]	1.62	1.15	1.38
Q=60 [l/s]	1.62	1.18	1.40

**Table 4.2:** Values of  $(\frac{u}{c})$  for the horizontal velocity at the free surface

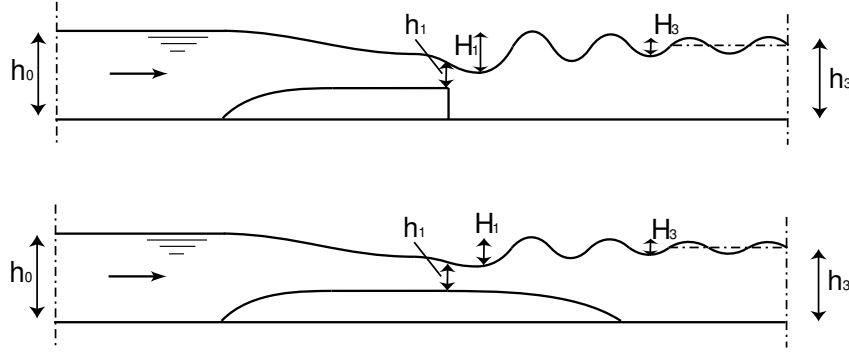
#### 4.4.3 Wave heights

The wave heights are determined from the photos of the water depth. Two wave heights are considered (see Figure 4.13):

- The height between the first wave trough and first wave top ( $H_1$ ). This is the biggest wave height due to the sharp drop in water level at the first wave trough.
- The wave height 1m downstream of the horizontal part of the weir ( $H_3$ ). This wave height is smaller due to damping of the waves.

The wave heights are made dimensionless by dividing it with the height of the weir, because the wave height is assumed to be proportional to the weir height. In Figure 4.14, the dimensionless wave height  $(\frac{H}{a_{weir}})$  is plotted against the Froude number. There is a distinct relation between the Froude number and dimensionless wave height at cross-section 3. This relation has the same shape as the analytical solution of the Boussinesq equation in case of a cosine shaped weir (see Chapter 5), which can be written as:

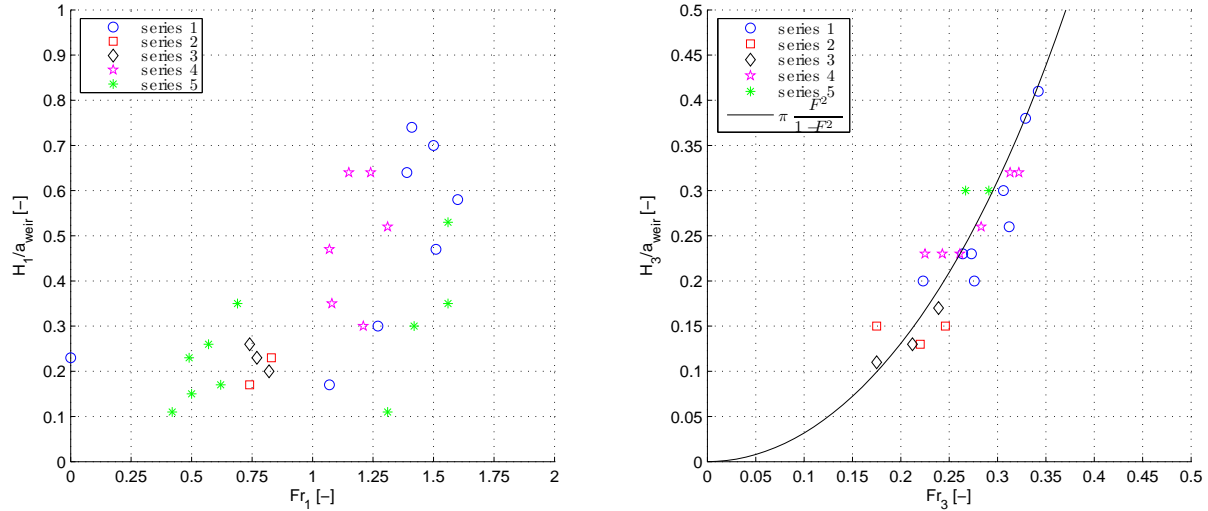
$$\frac{H_3}{a_{weir}} = \pi \frac{F^2}{1 - F^2}$$



**Figure 4.13:** Definition of the wave heights for weirs with and without a downstream part

A little variation can be expected due to the determination of  $H_3$ . The position of the wave top and wave trough 1m downstream of the horizontal part of the weir might vary for the different experimental runs. This causes some variation in the wave height due to the damping of the waves.

For series 1 and 4, the wave height is up to 4 times larger than for series 2 and 3. For series 5, undulations above the weir, the wave height also increases with the Froude number above the weir.



**Figure 4.14:** Dimensionless wave heights plotted against the Froude number for the first wave (section 1) and 1m downstream of the weir (section 3). The wave heights at section 3 have the same shape as an analytical solution of the Boussinesq equation (solid line).



#### 4.4.4 Error analysis

It is important to determine the accuracy of the used parameters for the reliability of the analysis of the experiment. The relative errors of these parameters can be derived from the errors in the measured variables (see chapter 3). It is assumed that the variables are normal distributed with a standard deviation equal to the absolute error as defined in Table 3.6. The absolute error of a function  $f(x, y)$  with measured parameters  $x$  and  $y$  is calculated as follows:

$$\sigma_f^2 = \sigma_x^2 \left( \frac{\partial f}{\partial x} \right)^2 + \sigma_y^2 \left( \frac{\partial f}{\partial y} \right)^2$$

For example the error in the degree of submergence is ( $S = \frac{h_3}{h_0}$ ):

$$\sigma_S^2 = \frac{1}{h_0^2} \left( \sigma_{h_3}^2 + \left( \frac{h_3}{h_0} \right)^2 \sigma_{h_0}^2 \right)$$

From this, the relative error can be calculated ( $\mu_{h_0} = h_0$ ,  $\mu_{h_3} = h_3$ ,  $\mu_S = S$ ):

$$r_S^2 = \left( \frac{\sigma_S}{\mu_S} \right)^2 = \left( \frac{\sigma_{h_0}}{\mu_{h_0}} \right)^2 + \left( \frac{\sigma_{h_3}}{\mu_{h_3}} \right)^2$$

This analysis is conducted for all the calculated parameters, resulting in the relative errors ( $r = \frac{\sigma_x}{\mu_x}$ ) given in Table 4.3. The largest errors occur in the wave numbers and wave heights due to the absolute errors in the wave length and wave height derived from the photos.

Parameter		Relative error	
Discharge	$Q$	$r_Q^2 = r_B^2 + \frac{9}{4}(2 - \frac{0.602}{C_E})^2 r_h^2$	1.6%
Velocity	$U$	$r_U^2 = r_Q^2 + r_h^2 + r_B^2$	2.0%
Froude number	$F$	$r_F^2 = r_Q^2 + \frac{9}{4} r_h^2 + r_B^2$	2.4%
Degree of submergence	$S$	$r_s^2 = r_{h_0}^2 + r_{h_3}^2$	1.2%
Wave number	$kh$	$r_{kh}^2 = r_h^2 + r_L^2$	5.1%
Wave celerity	$c$	$r_c^2 = \frac{1}{4}(1 - \beta)^2 r_L^2 + \frac{1}{4} \beta^2 r_h^2$	2.5%
		$\beta = \frac{kh}{\tanh kh \cosh^2 kh}$	
	$\frac{U}{c}$	$r^2 = r_U^2 + r_c^2$	3.2%
Wave height	$\frac{H}{a_{weir}}$	$r^2 = r_H^2 + r_{a_{weir}}^2$	5.1%

**Table 4.3:** Relative errors

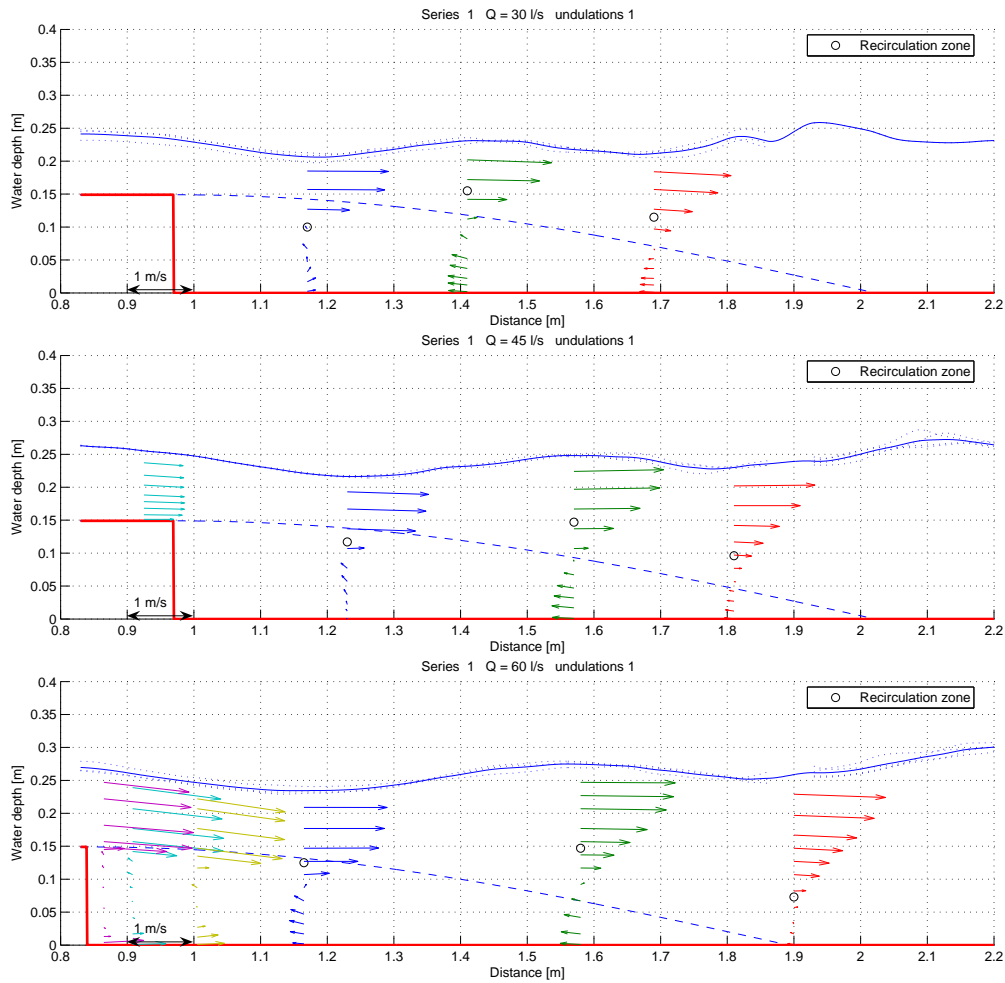
### 4.5 Interpretation velocity profile

From the velocity profiles given in Figure 4.11 and 4.12, other notable things needs to be mentioned concerning the recirculation zones and variation over the width.

### 4.5.1 Recirculation zones

Recirculation zones develop for the abrupt change in bottom profile in series 1. Because of the turbulent motions, the shape of the recirculation zone changes in time. But there is some average shape of the recirculation zone. This shape seems to be influenced by the undulations. At the wave trough, the recirculation zone drops and at the wave top it rises. This is visible in Figure 4.15, where the circles represent the boundary of the recirculation zone. This boundary is calculated as follows: The vertical position is determined, where the surface of the negative horizontal velocity is equal to the surface of the positive horizontal velocity. For this approach, the recirculation zone is also longer than the presumed recirculation zone of 7 times the weir height. It is interesting to know, if this is caused by the undulations. Velocity profiles for a classical jump and for the case of no undulations could confirm this.

No recirculation zones develop for the smooth downstream part in series 2. The smooth



**Figure 4.15:** Recirculation zone for series 1, the circles indicate the position of the recirculation zone. The recirculation zone seems to be influenced by the waves and is larger than the presumed 7 times the weir height.

downstream part has the same shape as the presumed recirculation zone for series 1. The idea was that the recirculation zone didn't affect the flow, so the undulations for series 1 and 2 should be more or less the same. But the wave characteristics differ a lot, so the recirculation zone has a distinct influence on the undulations.

#### 4.5.2 3D effects

The discharge is calculated from the velocity profile by means of integration of the measured horizontal velocities over the height. This value of the discharge is compared to the measured discharge from the Rehbock weir. The ratio of the integrated discharge from the velocity profile to the measured discharge from the Rehbock weir is given in Table 4.4. There seems to be a

Series	Position	Q=30[l/s]	Q=45 [l/s]	Q=60[l/s]
Series 1	first wavetrough	1.15	1.06	0.97
	first wavetop	0.92	1.05	0.93
	second wavetrough	1.01	0.98	0.92
	above weir	-	1.05	-
	behind weir 1	-	-	1.09
	behind weir 2	-	-	1.07
	behind weir 3	-	-	1.10
Series 2	first wavetrough	1.13	1.11	1.14
	first wavetop	1.29	1.34	1.27
	second wavetrough	1.41	1.39	1.26

**Table 4.4:** Comparison discharges, discharge calculated from the velocity profile divided by the measured discharge from the Rehbock weir.

significant difference between the discharges, especially in case of series 2. The accuracy of the velocity measurements needs to be considered to determine whether there is a measuring error or some other (physical) cause.

**Accuracy velocity profile** To ensure the reliability of the LDA-device, some verification measurements are conducted. These are described in Appendix C. From this, it can be concluded that the LDA-device works properly. Some deviations can be expected due to the measuring method:

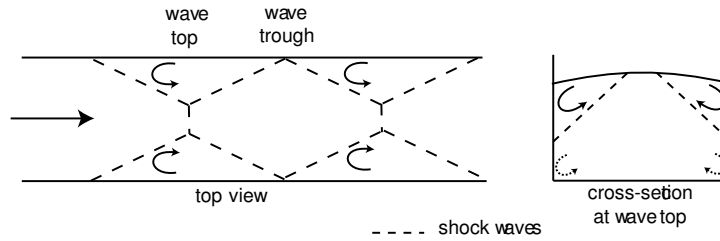
- The number of velocity points over the height is limited (about 11 points).
- Undulations tend to move a little in upstream and downstream direction.
- Measuring velocities too close to the free surface is not possible, because the undulations move a little up and down. In order to obtain a continuous signal of the LDA, measurements were possible up to 3cm of the free surface.
- Before the velocity profiles were integrated, a polynomial fit is applied to the velocity profile over the height. This fit has also some deviations, especially at the free surface (see velocity profiles Appendix D).

In Appendix D, the velocity profiles for each cross-section are given. For every velocity point, the standard deviation is given. The standard deviation of the discharge calculated by integration of the velocity profile depends on the correlation between the velocity points. The variation in the velocity is caused by the turbulent motions and the movement of the undulations. For the first one, the correlation between the velocity points is high, for the turbulent motions the correlation is low. The question is which effect has the largest influence on the variation. The effect of the turbulent motions is the largest at the shear layer, while the effect of the movement of the undulations should be more or less constant over the height. At the free surface, the variation is very little. So the effect of the movement of the undulations in the variance is very little. The turbulent motions have the largest influence in the variation of the velocity. The correlation between the velocity points due to this effect is assumed to be low. In this way, it is assumed that the velocity points are more or less uncorrelated. By means of this simplification, the relative errors are calculated (given in Table 4.5). It can be seen, that the largest relative errors occur for the undulations in series 1. This seems logical, because the recirculation zone causes larger turbulent motions. The relative errors for series 2 are much lower than the deviation in Table 4.4, which indicated that the higher discharge from the velocity profile has another (physical) cause.

Series	Position	Q=30[l/s]	Q=45 [l/s]	Q=60[l/s]
Series 1	first wavetrough	8.1%	7.4%	7.4%
	first wavetop	14.2%	12.8%	13.0%
	second wavetrough	14.2%	13.0%	11.9%
	above weir	-	0.7%	-
	behind weir 1	-	-	2.9%
	behind weir 2	-	-	2.1%
	behind weir 3	-	-	4.0%
Series 2	first wavetrough	1.0%	1.1%	0.9%
	first wavetop	1.3%	1.4%	1.5%
	second wavetrough	1.7%	1.8%	2.4%

**Table 4.5:** Relative error discharges

**Variation over the width** The cause of these large deviations might be a variation over the width. For series 2, variations over the width were already observed in the shape of the water surface: development of shockwaves at the sides, that intersect in the middle of the flume resulting in the wavetop. For undular hydraulic jumps in an open channel with horizontal bottom, Chanson and Montes (1995a) and Ohtsu et al. (2003) observed recirculation zones in the cross-sectional plane at the sides of the channel (at the bottom and at the free surface), see Figure 4.16. In this way, the flow in the middle of the flume accelerates, which could explain the higher velocities measured in the middle of the flume.



**Figure 4.16:** Sketch top view and cross-section, recirculation zones develop in lateral cross-direction (Chanson 1995a)

## 4.6 Hypothesis

The hypotheses and investigations formulated in the experimental program (section 3.3.1) are evaluated.

### 1. Influence separation zone on the undulations.

The velocity measurements show that for series 1 two separation zones develop and for series 2 no separation zone develops. There is a big difference between the undulations for series 1 and series 2. For series 1 (abrupt change in bottom profile):

- The undulations occur at a lower degree of submergence and the Froude numbers above the weir are higher.
- There is no variation over the width, no shock waves develop.
- Wavelength is two times larger than for series 2.
- Waveheight is up to four times bigger than for series 2.

So, this big difference between series 1 and series 2 might be caused by the separation zone. However, the same is valid for the hypothesis that the abrupt change in bottom profile causes undulations. But they are related to each other, because the separation zone is a result of the abrupt change in bottom profile.

### 2. Abrupt change in bottom profile causes undulations.

As mentioned for hypothesis 1, the differences between series 1 and series 2 could also be explained by the abrupt change in bottom profile. At least the abrupt change in bottom profile causes the separation zone. Also, undulations above the weir only develop for series 5 (block shape). This is the only series with an abrupt change in bottom profile on the upstream side of the weir. So, it seems that the abrupt change in bottom profile causes (in)directly undulations.

### 3. Undulations depend on the curvutare of the streamlines above the weir.

The difference between series 2 and series 3 (without middle part) is very small. The transition zone, where undulations occur, is at a somewhat higher degree of submergence for series 3. But the undulations look the same and the wave characteristics are the same. The difference between series 1 and series 4 is also very small. Also, the transition zone is

at a slightly higher degree of submergence, so the Froude numbers above the weir are a bit lower. But the wave characteristics are the same. It can be concluded that the curvatures of the streamlines above the weir seem to have little influence on the undulations.

4. Influence upstream shape of weir on the undulation.

The undulations behind the weir are almost similar for series 1 and series 5. So, the absence of the upstream part in series 5 doesn't make a difference.

## 4.7 Conclusion

Undulations occur for a certain range of the degree of submergence. This depends on the shape of the weir. For an abrupt change in bottom profile, the undulations occur for lower degrees of submergence than for a weir with a smooth downstream part. Also, the wave characteristics are different, for the former the undulations are more pronounced, the wave lengths are two times larger and the wave heights up to four times larger.

The wave lengths and the occurrence of undulations for the abrupt change in bottom profile are comparable to the investigations of the undular hydraulic jump on a horizontal bottom from the literature.

The wave heights 1m downstream of the weir have a distinct relation with the Froude number. A criterion for standing waves should be that the flow velocity is equal to the wave celerity. This depends on which flow velocity is used: the mean flow velocity is too low, because of the non-uniform velocity distribution, but the velocity at the free surface is too high. Furthermore, there seems to be a dependence of the factor  $\frac{U}{c}$  (flow velocity divided by wave celerity) with the Froude number.

The velocity profile has a large influence on the undulations. For the abrupt change in bottom profile, a recirculation zone is visible and it seems to have a wavy shape similar to the undulations.

Considerable 3D effects occur for the weir with the smooth downstream part, which is visible from the shock waves at the water surface and from the high velocities in the middle of the flume.

# Chapter 5

## Modelling

### 5.1 Introduction

The numerical models are described in this chapter. The first model is based upon the Boussinesq equations. The one-dimensional stationary equations are derived. A relative simple approach is to linearize the equations, which gives an indication of the wave characteristics. Another model is based upon the Euler equations (Stelling and Zijlema 2003). In this model multiple layers over the height can be applied. The one-layer case is considered. Also, a finite element model (Labeur and Pietrzak 2005) is described, that takes into account the variations over the height.

### 5.2 Boussinesq model

#### 5.2.1 Overview

A simple approach to get some insight in the undulations behind an obstacle is based upon the Boussinesq equations. The same approach is applied as for the description of internal lee waves in stratified flows (Pietrzak et al. 1988). The one-dimensional situation is considered.

#### One-dimensional

The boussinesq equations are based on the shallow water equations with a correction for the non-hydrostatic pressure. For an uneven bottom topography, this leads to following equations (friction neglected):

Continuity:

$$\frac{\partial h}{\partial t} + \frac{\partial}{\partial x}(hu) = 0 \quad (5.1)$$

Momentum (depth-averaged):

$$\frac{\partial u}{\partial t} + S_2 u \frac{\partial u}{\partial x} + g \frac{\partial}{\partial x}(h + h_b) - \frac{1}{3} h^2 \left( \frac{\partial^3 u}{\partial x^2 \partial t} + u \frac{\partial^3 u}{\partial x^3} \right) + \frac{1}{2} h u^2 \frac{\partial^3 h_b}{\partial x^3} = 0 \quad (5.2)$$

### Derivation of the Boussinesq equations

In the normal shallow water equations, the horizontal velocity is constant over the height and the vertical velocity is zero. In the Boussinesq equations, a correction ( $g\frac{\partial h'}{\partial x}$ ) is made on the hydrostatic pressure distribution. It uses an approximation for the vertical velocity distribution over the water height ( $w(z)$ ). The calculation steps are (see Figure 5.1 for the used variables):

**Step 1** An expression for  $w(z)$  is substituted in the vertical advection equation (steady state):

$$g\frac{\partial h'}{\partial z} = -u\frac{\partial w}{\partial x} - w\frac{\partial w}{\partial z}$$

**Step 2** This equation is integrated once from  $z$  to the water surface:

$$gh'(z) = \int_z^\eta \left( -u\frac{\partial w}{\partial x} - w\frac{\partial w}{\partial z} \right) dz$$

**Step 3** Averaging over the depth leads to:

$$gh' = \frac{1}{\eta - h_b} \int_{z_b}^\eta gh'(z) dz$$

**Step 4** Differentiating with respect to  $x$  leads to the correction in the horizontal momentum equation:

$$g\frac{dh'}{dx}$$

**Velocity distribution** An appropriate vertical velocity distribution has to be chosen for the derivation. A linear relation between the vertical velocity at the surface and at the bottom (steady state) is assumed (see Figure 5.1):

$$w_{top} = u\frac{\partial \eta}{\partial x}$$

$$w_{bottom} = u\frac{\partial h_b}{\partial x}$$

This leads to the following expression for the vertical velocity:

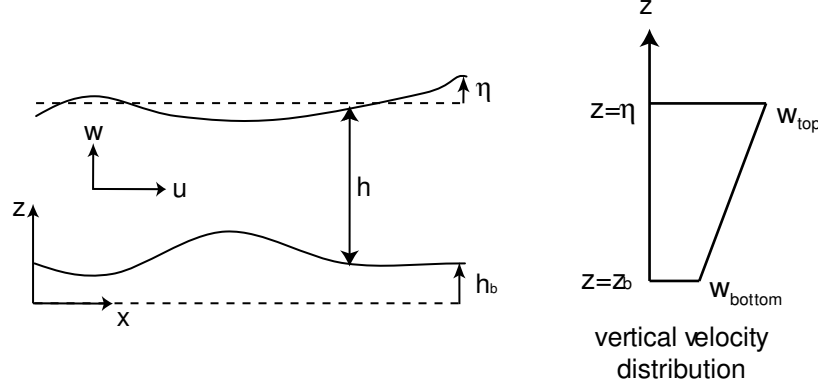
$$w(z) = u\frac{\partial \eta}{\partial x} \frac{z - h_b}{H} + u\frac{\partial h_b}{\partial x} \frac{\eta - z}{H} \quad (5.3)$$

with  $H = \eta - z_b$

This results in the following expression for the horizontal momentum:

$$g\frac{dh'}{dx} = -\frac{1}{2}u(\eta - h_b)\frac{\partial^2}{\partial x^2} \left( u\frac{\partial h_b}{\partial x} \right) + \frac{1}{3}(\eta - h_b)u\frac{\partial^2}{\partial x^2} \left( (\eta - h_b)\frac{\partial u}{\partial x} \right) \quad (5.4)$$





**Figure 5.1:** Definition of the variables in the Boussinesq equations

### 5.2.2 Linearized equations

In order to get more insight in the equations and derive an analytical solution, the equations are linearized. The bottom is horizontal with an obstacle of small amplitude. The equation is linearized by substituting the following expressions for the water depth and velocity:

$$h = \bar{h} + \eta - h_b \quad (5.5)$$

$$u = \bar{u} + v \quad (5.6)$$

The values with overbar present the values without obstacle, which are independent of  $x$ . Both  $\eta$  and  $h_b$  are assumed to be small compared to  $h$ . The term  $v$  is the velocity fluctuation in  $x$ -direction ( $u$ ). Higher order terms are neglected. For a steady flow situation, the continuity and momentum equations result in:

$$\bar{u}(\eta - h_b) + \bar{h}v = 0 \quad (5.7)$$

$$S_2 \bar{u} \frac{dv}{dx} + g \frac{d\eta}{dx} - \frac{1}{3} \bar{u} \bar{h}^2 \frac{d^3 v}{dx^3} + \frac{1}{2} \bar{h} \bar{u}^2 \frac{d^3 h_b}{dx^3} \quad (5.8)$$

Eliminating  $v$  gives the following equation for the free surface height  $\eta$  ( $S_2 = 1$ ):

$$\left. \begin{aligned} v &= -\frac{\bar{u}}{h}(\eta - h_b) \\ \frac{dv}{dx} &= -\frac{\bar{u}}{h} \left( \frac{d\eta}{dx} - \frac{dh_b}{dx} \right) \\ \frac{d^3 v}{dx^3} &= -\frac{\bar{u}}{h} \left( \frac{d^3 \eta}{dx^3} - \frac{d^3 h_b}{dx^3} \right) \end{aligned} \right\} \left( g - \frac{u^2}{h} \right) \frac{d\eta}{dx} + \frac{u^2}{h} \frac{dh_b}{dx} + \frac{1}{3} u^2 h \frac{d^3 \eta}{dx^3} + \frac{1}{6} h u^2 \frac{d^3 h_b}{dx^3} = 0$$

Making use of  $F^2 = \frac{\bar{u}^2}{gh}$  leads to the following linearized equation:

$$(1 - F^2) \frac{d\eta}{dx} + F^2 \frac{dh_b}{dx} + \frac{1}{3} F^2 h^2 \frac{d^3 \eta}{dx^3} + \frac{1}{6} F^2 h^2 \frac{d^3 h_b}{dx^3} = 0 \quad (5.9)$$

Integrating the equation once with respect to  $x$  gives:

$$(1 - F^2) \eta + F^2 h_b + \frac{1}{3} F^2 h^2 \frac{d^2 \eta}{dx^2} + \frac{1}{6} F^2 h^2 \frac{d^2 h_b}{dx^2} + C = 0 \quad (5.10)$$

C=integration constant, sort of reference level

Surface waves only develop if  $F^2 < 1$ , if the flow is subcritical (this is applicable to the flow behind the obstacle, not above the obstacle).

The obstacle occupies the interval  $-l \leq x \leq l$ .

For the part behind the obstacle ( $h_b = 0$ ), an expression for the wave length can be developed by substituting  $\eta = \hat{\eta} \cos(kx)$  and  $h_b = 0$  into equation 5.10:

$$kh = \sqrt{\frac{3(1 - F^2)}{F^2}} \quad (5.11)$$

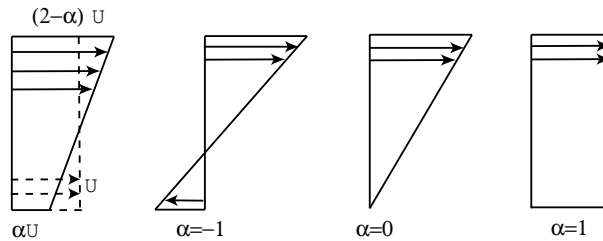
The dimensionless wave length only depends on the Froude number behind the weir. This expression for the wave length can be substituted in the linear dispersion relation. In this way, a criterion for the velocity divided by the wave celerity is formulated, which result in (substituting equation 5.11 into equation 2.7):

$$\frac{U}{c} = \frac{\sqrt{F \sqrt{3(1 - F^2)}}}{\sqrt{\tanh \sqrt{\frac{3(1 - F^2)}{F^2}}}} \quad (5.12)$$

This expression for  $\frac{U}{c}$  only depends on the Froude number.

**Influence velocity profile** So far, the assumption of an uniform velocity profile is used. But it can be seen from the measurements that the velocity profile is not uniform. The momentum equation needs to be corrected for the non-uniform velocity distribution. The flow behind the obstacle ( $h_b = 0$ ) is considered to determine the expression of the wave length. In that case, two terms need to be considered in the derivation of the Boussinesq equations: the advection term and the Boussinesq term. A constant velocity over the width and a linear variation of the velocity over the height (see Figure 5.2) is assumed, which leads to the following expression for the horizontal velocity ( $U$  is the mean velocity,  $\alpha$  determines the shape of the velocity profile):

$$u = U \left( \alpha + 2 \frac{z}{h} (1 - \alpha) \right)$$



**Figure 5.2:** Schematisation of the horizontal velocity profile

The correction in the advection term is defined by the profile coefficient  $S_2$  (see Equation 5.8), which is calculated as follows:

$$S_2 = \frac{\iint_A \rho u^2 dA}{\rho U^2 A} \quad (5.13)$$

The profile coefficient can be expressed as a function of  $\alpha$  (substituting the expression for  $u$  into 5.16):

$$S_2 = \frac{\alpha^2 - 2\alpha + 4}{3}$$

For the derivation of the Boussinesq term in the momentum equation, the same steps are followed as described previously in the derivation of the Boussinesq equations. For the vertical velocity distribution, again a linear relation between the velocity at the surface and at the bottom is assumed. The vertical velocity at the bottom is set to zero, because the flow behind the obstacle is considered. The vertical velocity at the surface is proportional to the horizontal velocity at the surface  $((2 - \alpha)U)$ . The Boussinesq term results in:

$$\frac{(\alpha - 2)(\alpha - 3)}{6} \frac{\partial^2}{\partial x^2} \left( h \frac{\partial U}{\partial x} \right) + \frac{(\alpha - 2)(\alpha - 1)}{6} U h \frac{\partial}{\partial x} \left( \frac{\partial h}{\partial x} \frac{\partial U}{\partial x} \right) \quad (5.14)$$

The second term can be neglected. After linearizing the equations and integrating once, the equation for the development of waves behind the obstacle yields:

$$(1 - S_2 F^2) \eta + \frac{(\alpha - 2)(\alpha - 3)}{6} F^2 h^2 \frac{d^2 \eta}{dx^2} = 0 \quad (5.15)$$

The expression for the wave length changes into:

$$kh = \sqrt{\frac{6(1 - S_2 F^2)}{(\alpha - 2)(\alpha - 3) F^2}} \quad (5.16)$$

### Analytical solution

From the linearized Boussinesq equations, derived for an uniform horizontal velocity profile, an analytical solution is constructed. The solution for the waves ( $x > l$ ) becomes:

$$\eta = \frac{3}{kh^2} \left\{ \cos(kx) \int_{-l}^l h_b(\xi) \sin(k\xi) d\xi - \sin(kx) \int_{-l}^l h_b(\xi) \cos(k\xi) d\xi \right\}$$

This represents a simple harmonic wave. By considering a cosine profile for the bottom obstacle, a relative simple expression for the wave length and wave height can be found.

If the obstacle has a cosine profile given by:

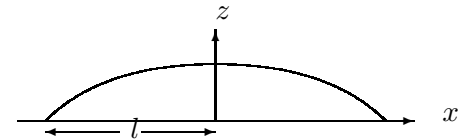
$$h_b = \hat{h}_b \cos\left(\frac{\pi x}{2l}\right)$$

The waves become:

$$\eta = \pi \frac{F^2}{1 - F^2} \phi(kl) \hat{h}_b \sin(kx) \quad (5.17)$$

$$\text{with } \phi(kl) = \frac{kl \cos(kl)}{(kl)^2 - \frac{\pi^2}{4}}$$

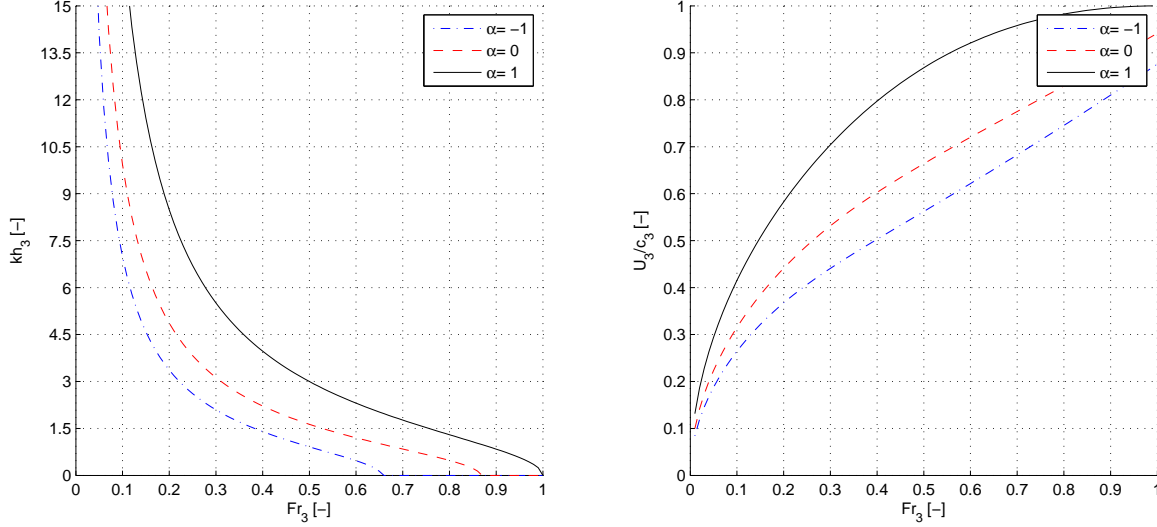
$$k = \frac{1}{h} \sqrt{\frac{3(1 - F^2)}{F^2}}$$



### Parameter analysis

The dimensionless wavelength ( $kh$ ) depends on the Froude number only (see Figure 5.3). Also, the flow velocity divided by the wave celerity depends on the Froude number only. This contradicts with the idea that  $\frac{U}{c}$  needs to be 1 as a criterion for the existence of undulations.

The amplitude of the undulations depend on the Froude number, the water depth, the length



**Figure 5.3:** Wavenumber against Froude for different horizontal velocity distributions

of the obstacle and the height of the obstacle (see Figure 5.4).

### Bottom friction

Until now, the bottom friction is neglected. The effect of the bottom friction will be investigated by adding a friction term to the original Boussinesq equations with an uniform horizontal velocity distribution. Adding friction to the system leads to the following friction term ( $\tau_b$ : bottom shear stress,  $f_b$ : friction factor):

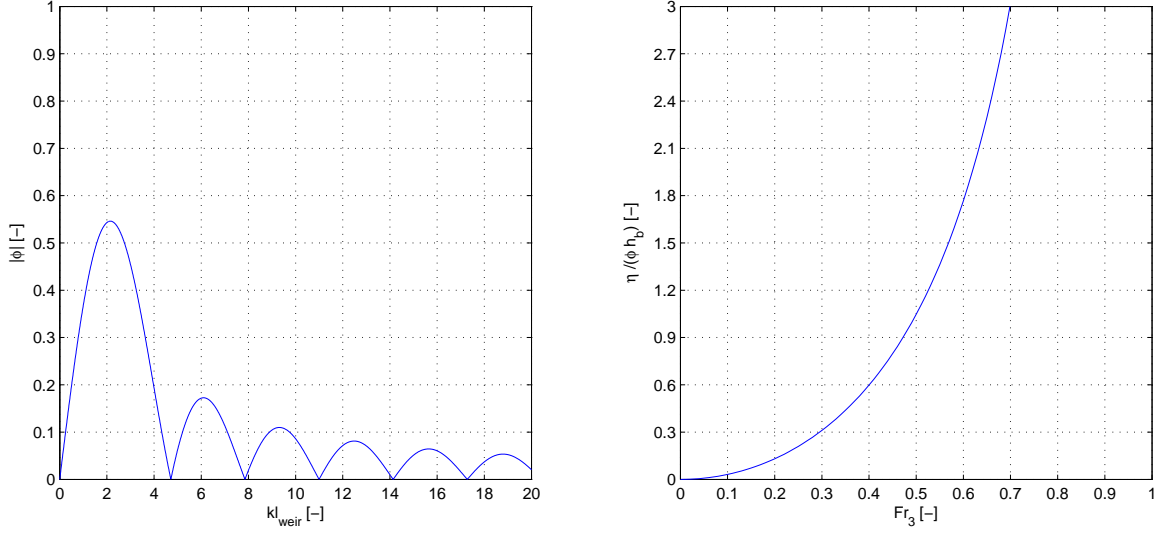
$$fric = \frac{\tau_b}{\rho h} = f_b \frac{u|u|}{h}$$

Linearizing the friction term leads to ( $u = \bar{u} + v$ ,  $h = \bar{h}$ ):

$$fric = f_b \frac{\bar{u}^2}{\bar{h}} + 2f_b \frac{\bar{u}}{\bar{h}} v = f_b \frac{\bar{u}^2}{\bar{h}} \left( 1 - 2 \frac{\eta - h_b}{\bar{h}} \right)$$

The second term corresponds to the bottom friction due to the waves. This term causes the damping of the waves. This (second) friction term (after division by  $g$ ) is added to equation 5.9:

$$-2f_b F^2 \frac{\eta - h_b}{h} \quad (5.18)$$



**Figure 5.4:** Expression for the waveheight defined by the analytical solution of the linear Boussinesq equation. The shape factor  $\phi$  depends on the length of the weir and the wave height is a function of the shape factor and the Froude number behind the obstacle.

Again, the part behind the obstacle is considered ( $h_b = 0$ ) for the linearized Boussinesq equations with an uniform horizontal velocity distribution, which leads to the following equation:

$$(1 - F^2) \frac{d\eta}{dx} + \frac{1}{3} F^2 h^2 \frac{d^3 \eta}{dx^3} - 2 f_b F^2 \frac{\eta - h_b}{h} = 0 \quad (5.19)$$

This equation is solved by substituting the expression for a damped harmonic wave:

$$\eta \sim \text{Re}(e^{-(m+ik)x})$$

The expression for the wave length becomes:

$$kh^2 = 3mh^2 + 3 \frac{1 - F^2}{F^2}$$

$$4mh^3 + 3 \frac{1 - F^2}{F^2} mh - 3f_b = 0$$

The parameter  $mh$  is the dimensionless damping rate. The damping rate is the largest for Froude numbers towards 1 and has some influence on the wave number for the higher Froude numbers. But this is still very small. Regarding the fact that the Froude numbers downstream of the bottom obstacle are much lower than 1 in the measurements, it can be concluded that the influence of the bottom friction on the wave lengths can be neglected.

### 5.2.3 Non-linear Boussinesq equations

The effect of the linearization of the Boussinesq equations is investigated by considering the non-linear Boussinesq equations. The original steady state continuity and momentum equations are considered. The bottom friction is neglected and an uniform velocity profile is assumed. The equations are discretized and solved numerically (see Appendix F).

### 5.2.4 Numerical implementation

The numerical implementation of the linear and non-linear Boussinesq equations are given in Appendix F.

## 5.3 Non-hydrostatic model

The Euler equations are used for the numerical modelling of non-hydrostatic free-surface flows. Multiple layers can be applied. In this thesis, the one-layer situation is considered only. For the mathematical description and numerical implementation of the model, one is referred to Stelling and Zijlema (2003).

## 5.4 FINEL 3D

FINEL 3D is a three-dimensional numerical model that uses the finite element method (Labeur and Pietrzak 2005). The model is based upon the full Navier Stokes equations. It is applicable to non-hydrostatic flow situations, because no assumptions have been made for the vertical velocity distribution. In this case, a 2-D flow simulation is considered. The computational grid consists of triangular elements and adapts to the position of the free surface. A turbulence model based on the mixing length theory is built in. The mixing length can be adjusted.

## 5.5 Conclusion

The Boussinesq equations are derived by adding a correction for the non-hydrostatic pressure distribution to the normal shallow water equations. The equations are linearized, which leads to a simple expression for the wave length. Taking into account a non-uniform horizontal velocity distribution leads to a different Boussinesq equation. The expression of the wave length changes resulting in longer waves for a triangular shaped velocity profile (the maximum velocity is at the free surface) than in case of a block shaped velocity profile. An analytical solution of the linearized Boussinesq equations also gives an expression for the wave height in case of a cosine shaped weir. Other models capable of calculating non-hydrostatic free-surface flows are the non-hydrostatic model based upon the Euler equations and a finite element model (FINEL 3D), based upon the full Navier Stokes equations.

## Chapter 6

# Numerical experiments

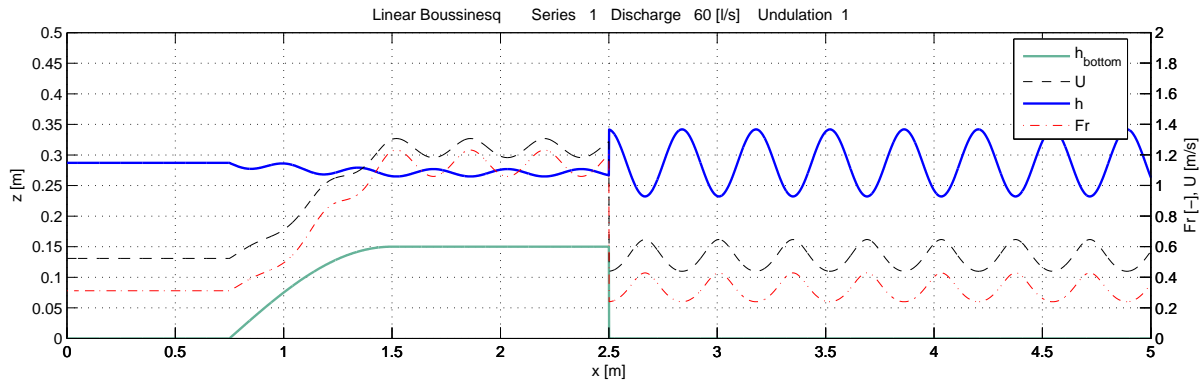
### 6.1 Introduction

For all the measured flow situations, numerical simulations are conducted for the models, described in chapter 5. In this way the different model approaches can be evaluated by comparing the results of the numerical experiments to the measurements for the occurrence of undulations and the wave characteristics.

### 6.2 Boussinesq model

#### 6.2.1 Linear Boussinesq model

The input parameters for this model are the downstream water depth and the discharge given by the measurements. Simulations are conducted for the linear Boussinesq model with an uniform horizontal velocity. An example of the results of a simulation of the model is given in Figure 6.1.



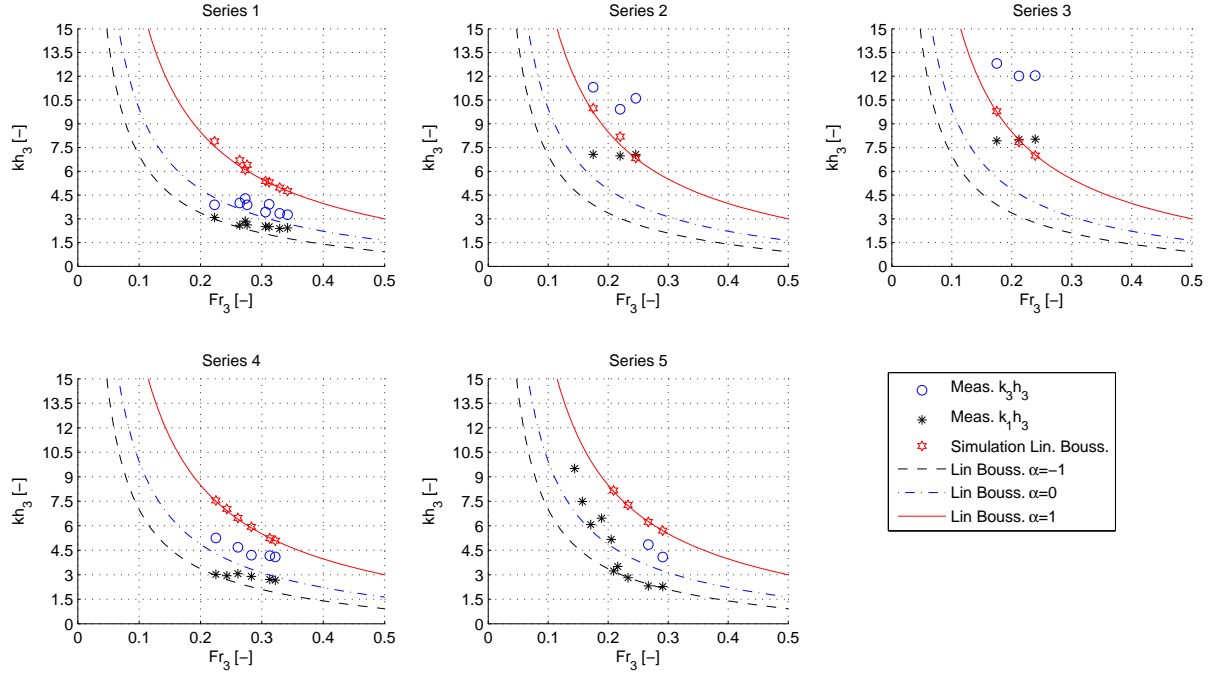
**Figure 6.1:** Example of a simulation of the linear Boussinesq model

### Occurrence of undulations

The linear Boussinesq model is not capable of describing the transition zones from undulations to no undulations. In fact, the linear Boussinesq model gives undulations in most cases.

### Wave characteristics

The indices of the wave characteristics correspond to the position in the flume, defined in Chapter 4.

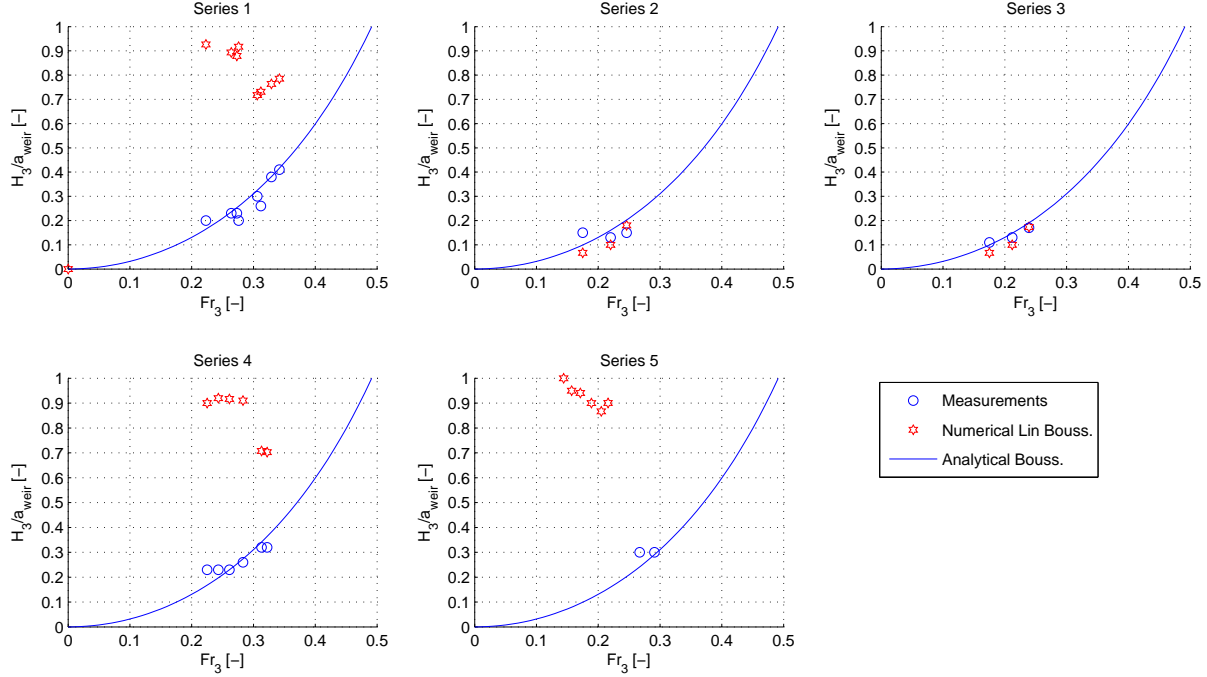


**Figure 6.2:** Comparison wave numbers measurements to linear Boussinesq model, the factor  $\alpha$  corresponds to the shape of the horizontal velocity profile ( $\alpha = 1$ : uniform velocity profile). Taking into account the velocity profile, the linear Boussinesq model gives a reasonable expression for the wave length.

**Wave lengths** In Figure 6.2, the wave numbers from the model are compared to the measurements. The dimensionless wave lengths are plotted as a function of the Froude number downstream of the weir (cross-section 3). Simulation runs are conducted for the linear Boussinesq model with an uniform horizontal velocity profile, which corresponds to the analytical expression for the wave length with  $\alpha = 1$ . For the weir with the smooth downstream part (series 2 and 3), where the velocity profile is almost uniform, modelling with an uniform flow velocity seems good enough: The waves above the downstream part of the weir ( $L_1$ ) are in good agreement with the model. But the waves behind the weir ( $L_3$ ) are too large in the model ( $L_1$  and  $L_3$  are the same in the model, but differ in the measurements). For the abrupt change in



bottom profile, a non-uniform horizontal velocity distribution has to be applied. The expression for the wavelength for a triangular shaped velocity profile ( $\alpha = 0$ ) corresponds to the measured wave lengths 1m downstream of the end of the weir ( $L_3$ ). In case of a negative horizontal velocity at the bottom ( $\alpha = -1$ ), wave lengths directly behind the weir show more resemblance with the model. This is consistent with the measured velocity profiles given in section 4.4.2: a substantial negative horizontal velocity develops directly behind the weir (separation zone), while the velocity profile further downstream looks more triangular shaped. The wave lengths can be predicted in a good manner with the linear Boussinesq model, when the velocity profile is taken into account.



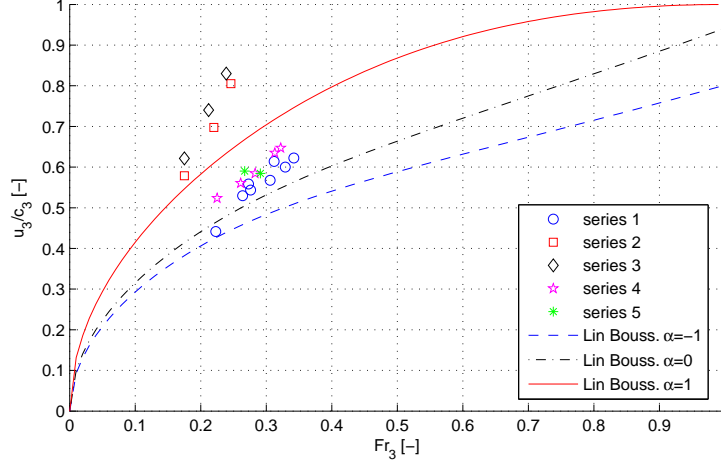
**Figure 6.3:** Comparison wave heights measurements to linear Boussinesq model, calculated wave heights are inaccurate for the weir with the abrupt change in bottom profile. The solid line represents an analytical solution in case of a cosine shaped weir.

**Wave heights** The dimensionless wave heights are plotted as a function of the Froude number downstream of the weir (cross-section 3), see Figure 6.3. The wave heights determined from the numerical simulations of the linear Boussinesq model, only show resemblance for series 2 and 3 (with downstream part). For the abrupt change in bottom profile, the amplitudes of the waves in the linear Boussinesq model are too high. A restriction to the linear Boussinesq model is that the wave height should be small compared to the water depth. In some cases, especially for the abrupt change in bottom profile, this is not valid any more, which may lead to unreliable results. The solid line in Figure 6.3 represents the wave amplitude for an analytical solution of the linear Boussinesq model in case of a cosine shaped weir, which is given by (shape factor

$\phi = 1$ ):

$$\frac{H_3}{a_{weir}} = \pi \frac{F^2}{1 - F^2}$$

This solution shows a much better agreement for the abrupt change in bottom profile than the previous one. This is remarkable, because the shape of the weir doesn't look like a cosine at all (for the abrupt change in bottom profile). This can be explained by looking at the streamlines, which follow more or less a cosine shape.



**Figure 6.4:** Comparison wave celerities measurements to linear Boussinesq model. The factor  $\alpha$  corresponds to the shape of the horizontal velocity profile ( $\alpha = 1$ : uniform velocity profile)

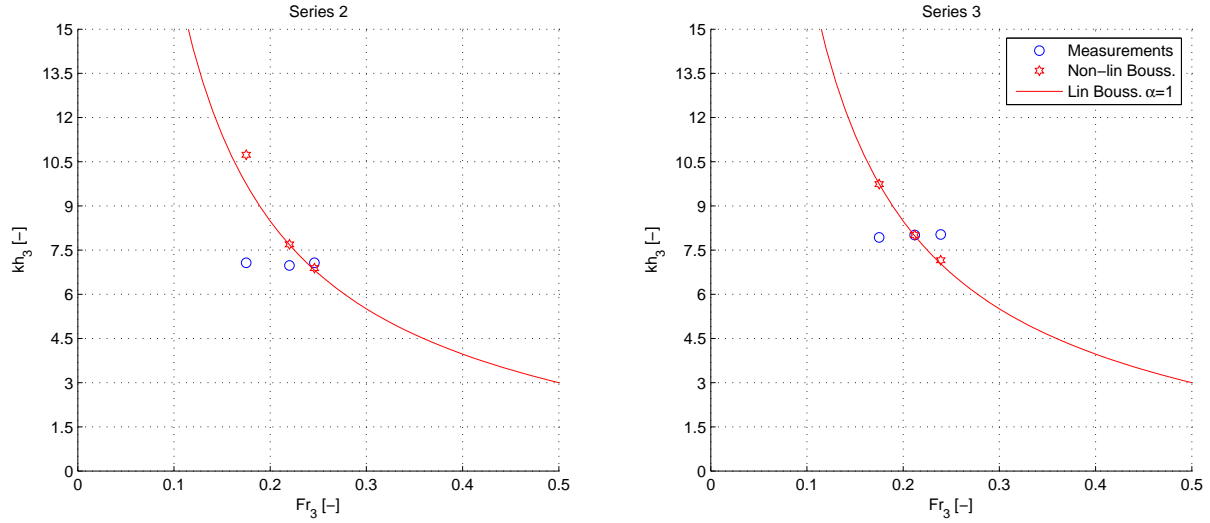
**Wave celerities** The flow velocity divided by the wave celerity is plotted against the Froude number downstream of the weir (cross-section 3) in Figure 6.4. The lines represent the relation of  $\frac{U}{c}$  and the Froude number for different velocity profiles, as given in equation 5.12. The expression of  $\frac{U}{c}$  shows some resemblance with the measurements: the expression is too large for both the abrupt change in bottom profile (compared to  $\alpha = 0$ , triangular shaped velocity profile) and the weir with the smooth downstream part (compared to  $\alpha = 1$ , uniform velocity profile). But it shows the same dependence with the Froude number.

### 6.2.2 Non-linear Boussinesq model

In order to investigate the effect of the linearization of the Boussinesq equations, the non-linear Boussinesq equations are considered. The non-linear Boussinesq model still uses the approximation of an uniform velocity profile. The model is not stable for the abrupt change in bottom profile. Probably because Froude numbers above the end of the weir are higher than 1, which doesn't happen for series 2 and 3, where the undulations occurred for higher degrees of submergence, which means lower Froude numbers. So, comparison with the measurements is only applicable for series 2 and 3.

### Wave characteristics

**Wave lengths** The dimensionless wave numbers for the non-linear Boussinesq model have the same relation with the Froude number downstream of the weir (cross-section 3) as in the linear Boussinesq model (see Figure 6.5). It seems that the linearization of the Boussinesq model has no influence on the wave lengths, at least in case of a weir with a smooth downstream part.



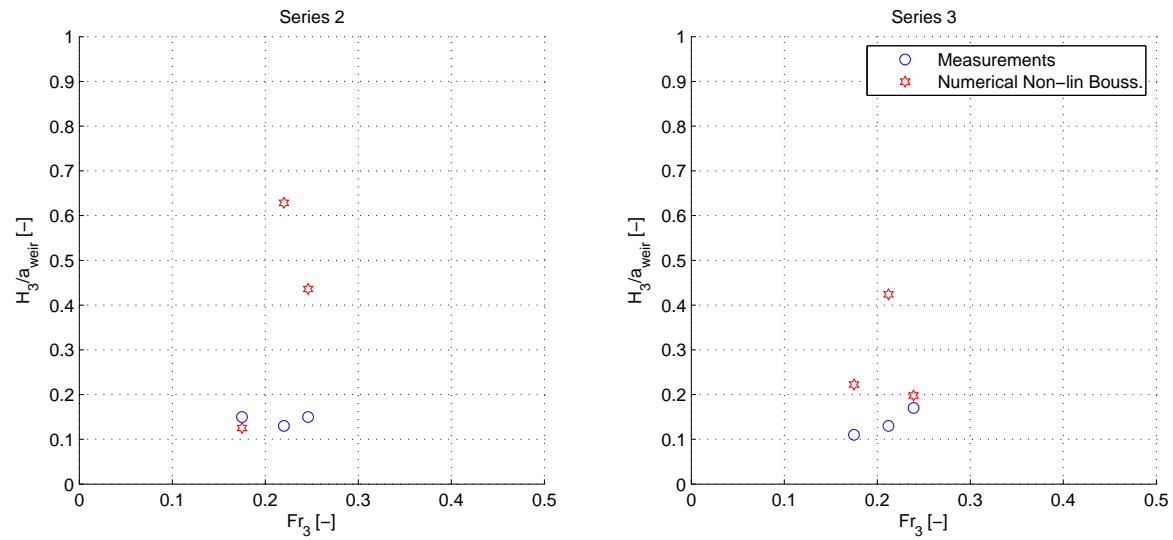
**Figure 6.5:** Comparison wave numbers measurements to non linear Boussinesq model, wave lengths are the same as for the linear Boussinesq model.

**Wave heights** The dimensionless wave heights are plotted against the Froude number (cross-section 3, downstream of the weir) in Figure 6.6. The wave heights for the non-linear Boussinesq model show less resemblance with the measurements than the linear Boussinesq model.

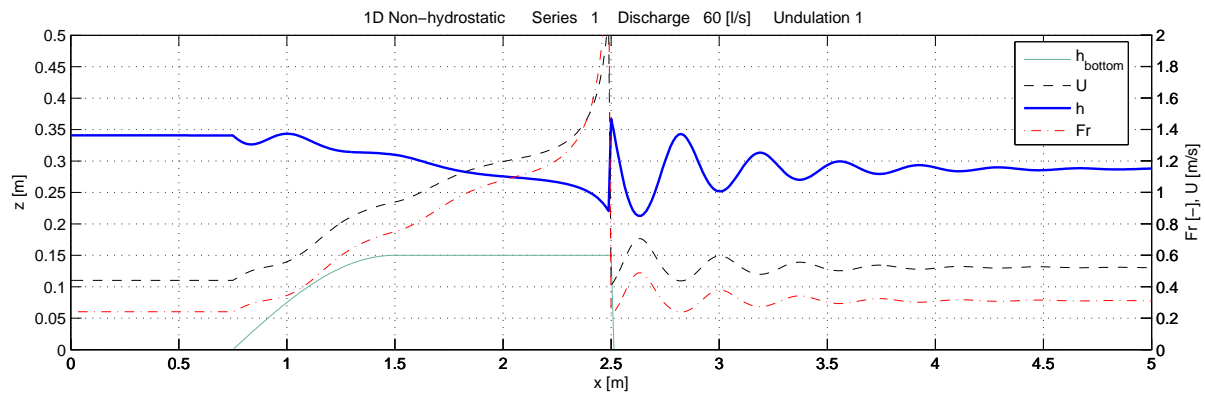
It can be concluded that the non-linear Boussinesq model has no added value to the linear Boussinesq model. Linearization of the Boussinesq equations leads to the same wave lengths and even better wave heights compared to the measurements.

## 6.3 Non-hydrostatic 1D

The boundary conditions are the downstream water depth ( $h_3$ ) and the discharge, which are adjusted to the values of these parameters in the measurements. An example of the output of a simulation of the model is given in Figure 6.7. The model has some difficulty with the abrupt change in bottom profile, which is visible at the high peak in the water surface directly behind the weir.



**Figure 6.6:** Comparison wave heights measurements to non linear Boussinesq model, wave heights are too large.



**Figure 6.7:** Example non-hydrostatic 1D model. Waves damp out fast.

### Occurrence of undulations

For the abrupt change in bottom profile, undulations occur for every degree of submergence. The model cannot predict the transition zones under which conditions undulations do and do not occur.

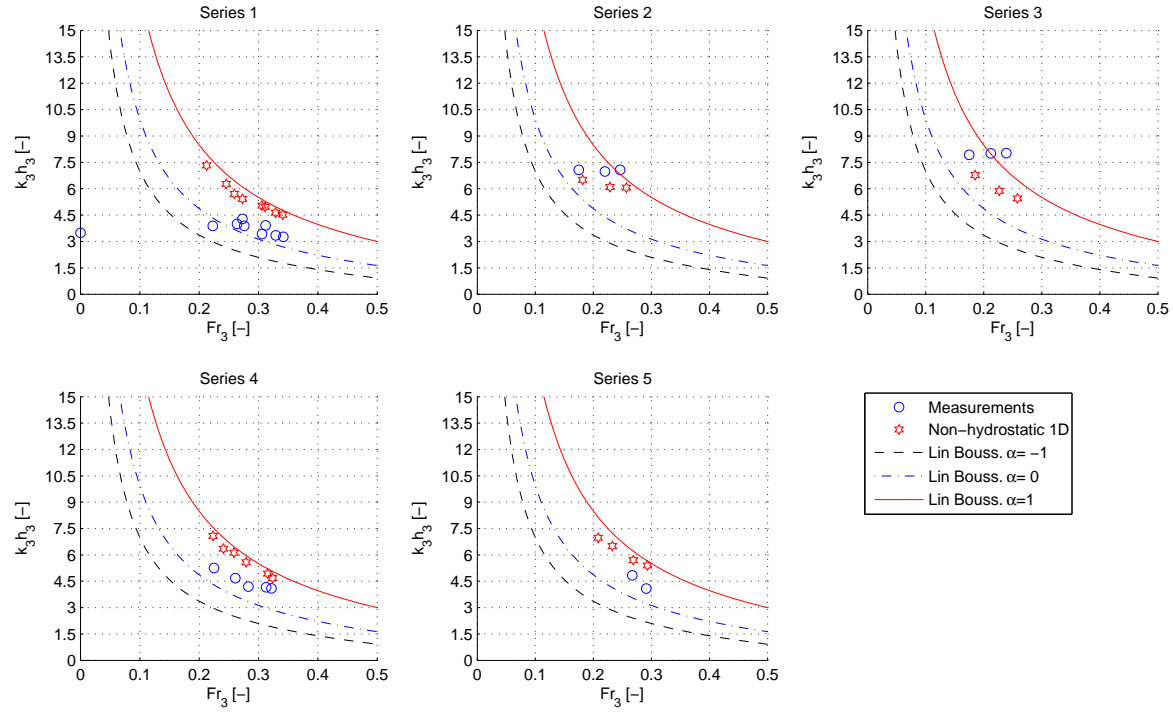
For the weir with the smooth downstream part (series 2 and series 3), there is an upper boundary for the degree of submergence ( $\frac{h_3}{h_0}$ ), above which no undulations occur. These values are a little higher than the measured values (Table 6.1). But this transition is not very sharp: the undulations dissappear gradually. By raising the downstream water depth, the wave height becomes smaller and smaller until the undulations are not visible any more. The model can't predict the lower boundary: For lower values of the degree of submergence, in case of a classical jump, undulations still develop.

	Model	Measurements
Series 2	S=0.98	S=0.97
Series 3	S=0.99	S=0.98

**Table 6.1:** Upper boundary occurrence of undulations for the weir with a smooth downstream part. In the model, undulations still develop for higher degrees of submergence than in the measurements.

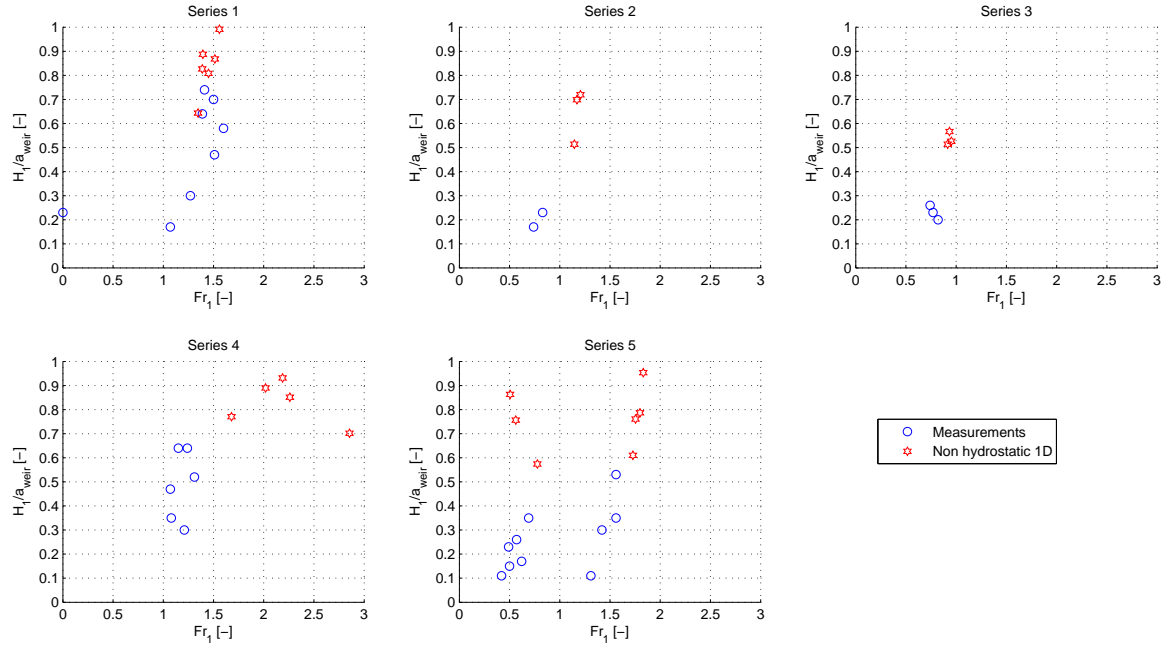
### Wave characteristics

**Wave lengths** Again, the dimensionless wave numbers are plotted as a function of the Froude number downstream of the weir (cross-section 3). The wave numbers for the non-hydrostatic 1D model resemble the expression given by the linear Boussinesq model for an uniform horizontal velocity profile (see Figure 6.8), although they are somewhat lower (larger waves). The shape of the weir does not influence the wave length, which contradicts with the measurements. For the smooth downstream part of the weir (series 2 and 3), the wave lengths in the model more or less resemble the wave lengths in the measurements. For the abrupt change in bottom profile, the measured wave lengths are two times larger. The shape of the velocity profile already suggested that the flow is not one-dimensional. It is not surprising that 1D modelling gives large deviations. For more reliable results, more layers have to be added to the model.



**Figure 6.8:** Comparison wave numbers measurements to non-hydrostatic 1D model. Calculated wave lengths are too small in case of a weir with an abrupt change in bottom profile

**Wave heights** In the model, the waves damp very fast, so it is difficult to choose an appropriate wave height for comparison with the model. In the measurements, there is a better relation between  $\frac{H_3}{a_{weir}}$  and  $Fr_3$ , but these waves are already damped out in the model (see Figure 6.7). The only reasonable comparison can be accomplished for  $H_1$ , the wave height between the first wave trough and first wave top. These wave heights are plotted against the Froude numbers above the end of the horizontal part of the weir (cross-section 1). But the model does not resemble the measurements much (see Figure 6.9). The model is not capable of predicting the correct wave heights.

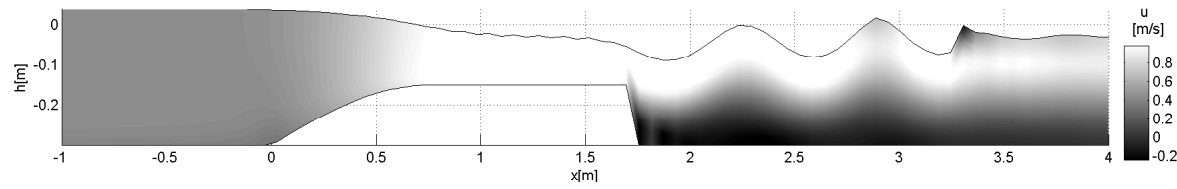


**Figure 6.9:** Comparison wave heights directly behind the weir (cross-section 1) of the measurements to the non-hydrostatic 1D model

It can be concluded that the non-hydrostatic model with one layer is not valid for the calculation of waves behind a weir.

## 6.4 FINEL 3D

The importance of the velocity profile is shown by the linear Boussinesq model and the non-hydrostatic model with one layer. The Finel3D model allows variations over the height, so that a non-uniform velocity profile is taken into account. It uses around 16 vertical grid points. It is expected that more reliable results will be achieved. The calculations are conducted for series 1 and series 2 only. An important parameter, that influences the flow pattern and wave characteristics is the mixing length. The mixing length is set to 1cm. An example of the output of the FINEL 3D model is given in Figure 6.10. It can be seen that the downstream part is not completely vertical for the weir with an abrupt change in bottom profile (series 1). Despite this inaccuracy, the results are still in good agreement with the measurements.



**Figure 6.10:** Example of a simulation of the FINEL3D model for series 1.

### Occurrence of undulations

For series 1 (abrupt change in bottom profile), undulations occur for Froude numbers above the end of the weir between 1 and 1.7 (see Figure 6.11). This is in good agreement with the occurrence of the undular jump on a horizontal bottom. A clear relation between the Froude number and the degree of submergence is visible. Undulations occur for degrees of submergence between 0.77 and 0.94, which are both a little higher than the measurements (between 0.75 and 0.90).

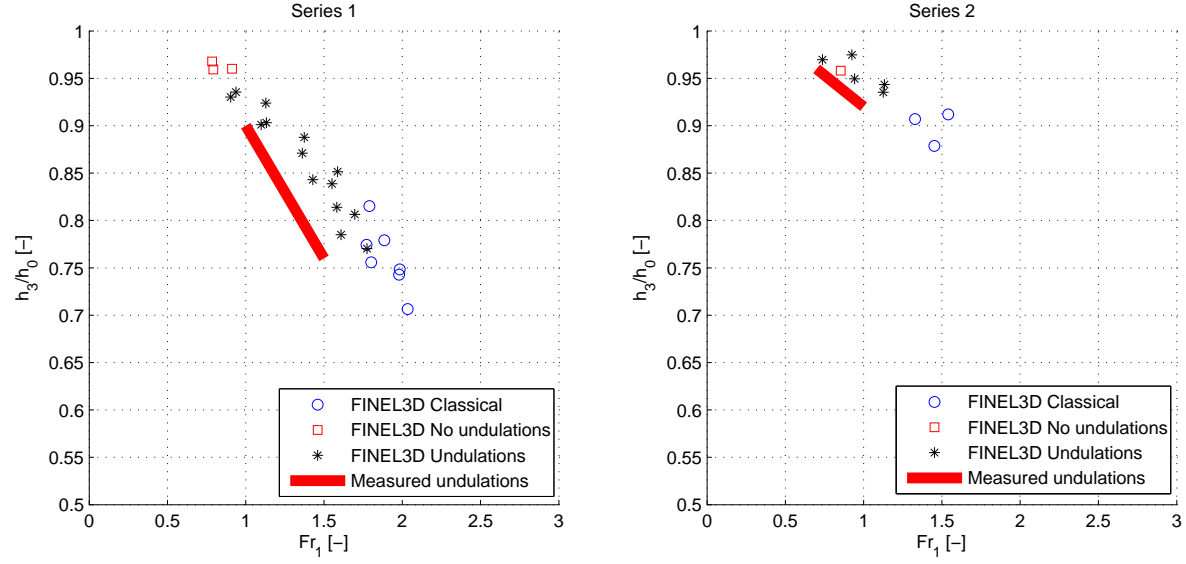
For series 2, undulations occur for degrees of submergence between 0.93 and 0.97, which is comparable to the measurements. The model can predict the occurrence of undulations in a fairly good manner.

### Wave characteristics

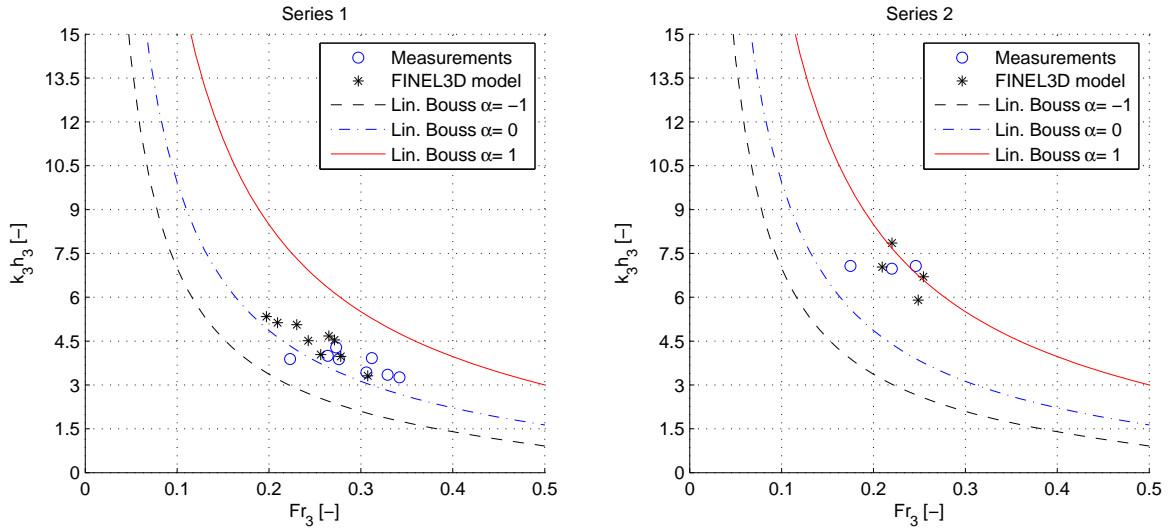
**Wave lengths** The dimensionless wave lengths are plotted against the Froude numbers downstream of the weir (cross-section 3) in Figure 6.12. The dimensionless wave lengths are in good agreement with the measurements for the weir with the abrupt change in bottom profile as well as the weir with a smooth downstream part. The FINEL 3D can predict the wave lengths in a good manner.

**Wave heights** In Figure 6.13, the dimensionless wave heights are plotted as a function of the Froude number behind the weir (cross-section 3). For the abrupt change in bottom profile (series 1), the dimensionless wave heights in the measurements are larger than in the model. The waves in the model damp out faster than in the measurements. For the weir with a smooth downstream part, the model predicts the correct wave heights.

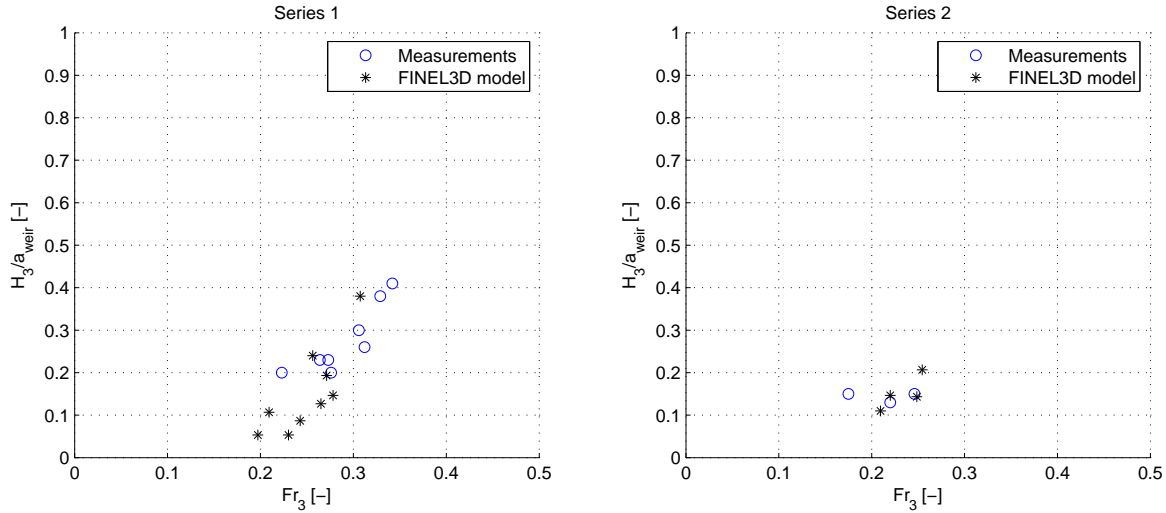




**Figure 6.11:** Occurrence of undulations for the FINEL 3D model, classical refers to a classical jump and no undulations to the submerged case, where no undulations occur.



**Figure 6.12:** Measured wave lengths compared to the FINEL 3D model.



**Figure 6.13:** Measured wave heights compared to the FINEL 3D model

## 6.5 Conclusions

In Table 6.2, an overview is given of the predicted wave lengths and wave heights of the numerical models compared to the measurements. It can be concluded that the wave lengths expressed by the linear Boussinesq model are in good agreement with the measurements when the shape of the horizontal velocity profile is taken into account. This is applicable to a weir with an abrupt change in bottom profile, where a triangular shaped velocity profile is used, as well as a weir with a smooth downstream part, where an uniform velocity profile is used. These velocity profiles correspond to the measured velocity profiles with the LDA-device. The results of the 1D non-hydrostatic and the FINEL 3D model confirm these observations. The non-hydrostatic model with one layer, making use of a depth-averaged approach, predicts incorrect wave lengths, while the FINEL 3D, making use of several grid points over the height, predicts the correct wave lengths.

Series	Shape weir	Boussinesq		1D Non-hydro		FINEL 3D	
		W.Length	W.Height	W.Length	W.Height	W.Length	W.Height
1		good	larger	smaller	larger	good	smaller
2		good	good	little larger	larger	good	good
3		good	good	little larger	larger	-	-
4		good	larger	smaller	larger	-	-
5		good	larger	smaller	larger	-	-

**Table 6.2:** Overview numerical models, wave heights and wave lengths of the model are compared to the measurements (smaller means that the wave property in the model is smaller than in the measurement)

## Chapter 7

# Conclusions and Recommendations

The undulations originated from the flow over a bottom obstacle are investigated. The objective of the research is to evaluate different modelling approaches and to get more insight in the phenomenon: under which conditions undulations occur and what the characteristics are. Experiments are conducted for different shapes of the weir and for various flow conditions. The measurements are compared to numerical models based on free-surface flows with a non-hydrostatic pressure distribution. Conclusions and recommendations are formulated from the experimental and numerical results.

### 7.1 Conclusions

Undulations behind a weir occur for a certain range of the degree of submergence (water depth downstream of the weir divided by upstream water depth). For lower values of the submergence, a classical hydraulic jump arises. Higher values lead to the disappearance of undulations. There is a big difference in the occurrence and the appearance of undulations between the weir with an abrupt change in bottom profile and the weir with a smooth downstream part.

**Abrupt change in bottom profile** Undulations occur for degrees of submergence between 0.75 and 0.90. By means of momentum balance and energy conservation, the degree of submergence can be written as the Froude number at the end of the weir. In this way, the upper and lower limit of the submergence, between which undulations occur, are analogue to the limiting Froude numbers of 1 and 1.7 for the undular hydraulic jump on a horizontal bottom. The wave lengths are comparable with empirical relations found for the undular jump on a horizontal bottom.

**Smooth downstream part of the weir** Undulations occur for higher degrees of submergence (between 0.90 and 0.98). The wave lengths are two times shorter and the wave heights up to four times smaller than for the abrupt change in bottom profile. The development of shock waves is visible at the water surface indicating the presence of considerable 3D effects. This is confirmed by integration of the velocity profile in the middle of the flume, which provides a significant higher discharge than the measured discharge (from the Rehbock weir).

**Discharge relation** The undulations do not seem to affect the discharge relation, because the expression for the discharge reduction coefficient is not influenced by the undulations.

**Influence velocity profile** The velocity profile has a large influence on the existence and characteristics of the undulations. This explains the difference between the weir with the abrupt change in bottom profile and the weir with a smooth downstream part. For the last one, no recirculation zone develops behind the weir, resulting in higher degrees of submergence favourable for the existence of undulations and lower wave lengths and wave heights. The wavy character of the recirculation zone shows that the undulations also affect the recirculation zone.

**Wave heights** A relation between the wave heights and the Froude number is found, which resembles an expression of an analytical solution of the linear Boussinesq equation based upon a cosine shaped weir.

The curvatures of the streamlines above the weir and the upstream shape of the weir hardly influence the characteristics of the undulations.

**Numerical modelling** For the description of the relatively short waves, a non-hydrostatic modelling approach is needed. The Boussinesq model, based upon the shallow water equations with a correction for the non-hydrostatic pressure provides an expression for the wave length depending on the Froude number only (1D model, linearized equations). The Boussinesq equations are also derived in case of a non-uniform horizontal velocity distribution, which results in a different expression for the wave length. For a weir with an abrupt change in bottom profile, a triangular shaped velocity profile (maximal velocity at free-surface), which corresponds to the measured velocity profile, is applied resulting in longer waves, which are in good agreement with the measurements. For a weir with a smooth downstream part, an uniform velocity profile is sufficient to predict the correct wave lengths.

The non-hydrostatic model (Stelling and Zijlema 2003) with one layer gives more or less the same results as the linear Boussinesq model with an uniform horizontal velocity distribution, indicating that more layers have to be added for proper results for the weir with the abrupt change in bottom profile. The large influence of the velocity profile also shows that one-dimensional modelling, making use of the mean velocity, is not valid for the description of the undulations. This is confirmed by the FINEL 3D model (Labeur and Pietrzak 2005), a finite element model that allows variations over the height, which provides the correct wave lengths. Only the FINEL 3D model can predict the upper and lower limit for the occurrence of undulations. In the other models, undulations develop for most flow conditions.

## 7.2 Recommendations

### Experimental setup

A better understanding of the 3D effects, especially for the weir with the smooth downstream part, will be achieved by measuring velocity profiles across the width. In this way, possible recirculation zones in lateral direction can be determined.

The velocity profiles for the classical jump and for the submerged case (no undulations) need to be measured to compare the shape of the recirculation zone in case of undulations to the case of no undulations. In the former case, it was found that the recirculation zone was longer than the presumed 7 times the weir height. It is interesting to find out whether this is caused by the undulations.

A more accurate measurement of the water depth can be obtained by using video recordings. This provides much more images of the water depth. The water depths can be derived from these images automatically by giving the water in the flume a colour.

Undulations were also observed in case a number of vertical rods are situated in the flow (grid). Due to the reduced cross-section, the Froude number between the bars increases resulting in undulations downstream of the bars. Measurements of this type of undulations could be compared to the measurements in the present research.

Compare results undulations behind the weir with the undular bore. It is interesting to find out whether the wave characteristics of the undulations behind the weir are comparable to the characteristics of the undular bore.

### **Numerical modelling**

The linear Boussinesq model indicates that the flow velocity divided by the wave celerity is a function of the Froude number, which contradicts with the criterion that the flow velocity should be equal to the wave celerity. Further investigation of this criterion is needed.

Numerical experiments for the non-hydrostatic model with multiple layers need to be conducted to compare it to the measurements. Because of the non-uniform velocity profile over the height, it is expected that this model will lead to a better agreement with the measurements.



# Notations

$a_{weir}$	Height of the weir	m
$B$	Width of the flume	m
$C_{dv}$	Discharge coefficient (perfect weir)	-
$C_*$	Discharge reduction coefficient	-
$c$	Wave celerity	$\frac{m}{s}$
$c_f$	Friction coefficient	-
$F$	Froude number	-
$F_{limit}$	Limiting Froude number, where the undular jump moves over to a classical jump	-
$g$	Gravitational constant $g = 9.81 \frac{m}{s^2}$	$\frac{m}{s^2}$
$h$	Water depth	m
$h_b$	Bottom profile	m
$H$	Wave height	m
$k$	Wave number	$\frac{1}{m}$
$L$	Wave length	m
$l$	Length half of the weir	m
$m$	Damping rate	$\frac{1}{m}$
$m$	Location x-direction in computational grid	-
$p$	Fit parameter for discharge reduction coefficient	-
$p$	Pressure	$\frac{N}{m^2}$
$q$	Specific discharge	$\frac{m^2}{s}$
$Q$	Discharge	$\frac{m^3}{s}$
$r$	Relative error	-
$Re$	Reynolds number	-
$S$	Degree of submergence $S = \frac{h_3}{h_0}$	-
$S_2$	Velocity profile coefficient	-
$U$	Mean horizontal flow velocity	$\frac{m}{s}$

$u$	Horizontal velocity	$\frac{m}{s}$
$v$	Horizontal velocity fluctuation	$\frac{m}{s}$
$w$	Vertical velocity	$\frac{m}{s}$
$x$	Horizontal coordinate	m
$y_c$	Critical water depth ( $Fr = 1$ )	m
$z$	Vertical coordinate	m
$\alpha$	Ratio velocity at bottom to velocity at free surface	-
$\Delta x$	Distance between grid points in horizontal direction	m
$\delta$	Thickness of boundary layer	m
$\zeta$	Free surface elevation	m
$\eta$	Free surface elevation	m
$\nu$	Kinematic viscosity	$\frac{m^2}{s}$
$\rho$	Density	$\frac{kg}{m^3}$
$\sigma$	Standard deviation of arbitrary parameter	
$\phi$	Shape factor in analytical Boussinesq solution	-



# References

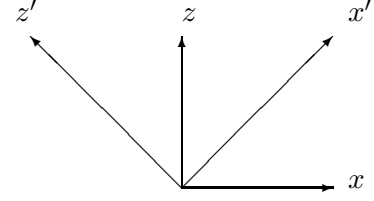
- Bradley, J. N. and A. J. Peterka (1957). The hydraulic design of stilling basins: hydraulic jumps on a horizontal apron (basin i). *Journal of the Hydraulics Division* 83(HY5), 1401(1–24).
- Chanson, H. and J. S. Montes (1995a). Characteristics of undular hydraulic jumps: experimental apparatus and flow patterns. *Journal of hydraulic engineering* 121(2), 129–144.
- Chanson, H. and J. S. Montes (1995b). Characteristics of undular hydraulic jumps: experiments and analysis. *Journal of hydraulic engineering* 124(2), 192–205.
- Chow, V. T. (1973). *Open channel hydraulics*. New York, USA: McGraw-Hill International.
- Darcy, H. and H. Bazin (1865). *Recherches hydrauliques. Imprimerie Imperiale Parties 1e et 2e*.
- Frazao, S. S. and Y. Zech (2002). Undular bores and secondary waves - experiments and hybrid finite-volume modelling. *Journal of hydraulic research* 40(1), 33–43.
- Hager, W. H. and K. Hutter (1984). On pseudo-uniform flow in open channel hydraulics. *Acta Mechanica* 53, 183–200.
- Henderson, F. M. (1966). *Open channel flow*. New York, USA: MacMillan.
- Ippen, A. T. and D. R. F. Harleman (1954). Verification of theory for oblique standing waves. *Proceedings of the Am. Soc. of Civ. Eng.* 80, 526(1–17).
- Iwasa, Y. (1955). Undular jump and its limiting condition for existence. *Proceedings of the 5th Japan National Congress for Applied Mech.*, 315–319.
- Kolkman, P. A. (1989). Discharge relations for hydraulic structures and head losses from different components. *Q965-C67*.
- Labeur, R. and J. D. Pietrzak (2005). A fully three dimensional unstructured grid non-hydrostatic finite element coastal model. *Ocean Modelling* 10(1-2), 51–67.
- Montes, J. S. (1978). A study of the undular jump profile. *Proc. 9th Australasian Fluid Mechanics Conf.*, 148–151.
- Ohtsu, I., Y. Yasuda, and H. Gotoh (2001). Hydraulic condition for undular jump formations. *Journal of hydraulic research* 39(2), 203–209.
- Ohtsu, I., Y. Yasuda, and H. Gotoh (2003). Flow conditions of undular hydraulic jumps in horizontal rectangular channels. *Journal of hydraulic engineering* 129(12), 948–955.
- Pietrzak, J., C. Kranenburg, and G. Abraham (1988). *Stratified flows*. Rijkswaterstaat, Delft hydraulics, TU Delft.

- Reinauer, R. and W. H. Hager (1995). Non-breaking undular hydraulic jump. *Journal of hydraulic research* 33(5), 683–698.
- Ryabenko, A. A. (1990). Conditions favorable to the existence of an undulating jump. *Gidrotechnicheskoe Stroitel'stvo, translated in Hydrotechnical Constructions*, 762–770.
- Stelling, G. and M. Zijlema (2003). An accurate and efficient finite-difference algorithm for non-hydrostatic free-surface flow with application to wave propagation. *Int. Journal for numerical methods in fluids* 43, 1–23.

# Appendix A

## Dataprocessing

### A.1 Velocities



The velocities at a certain point are measured at an angle of  $45^\circ$  ( $x'$  and  $z'$ ) of the horizontal and vertical direction (duration of 10 minutes, 200 measurements per second). The horizontal and vertical velocities are calculated from these signals. The mean velocities are calculated by ensemble averaging:

$$\bar{u}(x_i) = \frac{1}{N} \sum_{n=1}^N u^{(n)}(x_i)$$

The variance is calculated:

$$\sigma^2(x_i) = \frac{1}{N} \sum_{n=1}^N \left( u^{(n)}(x_i) - \bar{u}(x_i) \right)^2$$

The velocity fluctuations are determined by subtracting the mean velocity from the velocity signal:

$$u'^{(n)}(x_i) = u^{(n)}(x_i) - \bar{u}(x_i)$$

The Reynold-stresses are calculated from the velocity fluctuations:

Normal stresses:

$$q_{uu} = \rho \overline{u' u'} \quad q_{ww} = \rho \overline{w' w'}$$

Shear stresses:

$$q_{uw} = \rho \overline{u' w'}$$

The correlation between the horizontal and vertical velocity is expressed as:

$$R_{u'w'} = \frac{\overline{u' w'}}{\sqrt{\overline{(u')^2} \overline{(w')^2}}} = \frac{q_{uw}}{\sqrt{q_{uu} q_{ww}}}$$

The power spectrum is calculated by means of a Fourier transform.

## A.2 Water depths

The water depths are determined from the photos. The photos are taken for a few glass windows (100cm long, 40cm high), where the undulations occur. The photos are edited in such a way that the rectangular glass windows are also rectangular in the photo. By means of a special software program the water depth is identified.

For every window in each experiment a few photos are taken to get some sort of mean water depth. These water depths are verified by a pointer gauge at some points (end of the weir, first wavetrough, first wavetop and second wavetrough).

## A.3 Pressure

To obtain a reference value for the Pitot-tube, the pressure is measured in case of a hydrostatic distribution. The difference with the water depth provides the reference level of the Pitot tube.

## A.4 Discharge

The discharge is determined by a Rehbock weir. The water depth in the Rehbock weir, which corresponds with a certain discharge, is measured with a pointer gauge. The discharge is calculated as follows:

$$Q = C_e \frac{2}{3} b h_e \sqrt{2g h_e}$$

$$C_e = 0.602 + 0.083 \frac{h}{p}$$

$$h_e = h + 0.0012$$

$h$ =waterdepth above the weir

$p$ =height of the weir

$b$ =width of the weir

## Appendix B

# Water Profiles

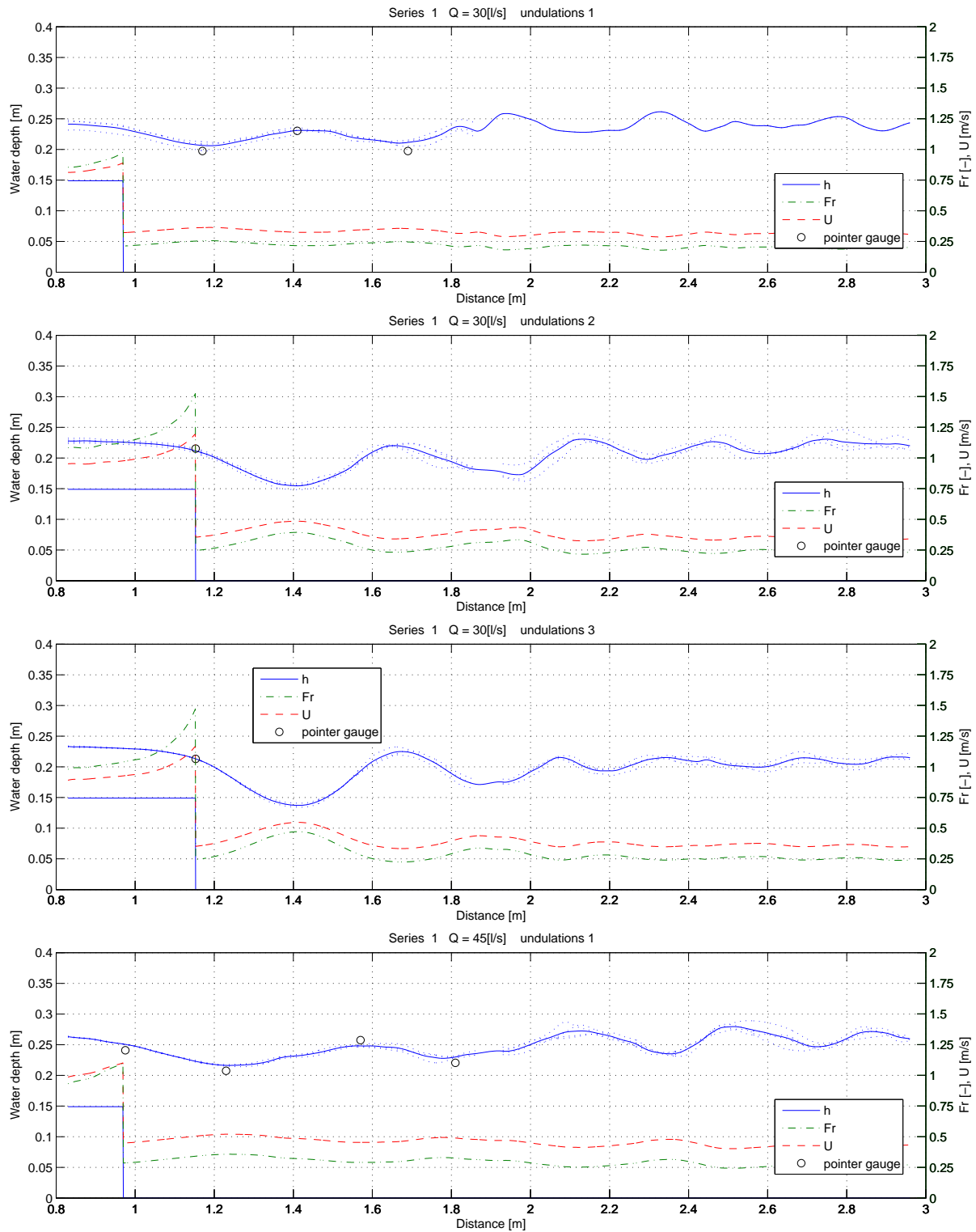
The water profiles of all the conducted experiments are given. The water flows from the left to the right. The obstacle is visible in the left corner. The dotted lines are the water depths derived from the photos. These lines show some variation caused by:

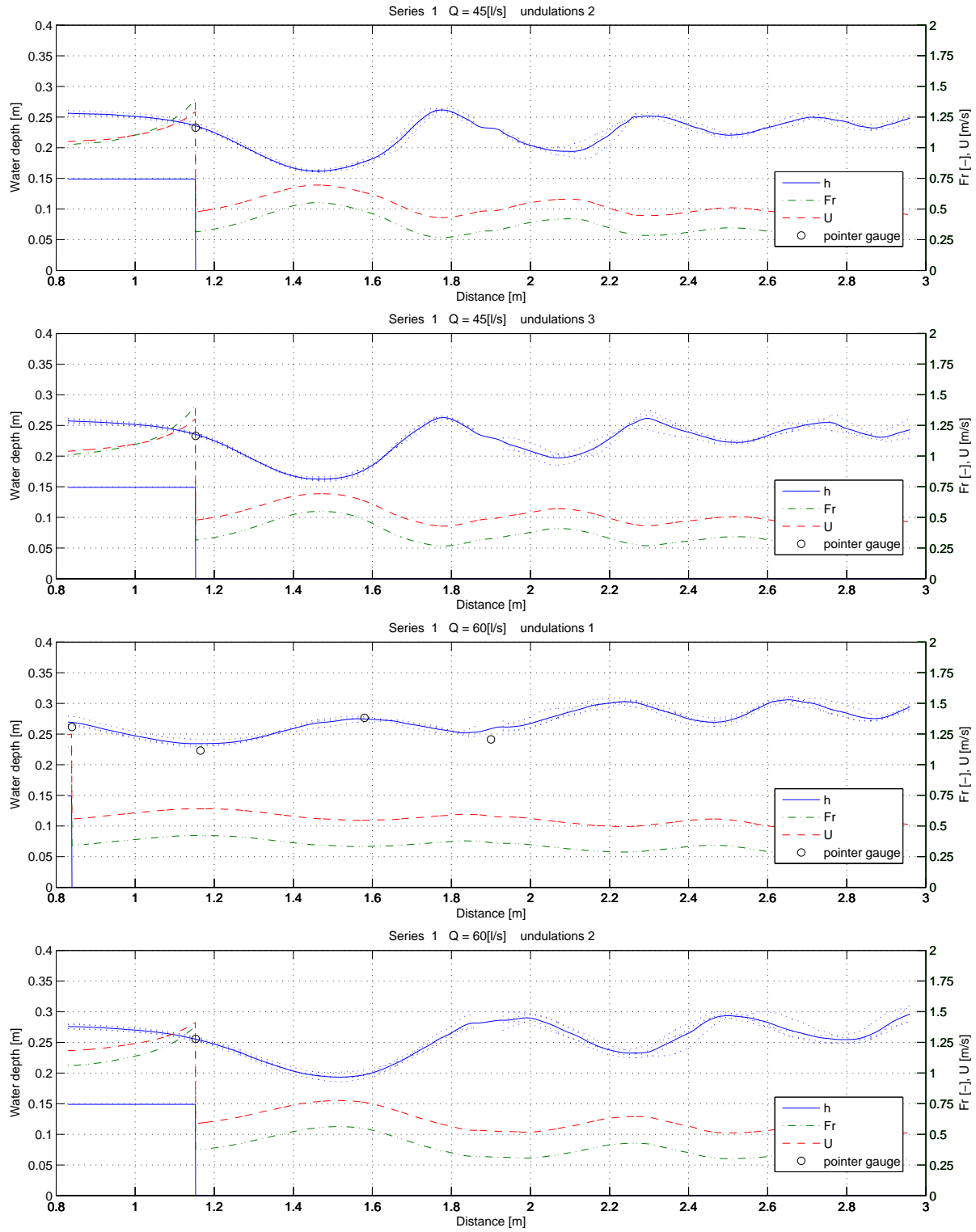
- In some cases, mainly for lower degrees of submergence, the undulations are not stable. They become steeper and steeper until they break. This process repeats itself. In this way, a photo of the water depth just before breaking of the wave differs from a photo after breaking.
- The undulations move a little up and downstream, depending on the natural frequency of the flume.
- The method of obtaining the water depths from pictures is slightly inaccurate, especially when the water depth in the middle of the flume differs from the water depth on the sides. This occurs for series 2 and 3 (smooth downstream part of the weir), where the water depth varies over the width.

The solid line is the average of the dotted lines and gives a good impression of the waves behind the obstacle. In the middle of the figure (between  $x=1.8\text{m}$  and  $x=1.9\text{m}$ ), the steel girders block the view of the camera, so the mean water depth between these windows is interpolated. The water depth measured with the pointer gauge is given by the circle, which forms a check to the water profile.

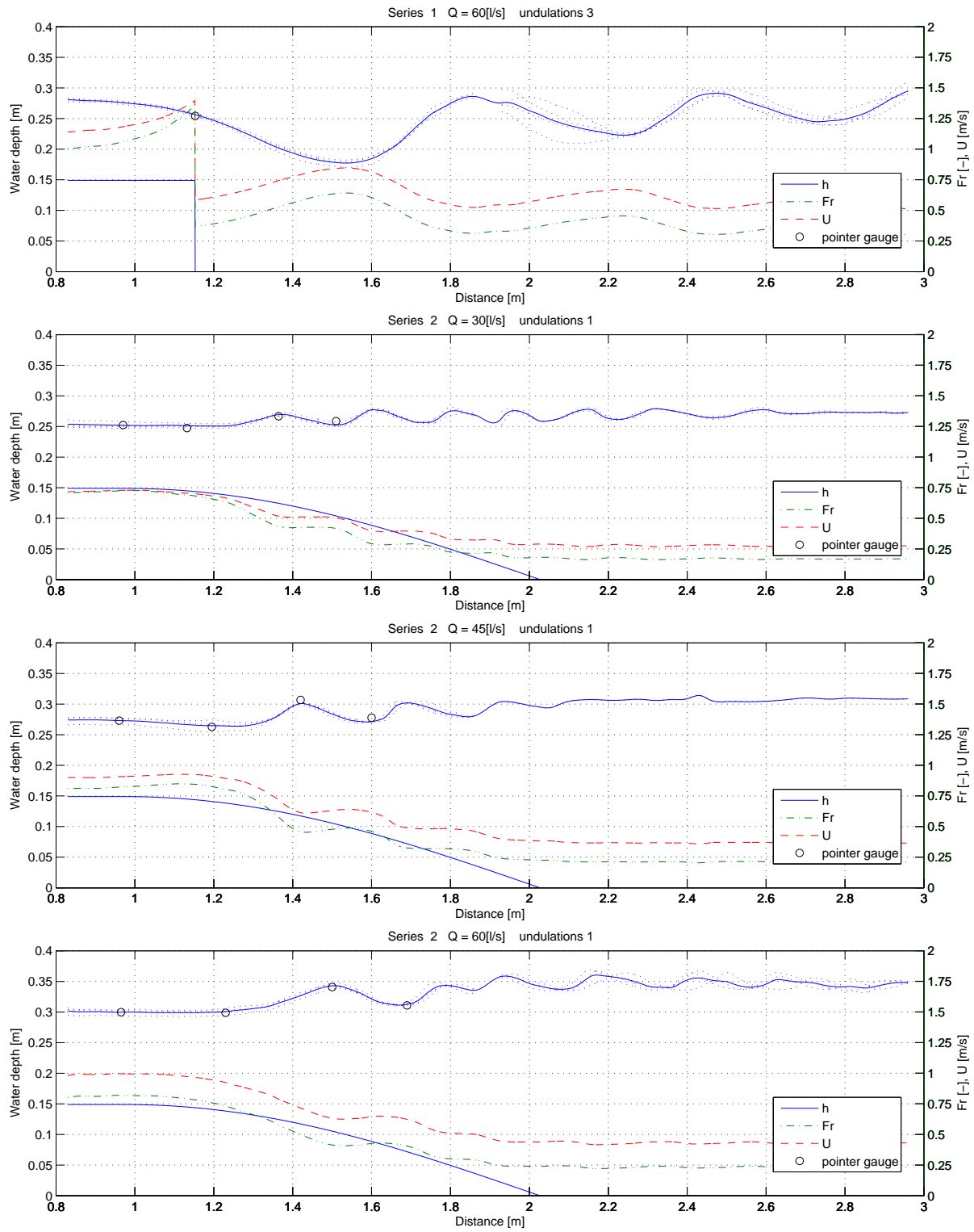
The mean velocities and the Froude numbers are plotted on the secondary axis. The wave lengths and wave heights are derived from these figures.

## B. Water Profiles

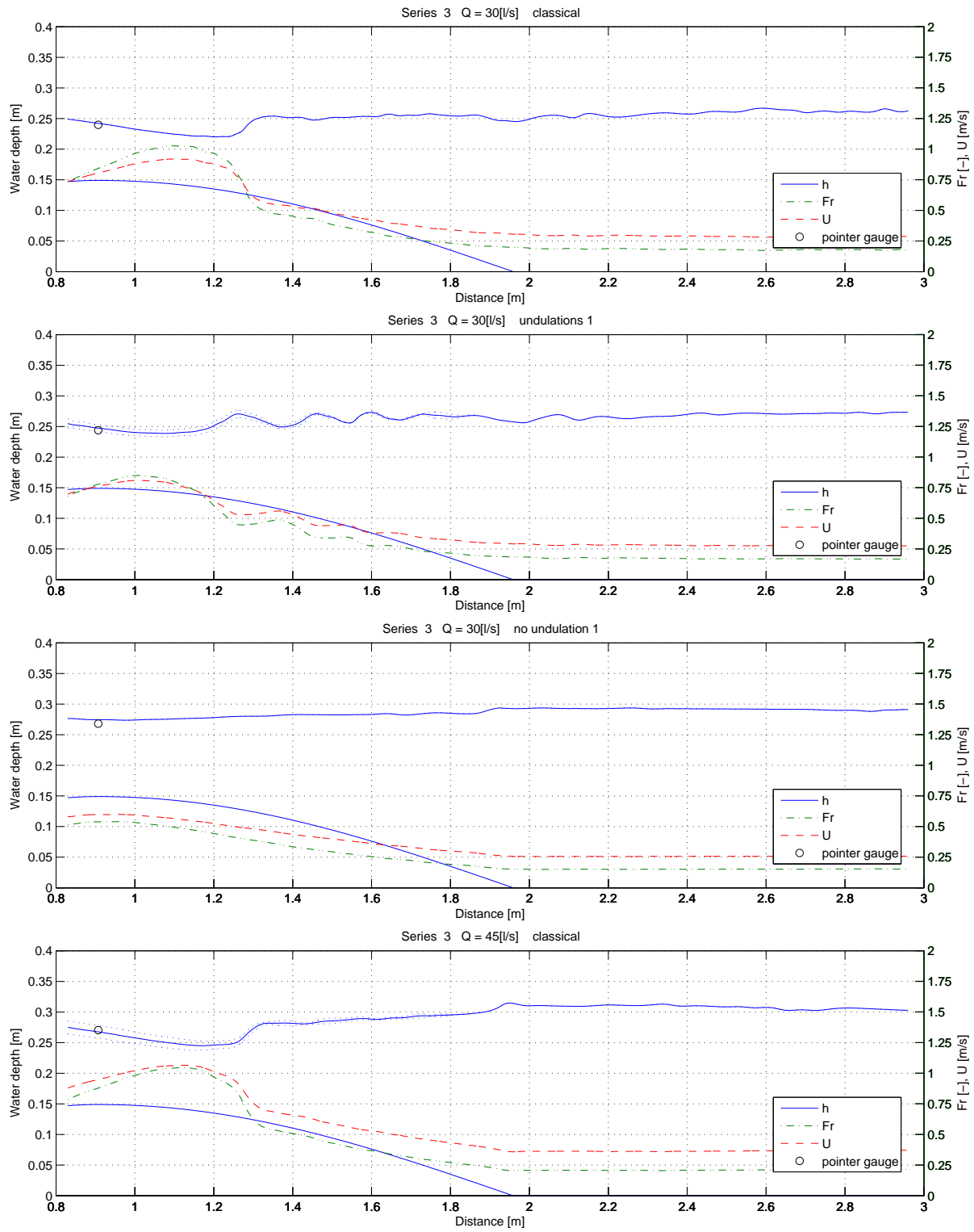




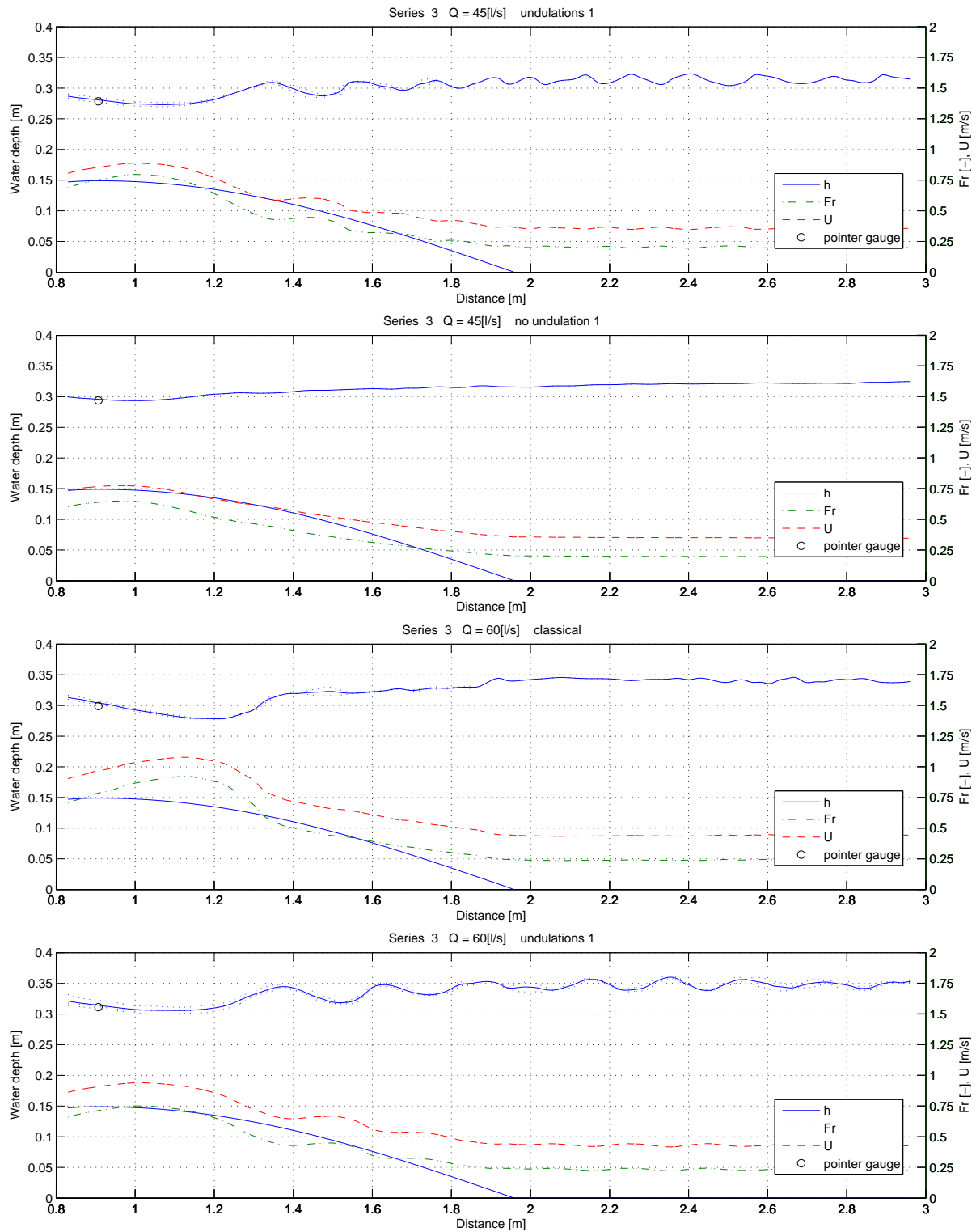
## B. Water Profiles

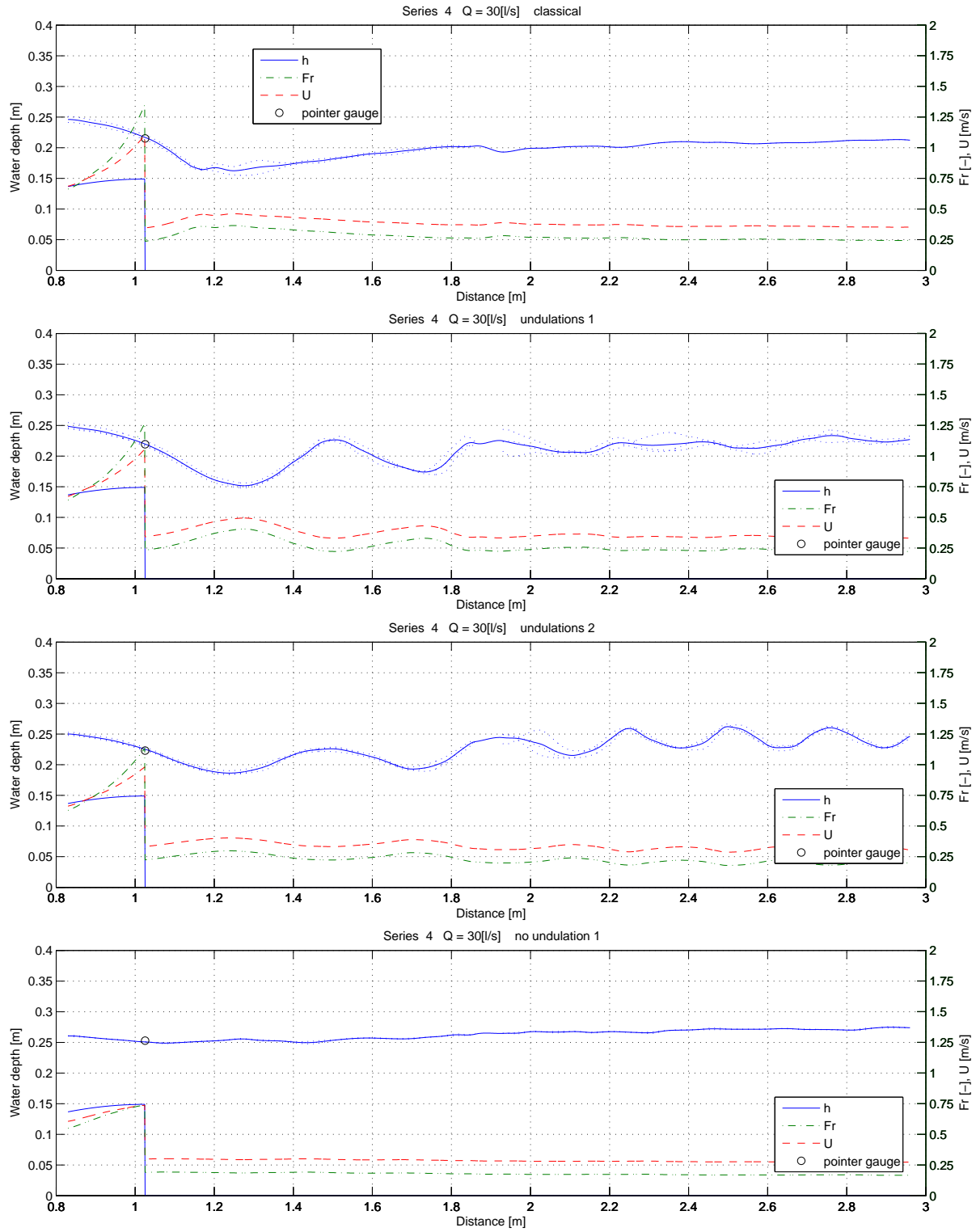




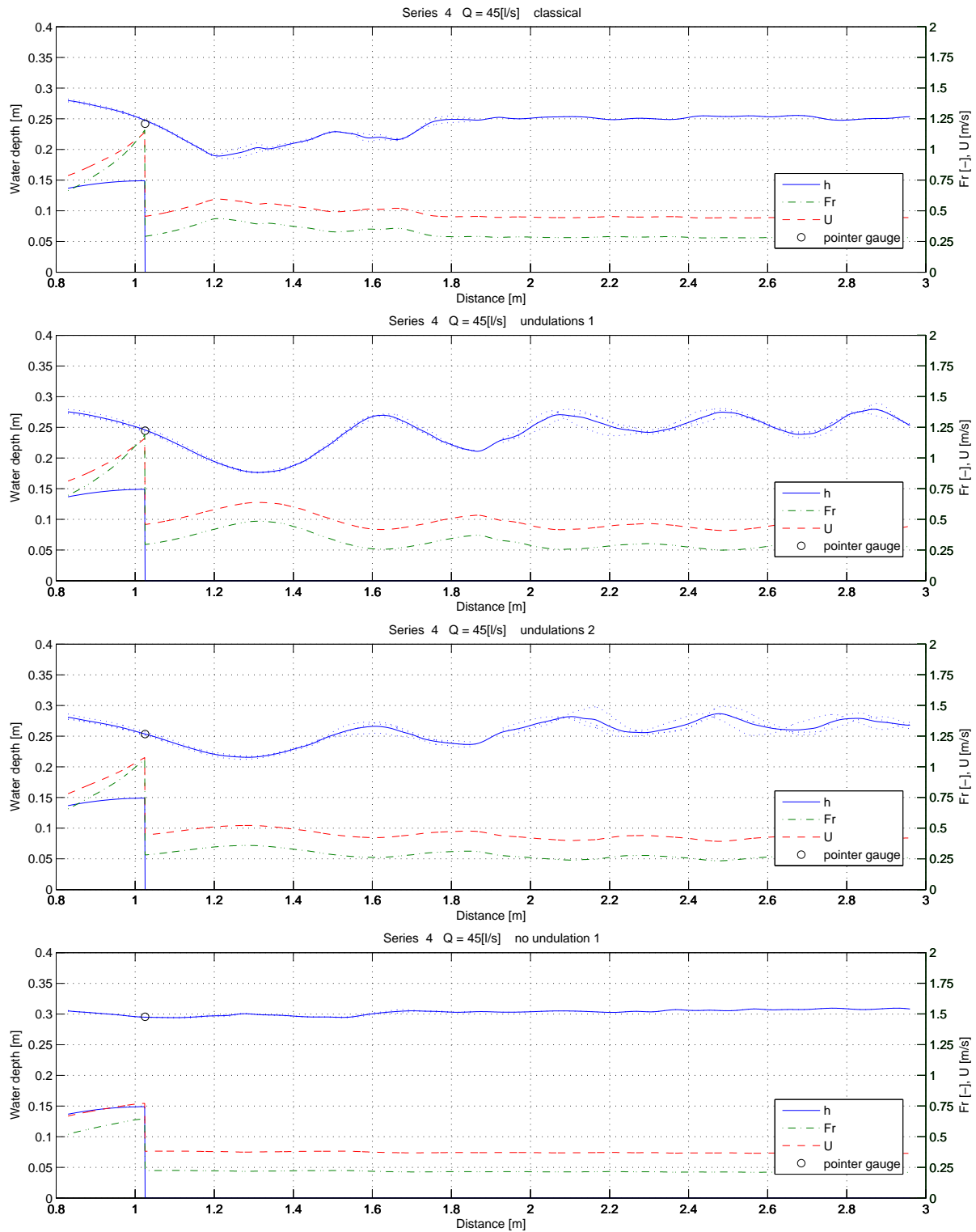


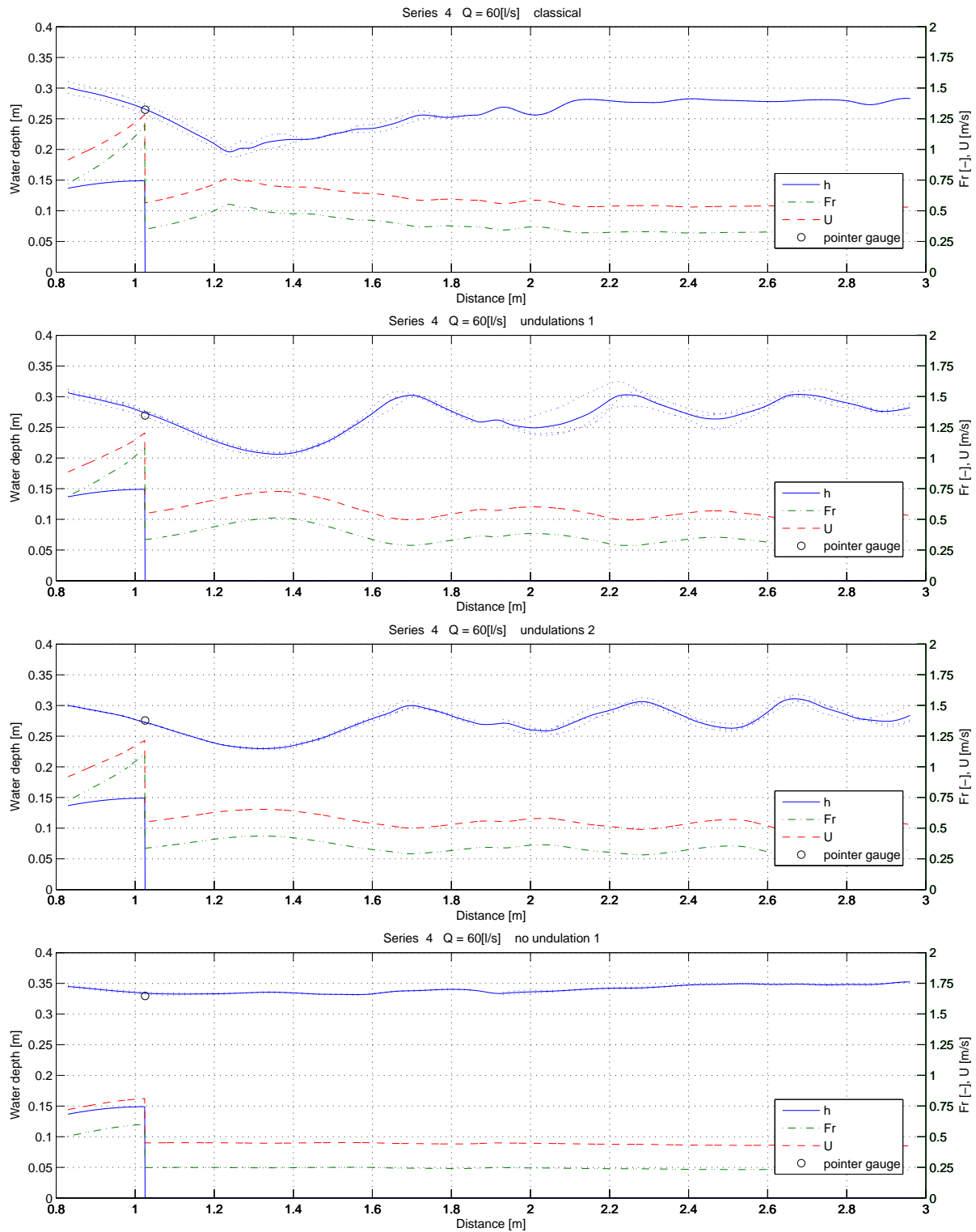
## B. Water Profiles



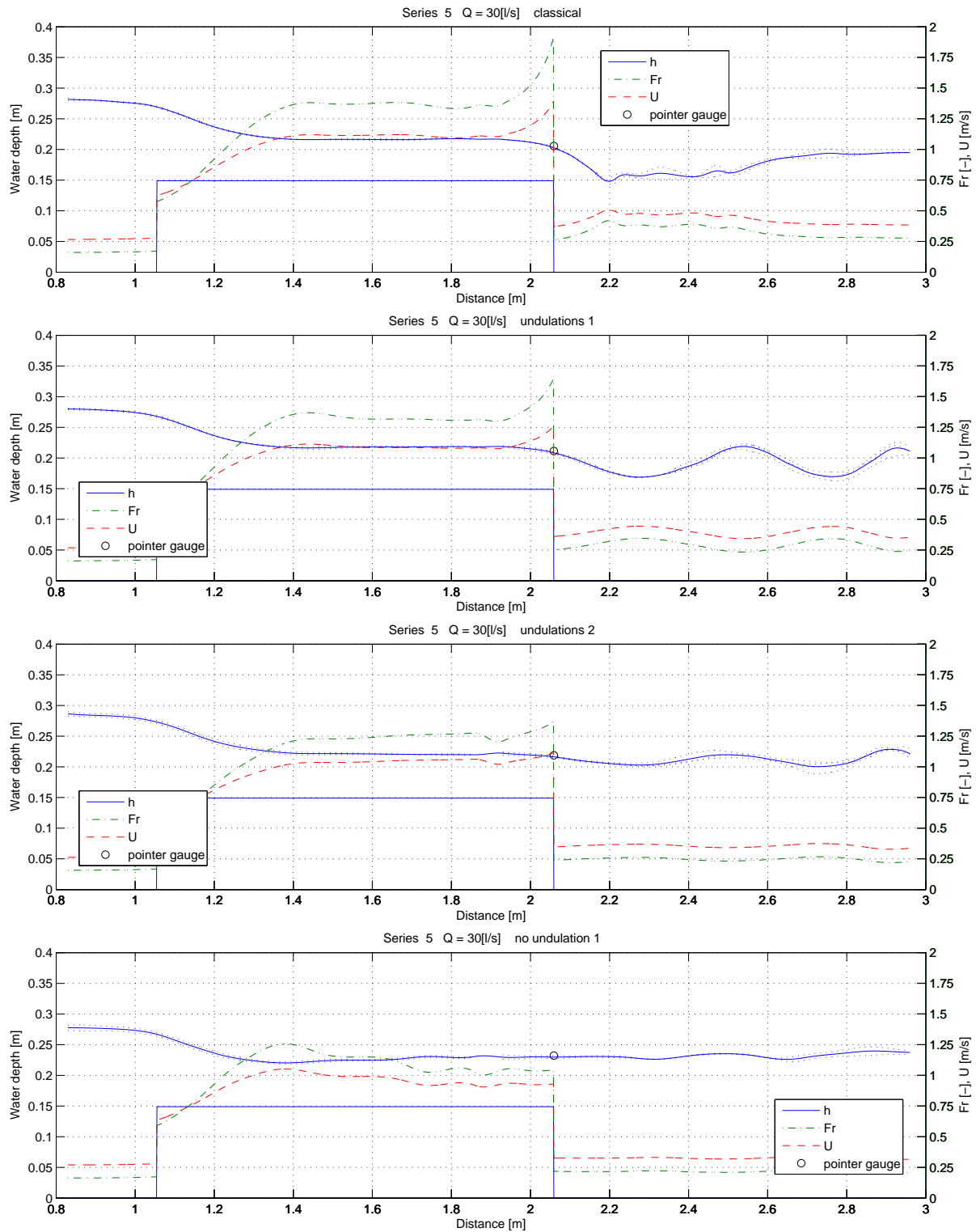


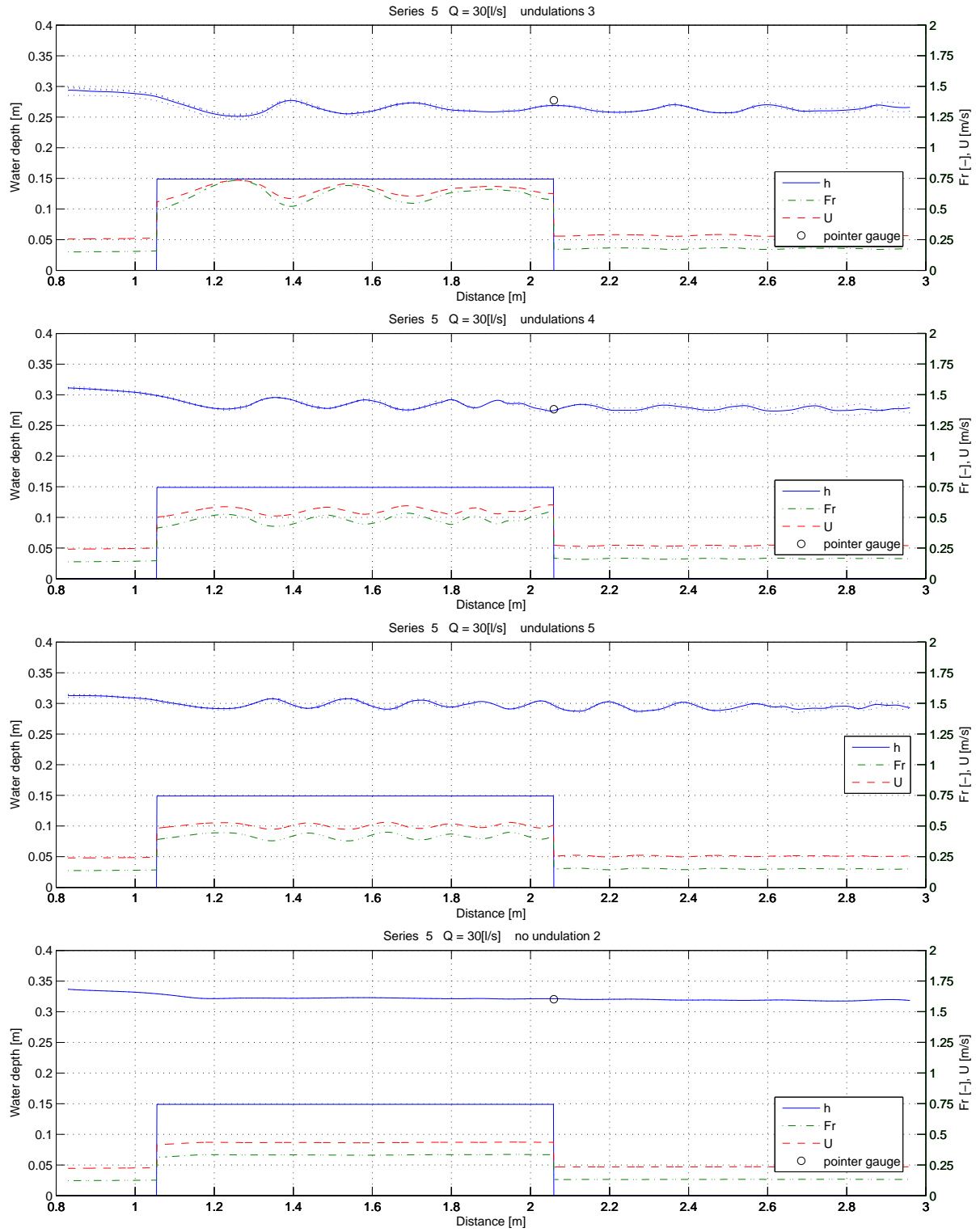
## B. Water Profiles



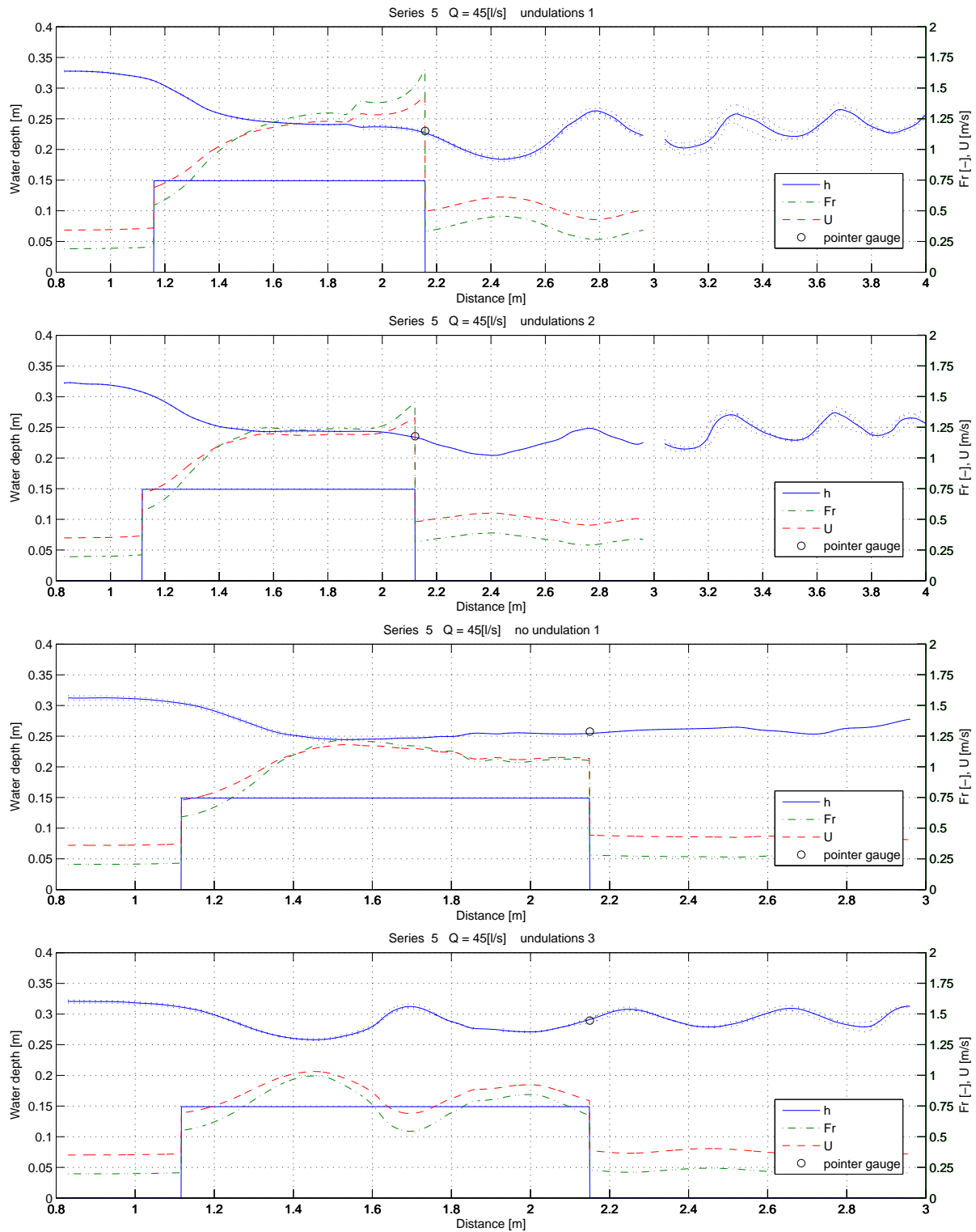


## B. Water Profiles

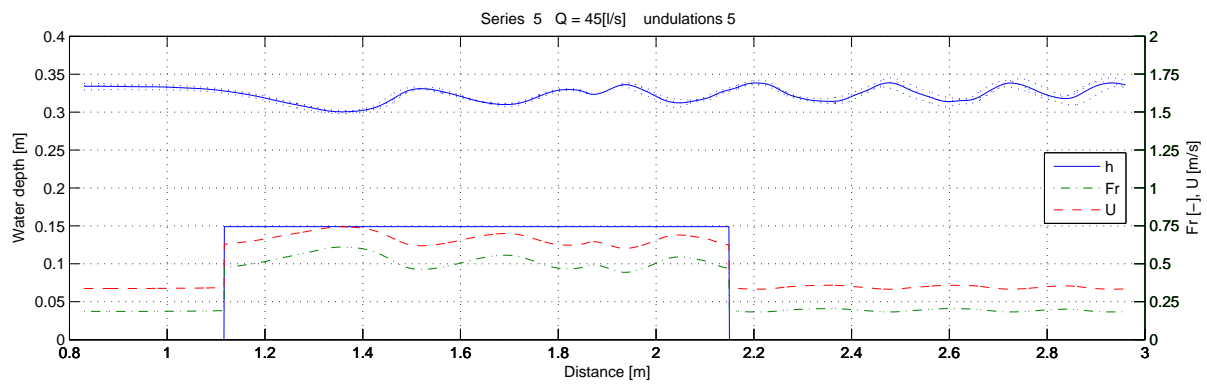
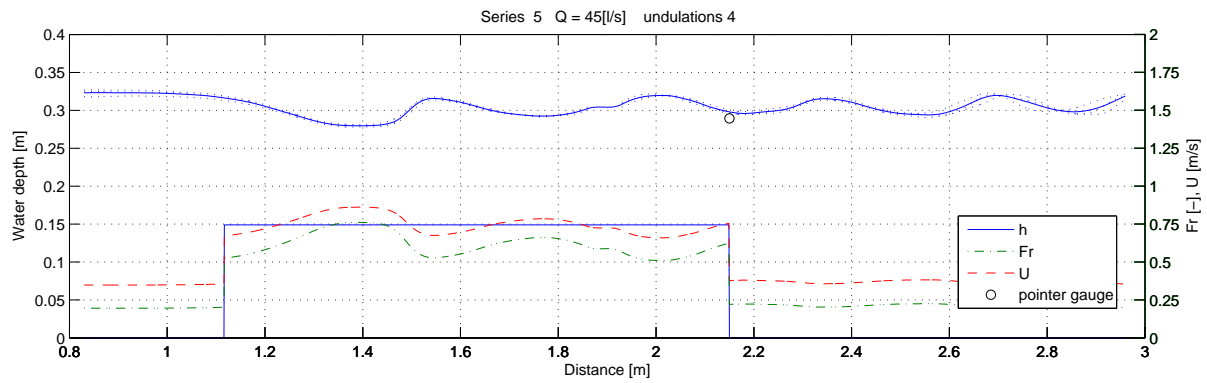




## B. Water Profiles









## Appendix C

# Verification LDA-measurement

The values of the velocities are verified by comparing the measured discharge with the calculated discharge from the velocity profile. The discharge is calculated in the following manner ( $h$ =water depth):

$$Q = B \int_0^h u(z) dz$$

For the velocity profiles under the waves, there were some large deviations (up to 1.4). Two calibration measurements are conducted to verify the measurements of the LDA:

- Flow above a sharp weir, the flow is critical above the weir, so the velocity can be calculated from the water depth ( $Fr = 1 \implies U = \sqrt{gh}$ ). The mean velocity calculated from the velocity profile in Figure C.1 is in good agreement with the velocity calculated from the water depth. The discharge determined by integrating the velocity profile is also in good agreement with the discharge measured from the Rehbock weir (see Table C.1).

	$Q_r$ [l/s]	$h$ [m]	$U$ [m/s]
Measurement (pointer gauge)	23.5	7.12	0.836
LDA	24.3		0.85

**Table C.1:** Sharp weir

- Flow over a horizontal bottom, no weir. The discharge calculated from the velocity profile is somewhat higher than the measured discharge (see Table C.2).

	$Q_r$ [l/s]
Measurement (pointer gauge)	45.4
LDA	49.5

**Table C.2:** Flow over a horizontal bottom

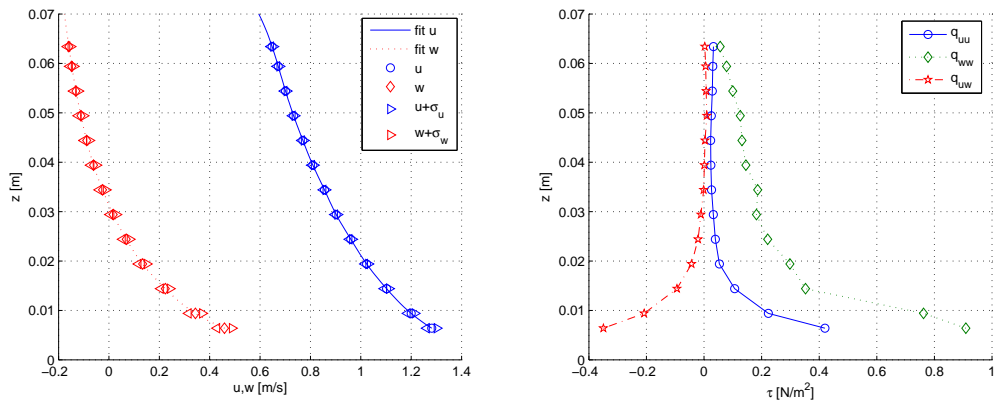


Figure C.1: Calibration sharp weir

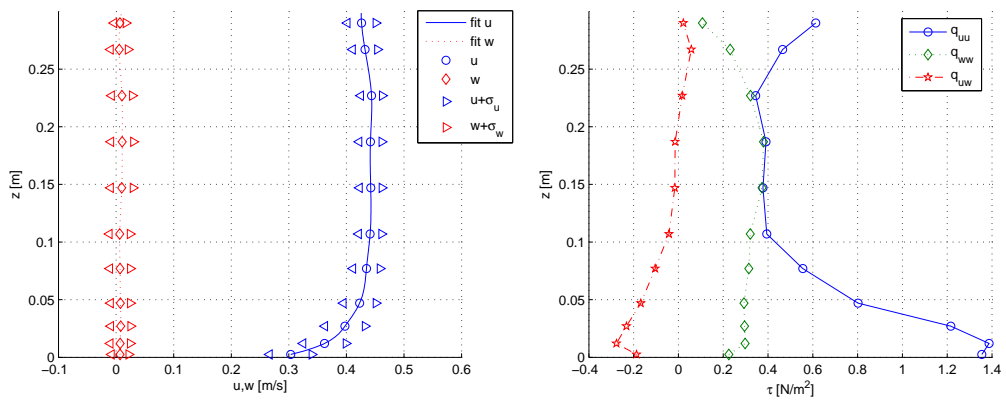
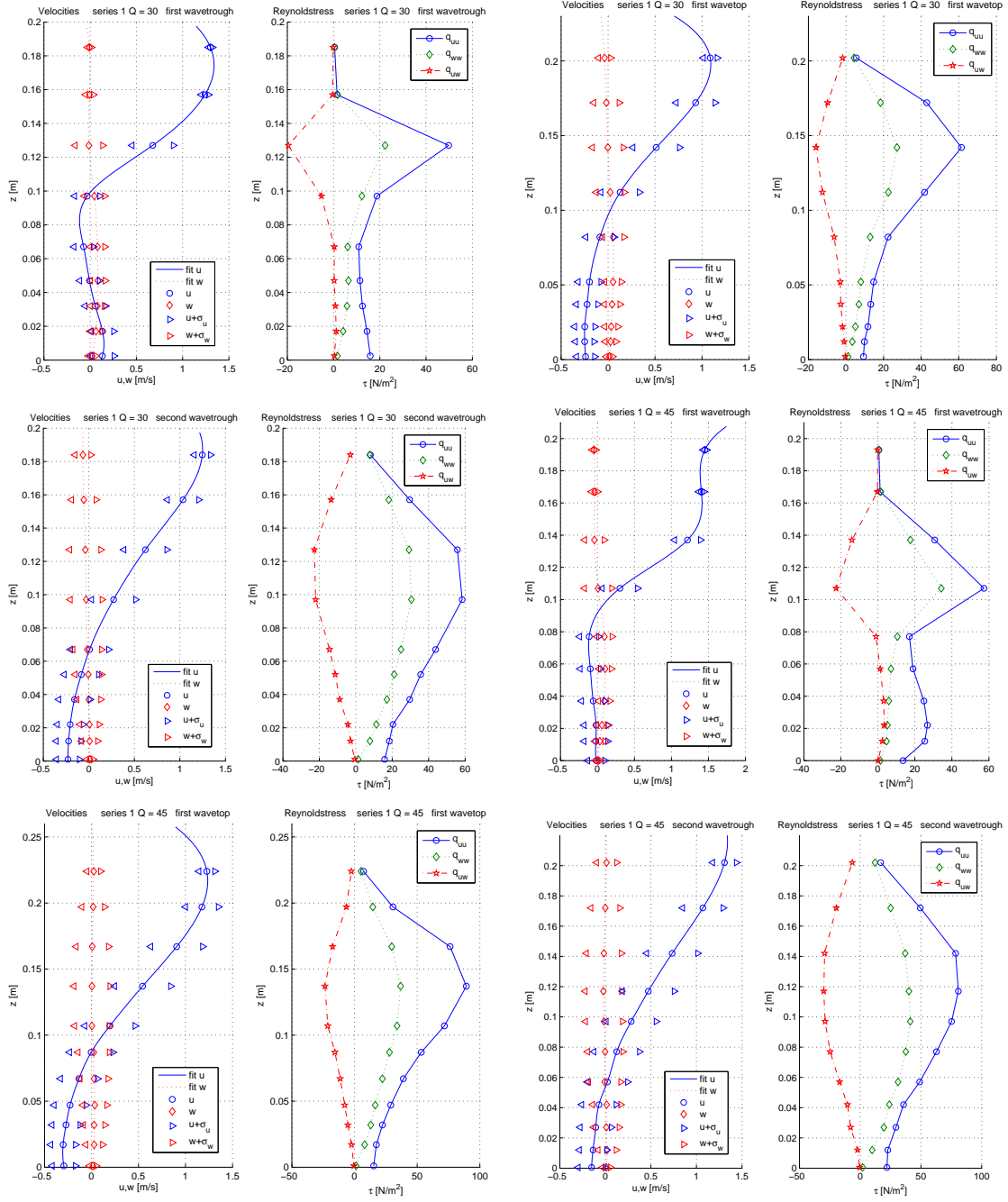


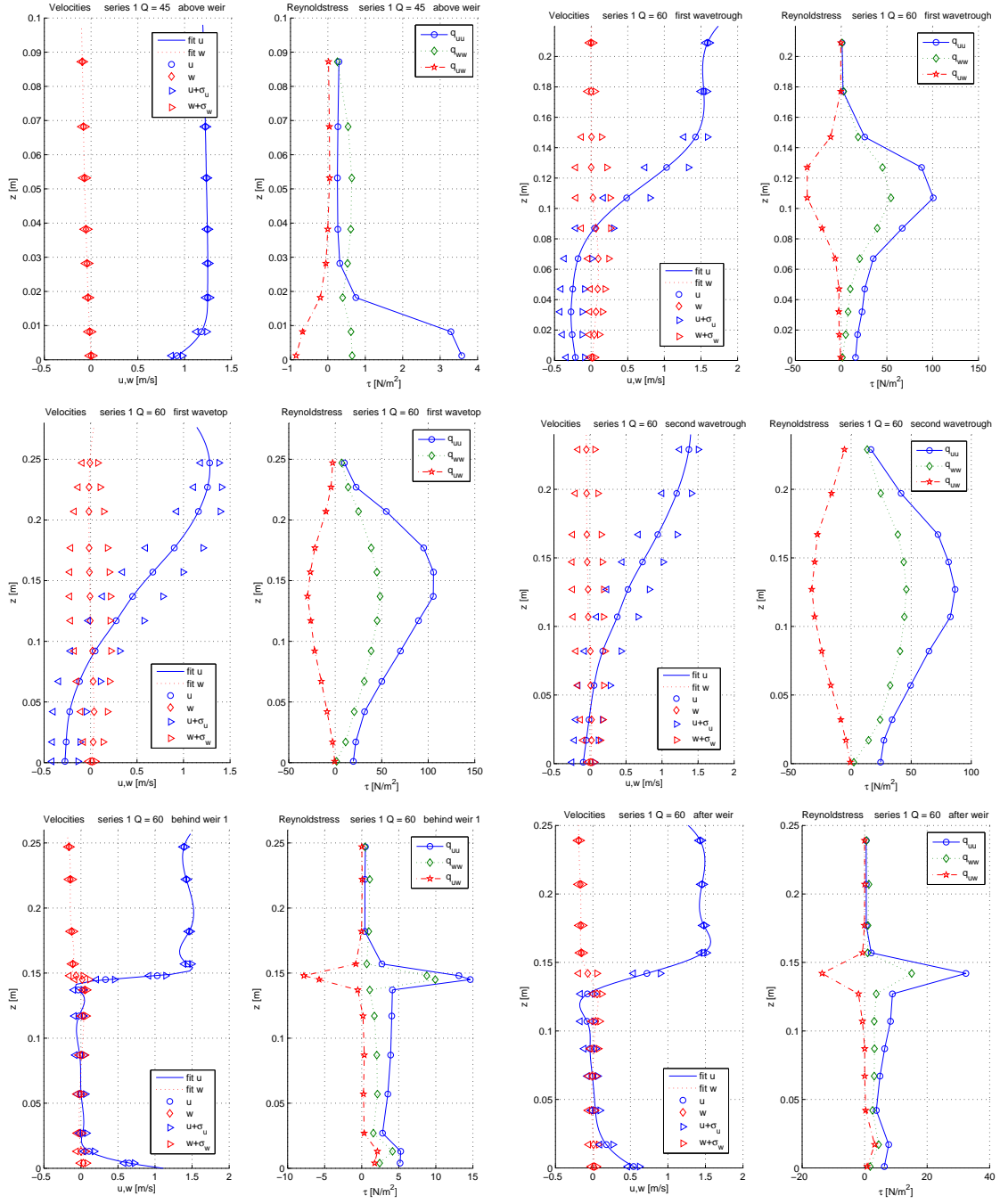
Figure C.2: Calibration horizontal bottom

## Appendix D

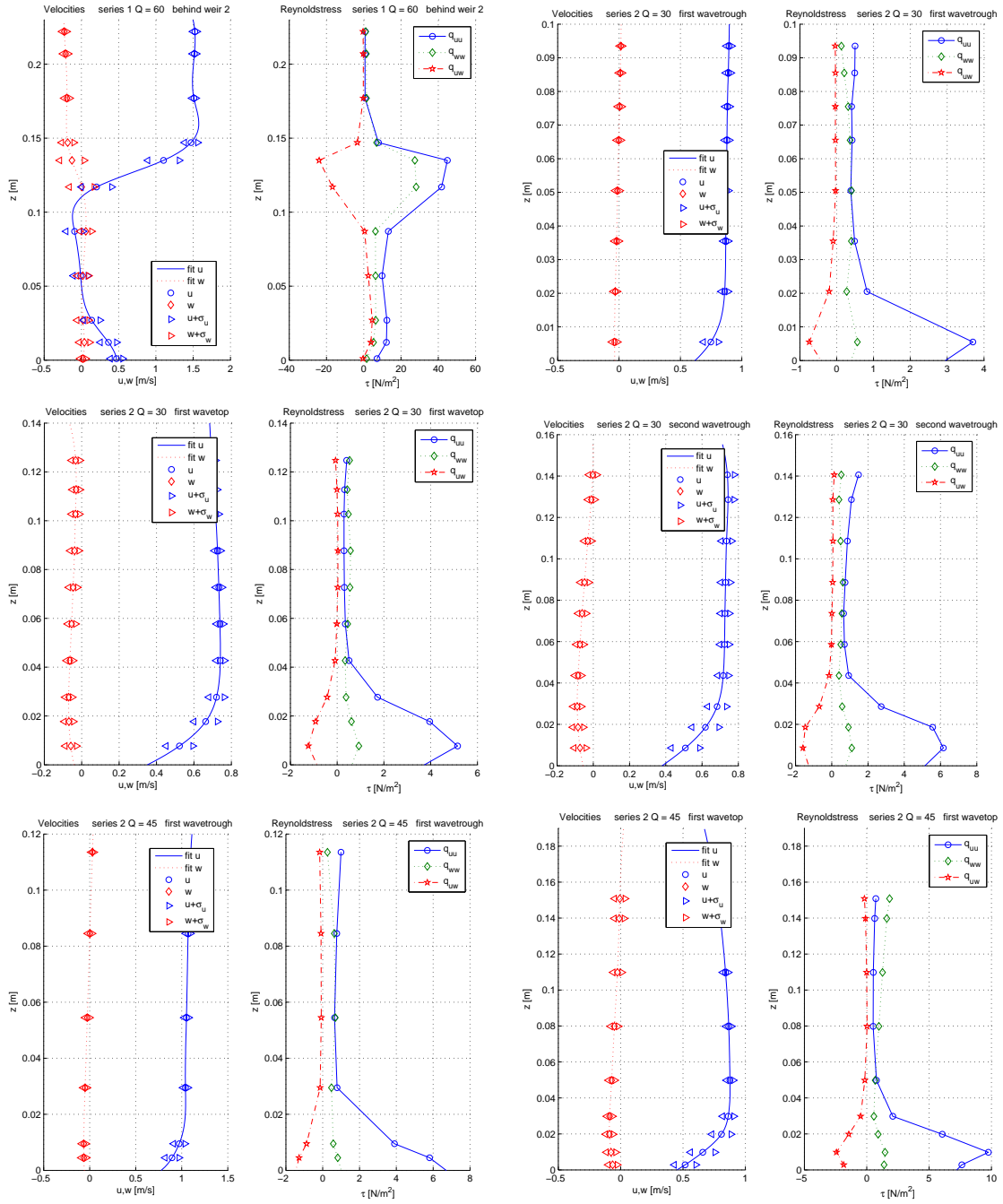
# Velocities and Reynoldsstresses

## D. Velocities and Reynoldsstresses

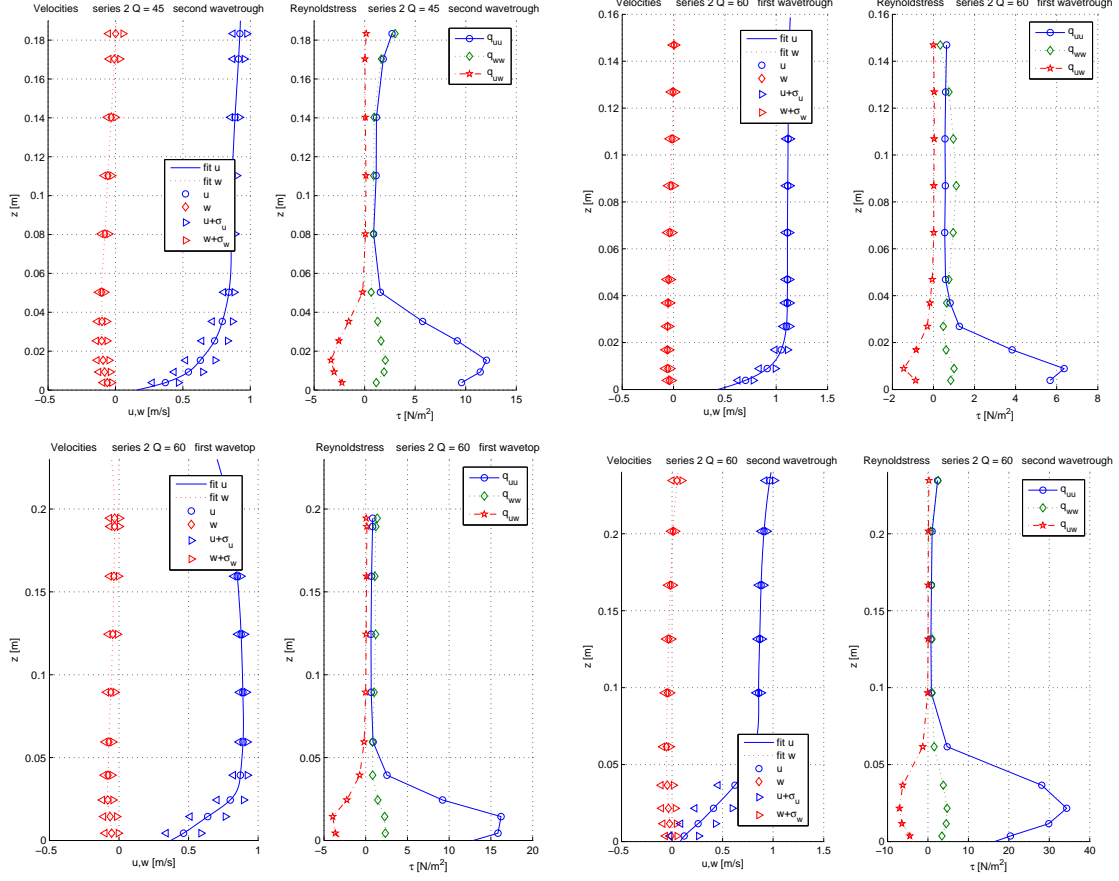




## D. Velocities and Reynoldsstresses





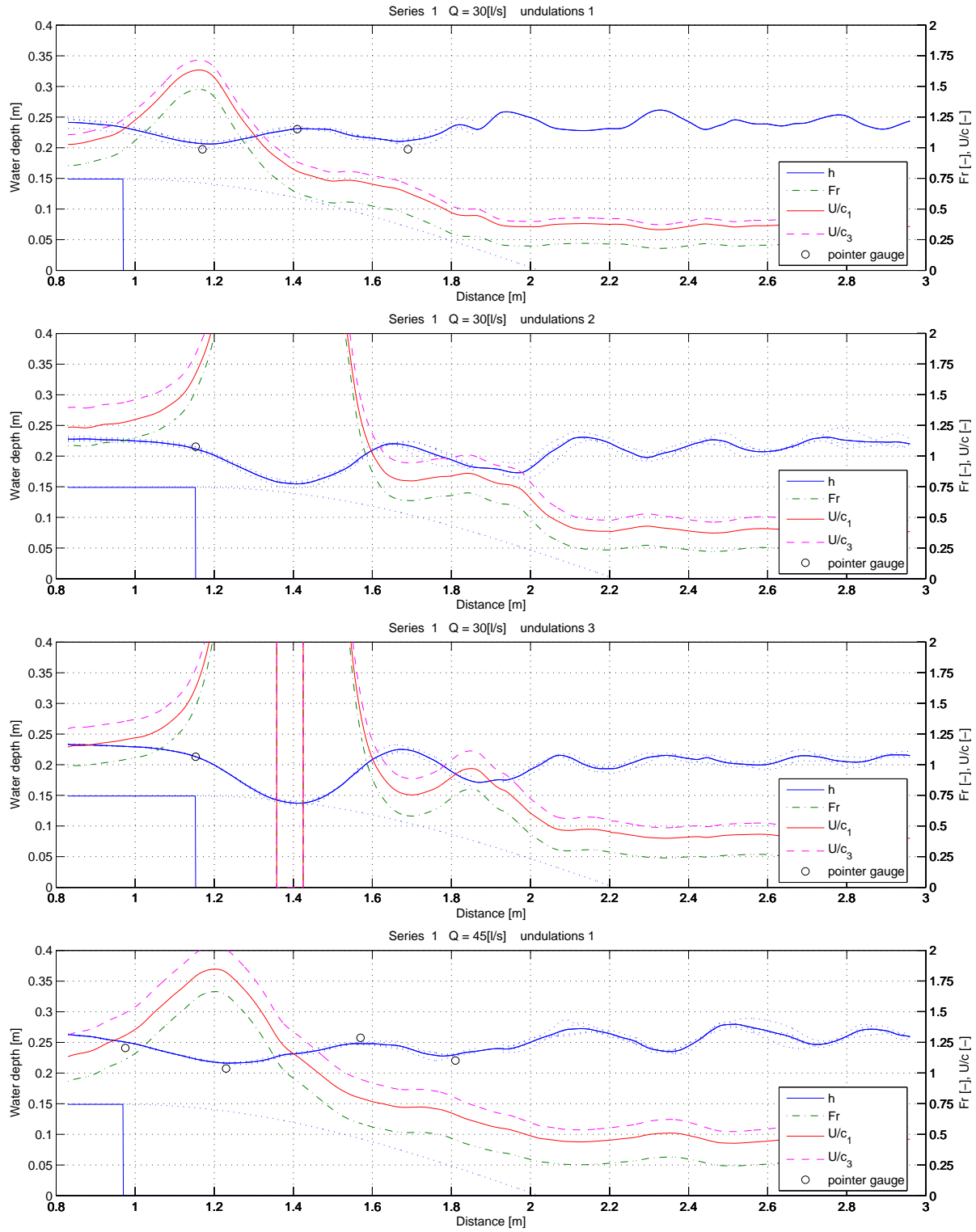


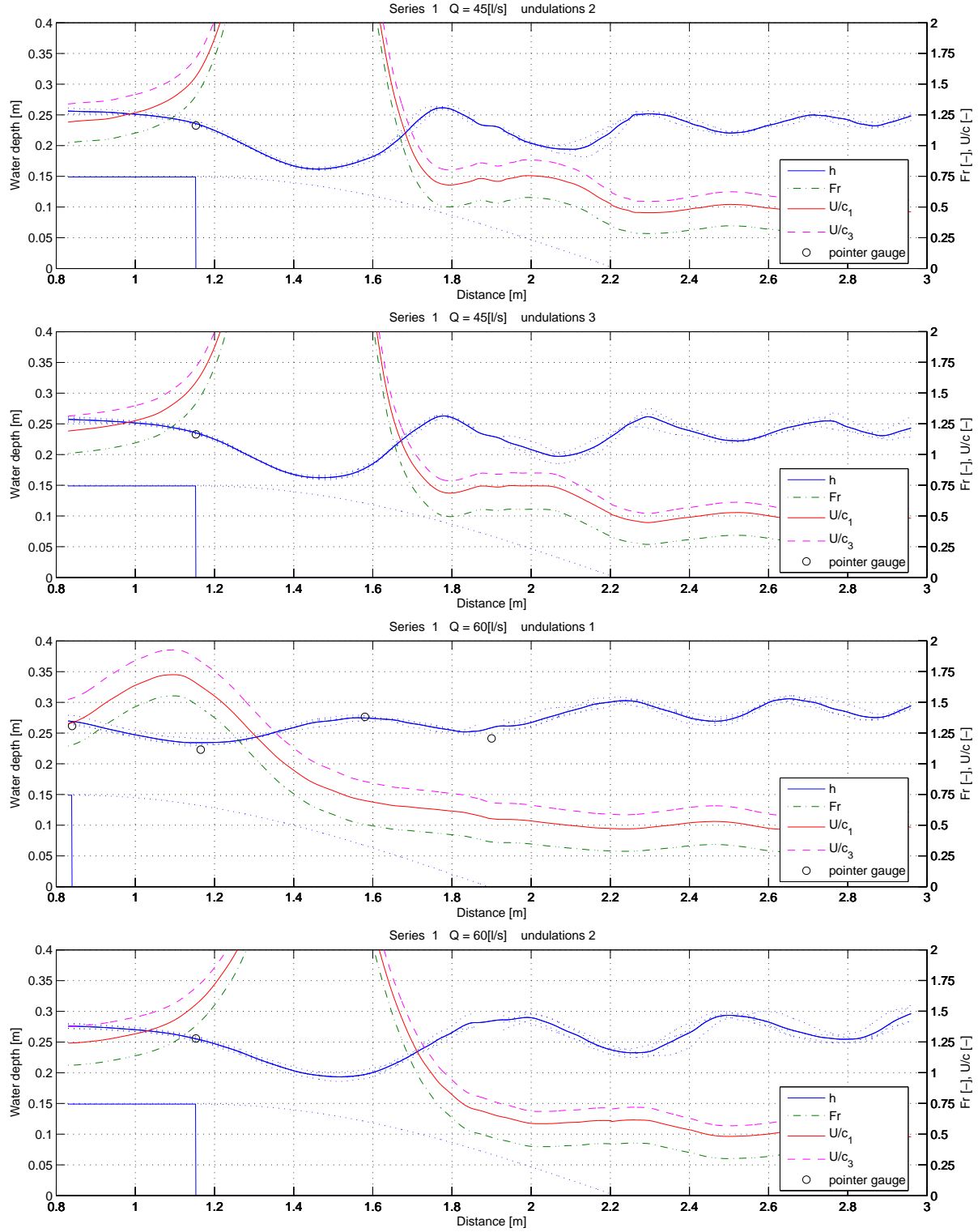


## Appendix E

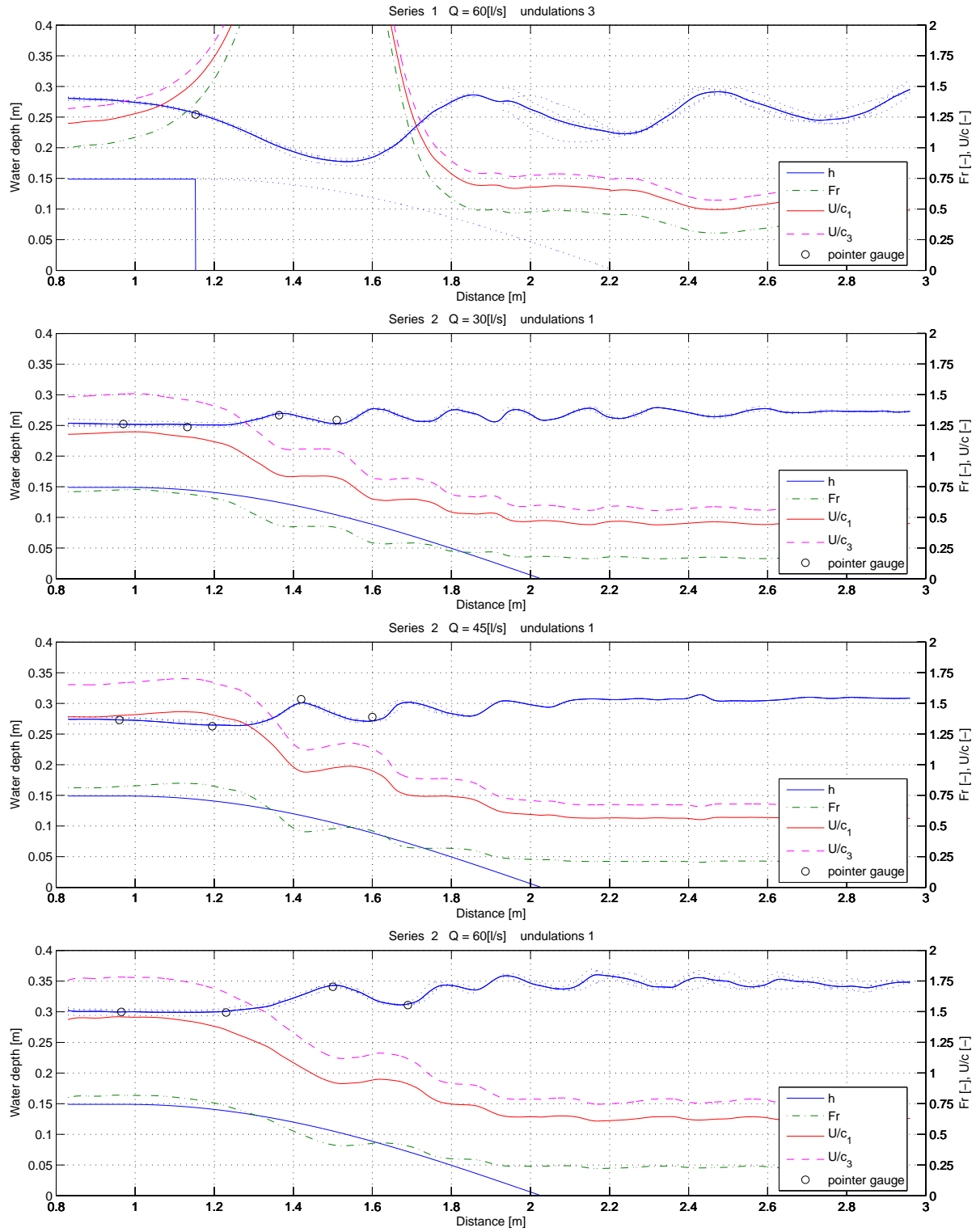
### Water Profiles Wave celerity

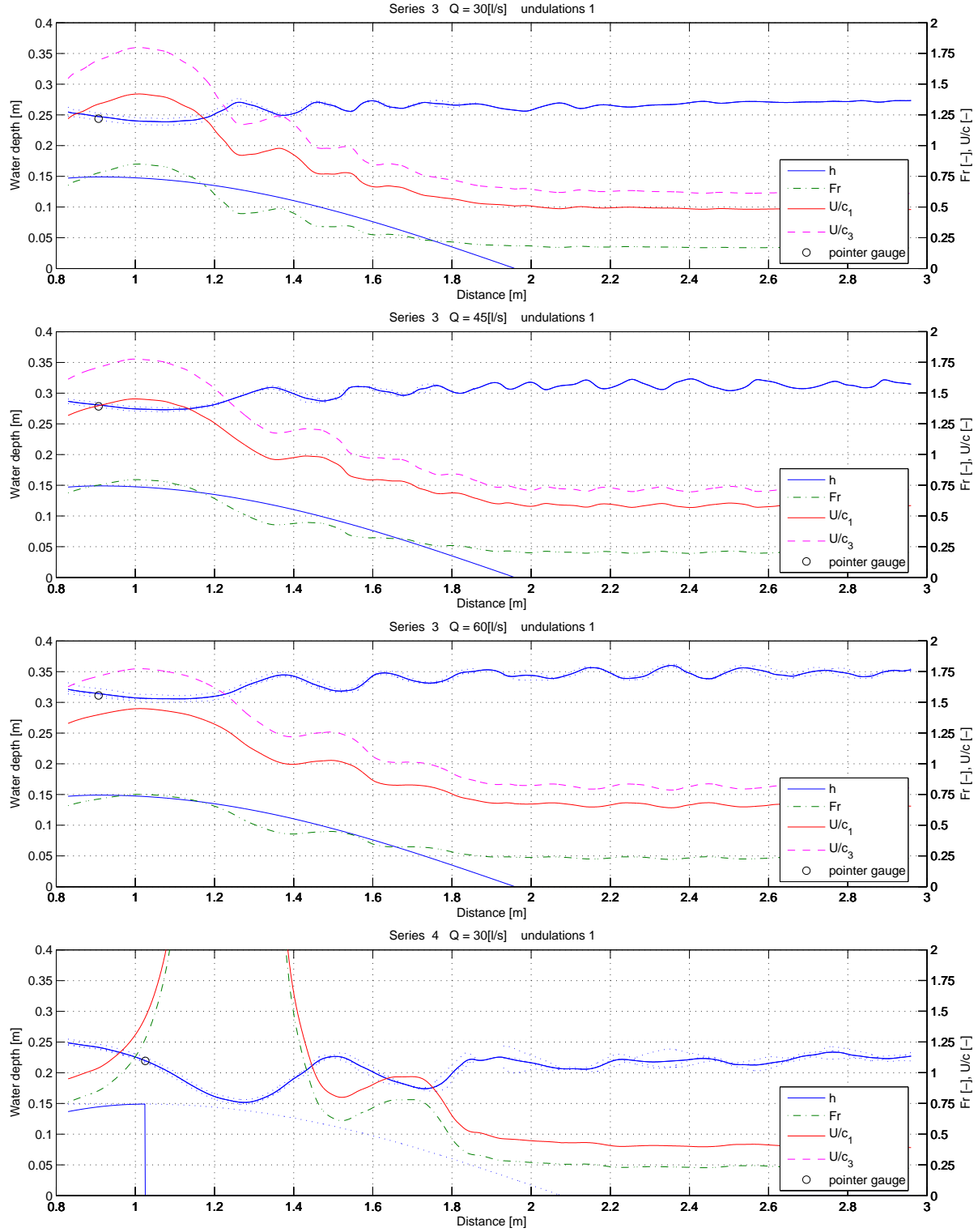
## E. Water Profiles Wave celerity



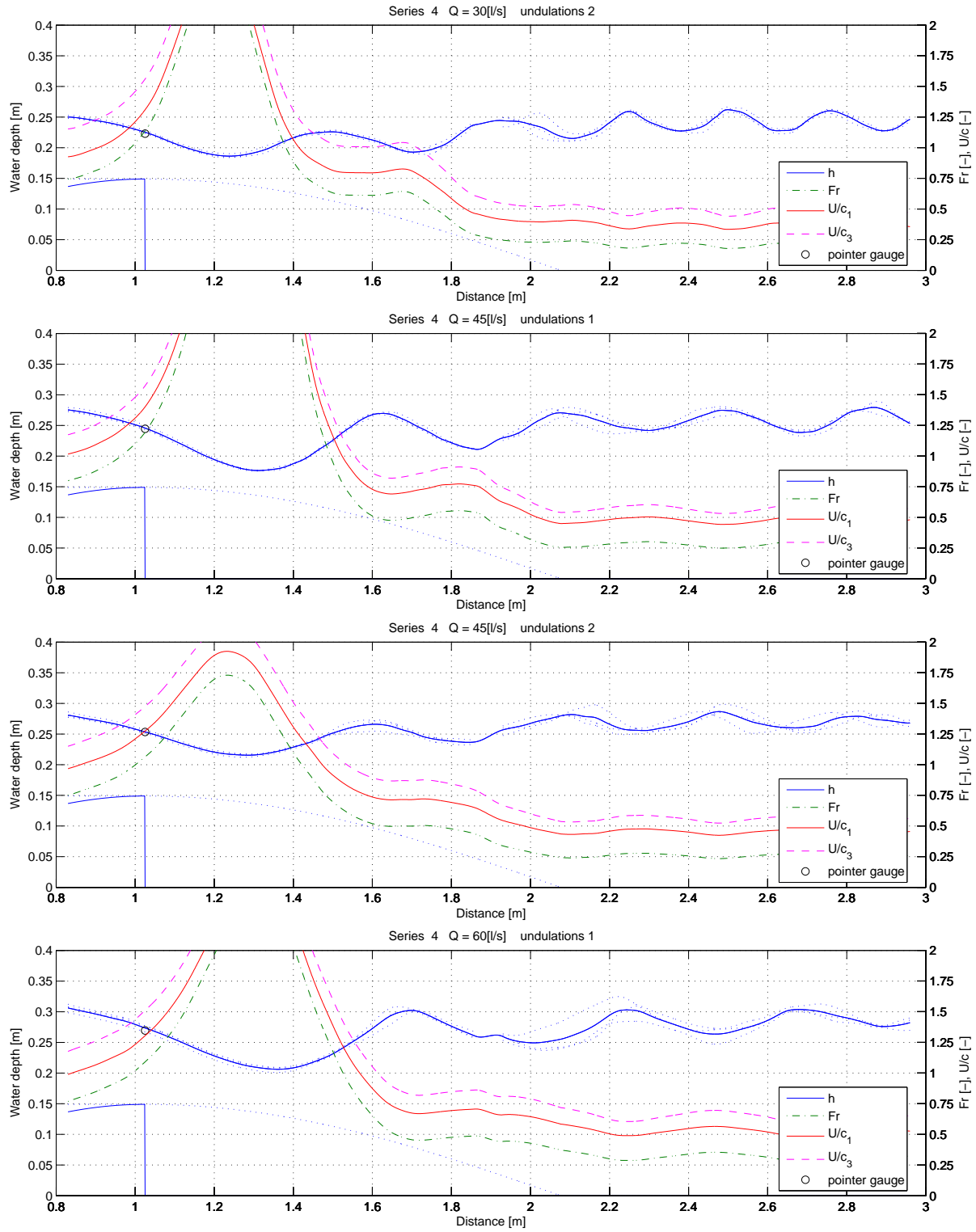


## E. Water Profiles Wave celerity

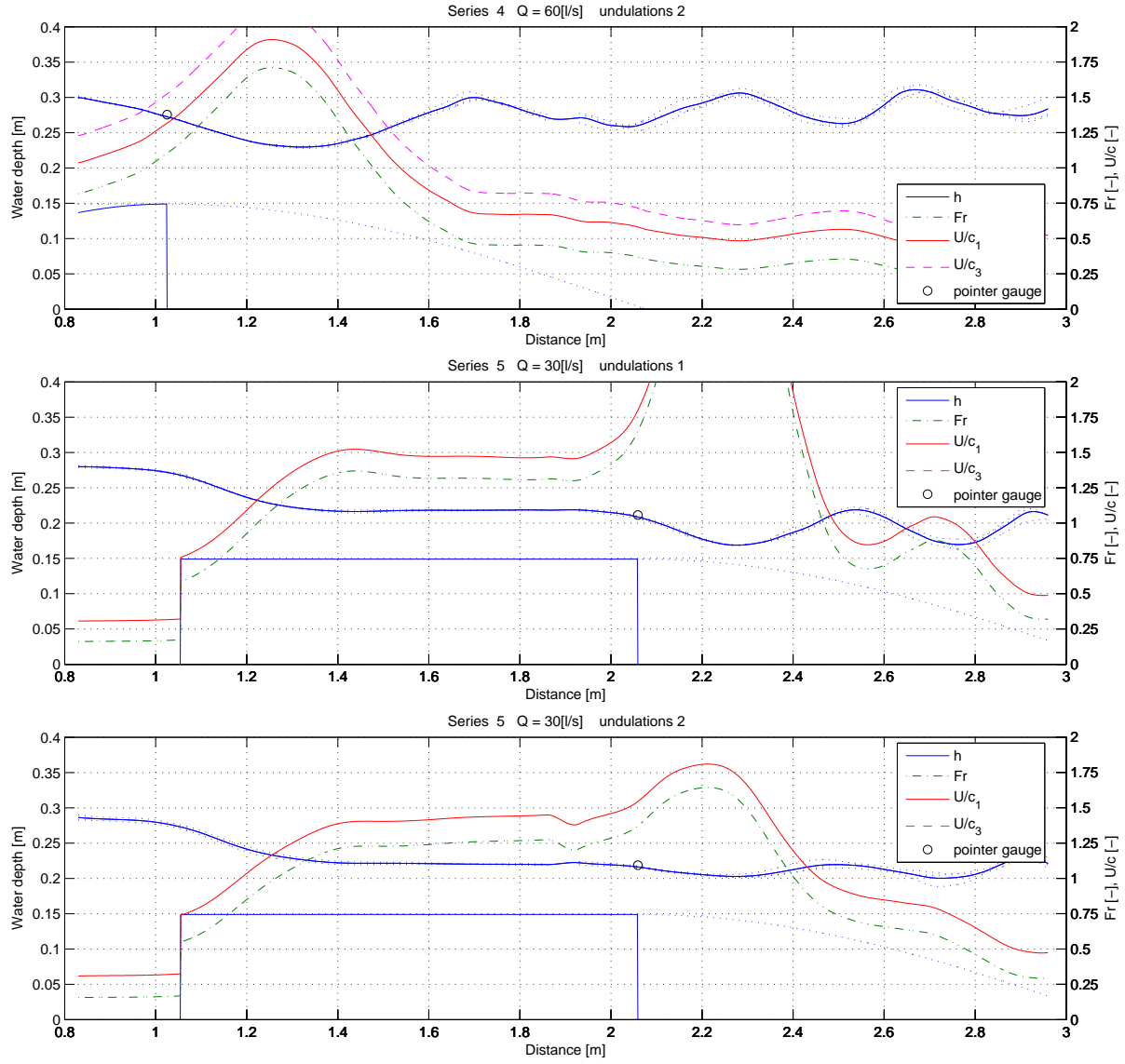




## E. Water Profiles Wave celerity









## Appendix F

# Numerical implementation Boussinesq equations

### F.1 Linearized equations

The linear Boussinesq equations is given by:

$$(1 - F^2) \eta + F^2 h_b + \frac{1}{3} F^2 h^2 \frac{d^2 \eta}{dx^2} + \frac{1}{6} F^2 h^2 \frac{d^2 h_b}{dx^2} = 0 \quad (\text{F.1})$$

Discretization of the equation F.1 leads to:

$$(1 - F^2) \eta^m + F^2 h_b^m + \frac{1}{3} \frac{1}{\Delta x^2} (\eta^{m-1} - 2\eta^m + \eta^{m+1}) + \frac{1}{6} F^2 h^2 \frac{1}{\Delta x^2} (h_b^{m-1} - 2h_b^m + h_b^{m+1}) = 0$$
$$\eta^{m+1} = -\eta^{m-1} + 2\eta^m - 3 \frac{\Delta x^2}{h^2} \left( \frac{1 - F^2}{F^2} \eta^m + 3h_b^m \right) - \frac{1}{2} (h_b^{m-1} - 2h_b^m + h_b^{m+1}) \quad (\text{F.2})$$

**Adding bottom friction** The term for the bottom friction is given by (expression

$$-2f_b F^2 \frac{\eta - h_b}{h} \quad (\text{F.3})$$

For the substitution of the friction term into equation F.1, expression F.3 is integrated once:

$$-2 \frac{f_b F^2}{h} \int (\eta - h_b) dx$$

Discretizing this term in the same way as in equation F.2 gives:

$$-3 \frac{f_b \Delta x^2}{h^3} \sum_{m=1}^{mmax} ((\eta - h_b)^m + (\eta - h_b)^{m-1}) \Delta x$$

## F.2 Non-linearized equations

The original steady state equations without friction are considered again:

Continuity:

$$\frac{\partial h}{\partial t} + \frac{\partial}{\partial t}(hu) = 0 \quad (\text{F.4})$$

Momentum (depth-averaged):

$$u \frac{\partial u}{\partial x} + g \frac{\partial}{\partial x}(h + h_b) - \frac{1}{3}h^2 u \frac{\partial^3 u}{\partial x^3} + \frac{1}{2}hu^2 \frac{\partial^3 h_b}{\partial x^3} = 0 \quad (\text{F.5})$$

Momentum is written as:

$$q \frac{\partial u}{\partial x} + gh \frac{\partial}{\partial x}(h + h_b) - \frac{1}{3}qh^2 \frac{\partial^3 u}{\partial x^3} + \frac{1}{2}q^2 \frac{\partial^3 h_b}{\partial x^3} = 0 \quad (\text{F.6})$$

Discretization of this equations leads to:

$$\begin{aligned} q \frac{u^{m+1} - u^m}{\Delta x} + gh \frac{h^{m+1} - h^m + h_b^{m+1} - h_b^m}{\Delta x} - \frac{q(h^m)^2}{3\Delta x^3} (u^{m+1} - 3u^m + 3u^{m-1} - u^{m-2}) + \\ + \frac{q^2}{2\Delta x^3} (h_b^{m+1} - 3h_b^m + 3h_b^{m-1} - h_b^{m-2}) = 0 \end{aligned} \quad (\text{F.7})$$

This gives a solution for  $u^{m+1}$

$$u^{m+1} = \frac{(a_m + 3c_m)u^m - 3c_m u^{m-1} + c_m u^{m-2} - K}{a_m + c_m} \quad (\text{F.8})$$

$$K_m = b_m(h^{m+1} - h^m) + d_m(h_b^{m+1} - 3h_b^m + 3h_b^{m-1} - h_b^{m-2})$$

$$a_m = q$$

$$b_m = \frac{gh^m}{\Delta x}$$

$$c_m = -\frac{q(h^m)^2}{3\Delta x^3}$$

$$d_m = \frac{q^2}{2\Delta x^3}$$

In this way, the velocity is solved in upstream direction. Discretization of the continuity equation gives an expression for  $h^{m+1}$

$$h^{m+1} = \frac{q}{u^{m+1}}$$

In case of subcritical flow, the information comes from the upstream and the downstream direction, so the equations also needs to be solved backwards (downstream direction):

$$a_m(u^m - u^{m-1}) + c_m(u^{m+1} - 3u^m + 3u^{m-1} - u^{m-2}) + K = 0$$

$$u^{m-1} = \frac{c_m u^{m+1} + (c_1 + 3c_3)u^m - c_m u^{m-2} + K}{a_m - 3c_m}$$

$$h^{m-1} = \frac{q}{u^{m-1}}$$

The modified momentum equation can also be solved implicit by using a set of equations:

$$a_m(u^{m+1} - u^m) + c_m(u^{m+1} - 3u^m + 3u^{m-1} - u^{m-2}) + K_m = 0$$

Boundary conditions:

$$u^1 = u^2 = u_{upstreamboundary}$$

$$u^{mmax+1} = u_{downstreamboundary}$$

$$\begin{pmatrix} 1 & 0 & 0 & 0 & 0 & 0 \\ 0 & 1 & 0 & 0 & 0 & 0 \\ a_3 & b_3 & c_3 & d_3 & 0 & 0 \\ 0 & a_4 & b_4 & c_4 & d_4 & 0 \\ 0 & 0 & a_m & b_m & c_m & d_m \end{pmatrix} \begin{pmatrix} u_1 \\ u_2 \\ u_3 \\ u_4 \\ u_m \\ u_{m+1} \end{pmatrix} = \begin{pmatrix} K_1 \\ K_2 \\ K_3 \\ K_4 \\ K_m \\ K_{m+1} \end{pmatrix}$$

This solves the velocity u over the x-direction. The waterdepth h is solved with the continuity equation:

$$h^m = \frac{q}{u^m}$$